# Dissertation

Baricitinib reduces inflammation and improves cell homeostasis of HGPS fibroblasts by inhibiting JAK-STAT signaling

Chang Liu

Fakultät für Medizin

Lehrstuhl Epigenetik der Hautalterung

# Baricitinib reduces inflammation and improves cell homeostasis of HGPS fibroblasts by inhibiting JAK-STAT signaling

Chang Liu

Vollständiger Abdruck der von der Fakultät für Medizin der Technischen Universität München zur Erlangung des akademischen Grades eines Doktors der Naturwissenschaften (Dr. rer. nat.) genehmigten Dissertation.

**Vorsitzende(r):** **Prof. Dr. Jürgen Ruland**

**Prüfer der Dissertation:**

**1. Prof. Dr. Karima Djabali**

**2. Prof. Dr. Thomas Brück**

Die Dissertation wurde am 30.09.2020 bei der Technischen Universität München eingereicht und durch die Fakultät für Medizin am 16.02.2021 angenommen.

# Table of Contents

# Abstract

Hutchinson–Gilford progeria syndrome (HGPS, OMIM 176670) is a rare disorder of premature ageing, with an average life span of 14.7 years and induced by myocardial infarction or stroke. Ninety percent of HGPS cases are caused by the mutation within exon 11 of the lamin A gene (GGC > GGT, G608G). This results in a new cleavage site, which leads to a 50 amino acid deletion in the carboxy-terminal tail of prelamin A. This removal eliminates the cleavage site of ZMPSTE24 during the lamin A formation process, resulting in a permanent farnesylation protein, which is also called progerin. Accordingly, progerin is firmly anchored to the nuclear envelope, causing nuclear blebbing, heterochromatin disorganization and DNA double-strand break (DSB) accumulation. Eventually, the aggregation of progerin induces the accelerated senescence of cells.

In addition to causing senescence at the cellular levels, the accumulation of progerin in children with HGPS leads to ageing at the organismal levels. Children with HGPS often develop a variety of phenotypes, including atherosclerosis, arthritis, alopecia and lipodystrophy; these also regularly appear during the ageing process of ordinary older adults. These characteristics are all associated with tumor necrosis factor-alpha (TNFa), interleukin 6 (IL-6), interferon (IFN) and other cytokines, and they often coincide with other progeroid syndromes, such as mandibuloacral dysplasia (MAD), restrictive dermopathy (RD) and Malouf syndrome. To determine if the development of these four characteristics might participate in an aberrant signaling pathway, we conducted a text mining analysis of scientific literature and databases to find the genes related to each of the characteristics.

Among thousands of relevant genes, we found a total of 17 essential genes correlated to 4 diseases simultaneously, 14 of which were linked to the JAK1/2-STAT1/3 signaling pathway. We then established the replicative senescence model in both HGPS and control cells. After a long term cell culture, we found that the JAK1/2-STAT1/3 signaling pathway was over-activated with propagated inflammation cytokines, while cell senescence increased.

In addition to telomere attrition, many other stresses can also cause the occurrence of cell senescence. We used etoposide to induce the senescence of the control and HGPS fibroblasts via DNA damage. Notably, the over-activation of the JAK1/2-STAT1/3 signaling pathway could be found in cells after injury using etoposide, like replicative senescence. Therefore, we conclude that the JAK-STAT pathway's excessive activation during senescence depends on a common mechanism. Although this mechanism is always accompanied by ageing, the generation of ageing can be induced by multiple sources. It can be caused by telomere attrition or promoted by the progerin expression, or it can be affected by DNA damage.

baricitinib is a potent, selective, and reversible JAK1/2 inhibitor, approved by the Food and Drug Administration (FDA). We report the inhibition of the JAK1/2-STAT1/3, signaling pathway restored cellular homeostasis, delayed senescence and decreased pro-inflammatory markers, in both control and HGPS cells. Our in vitro data using human fibroblast models indicate that the over-activation of the JAK-STAT signaling mediates premature senescence, replicative senescence and DNA damaged senescence; the inhibition of this pathway could present as a promising treatment for HGPS and age-related pathologies.

# 1.Introduction

## 1.1. Theories of senescence

Biological ageing, known as senescence, is one of the most complex biological processes and has attracted the attention of scientists and philosophers throughout history. During the process of human ageing, the complexity of various physiological processes and anatomical structures gradually disappears [1]. Additionally, different kinds of damage are accumulated from small molecular level to cellular level, and then to tissue levels, progressively leading to the loss of function and greater vulnerability to various diseases over time, and eventually resulting in death [2].

Compared to centuries ago, not only has the average life expectancy of humans across the globe been extended, but the percentage of elderly people in the population has increased dramatically, especially in certain developed countries [3]. Although biologists and demographers have proposed several theories to explain the ageing process, the molecular mechanisms of physiological ageing are still not yet fully understood. Among these theories, the most widely known are the programmed ageing theory and the damage or error ageing theory [4]. According to the "programmed" hypothesis, ageing depends on the circadian clock, which regulates the stages of life through growth, development, maturity and ageing [5]. This regulation depends on genes sequentially switching the nerve, endocrine and immune systems on and off, which are responsible for maintaining homeostasis and activating defense response [6]. The "error" hypothesis emphasizes the effects of environmental changes on organisms that cause progressive damage at various cellular levels (e.g., telomere shortening, DNA (deoxyribonucleic acid) polymerase errors, mitochondrial DNA damage, radical oxygen accumulation, cross-linking) [7]. Inevitably, reactive oxygen species (ROS) are consistently produced as a by-product in our daily metabolism, resulting in damage to large molecules and cellular structures [8]. But all theories ultimately lead to the accumulation of DNA damage,

which in turn leads to senescence and cancer through genome instability.

Although almost everyone wants to be healthy and have a long life; in reality, most people live to about 70–80 years [9]. However, there are particular patients with what is known as progeroid syndrome or progeria, who have accelerated ageing and a shortened life span [10]. Premature ageing syndrome contains two categories: unimodal syndrome and segmental syndrome [11]. Unimodal early ageing syndrome displays significant aspects of healthy ageing, such as Alzheimer's disease [12]. In contrast, segmental premature ageing syndrome displays multiple aspects of the ageing phenotype affecting several but not all tissue types, such as Werner's syndrome and Hutchinson–Gilford progeria syndrome (HGPS) [13].

## 1.2. Hutchinson–Gilford progeria syndrome

Hutchinson–Gilford premature ageing syndrome (HGPS, OMIM 176670) is a rare catastrophic premature ageing disease characterized by severe stunting and early death. HGPS patients are usually associated with a number of conditions [14]. These diseases include bone changes (arthritis, osteolysis, osteoporosis), obvious fat malnutrition, skin atrophy with scleroderma lesions, hair loss and vascular diseases [15]. Among these diseases, vascular disease is the most harmful, which always leads to death. Jonathan Hutchinson first reported a unique patient in 1886 [16]. Although the patient was a six-year-old boy, his overall appearance was that of an older man. Shortly after that, in 1897, Hastings Gilford found another child patient with similar symptoms [17]. Through continuous research, Guildford defined this disease, which displays similar properties to those of older adults, as progeria syndrome.

Children with HGPS do not have any abnormal phenotypes at birth or in infancy, but, within 12 to 24 months after birth, various symptomatic phenotypes gradually begin to appear [18]. With the passage of time, HGPS patient growth changes from ordinary to that of retardation, and the rate of weight gain has steadily decreases [19]. Alopecia occurs in the first year,

following the loss of subcutaneous fat, mid-facial cyanosis and skeletal abnormalities (low bone density, stiffness of joints) develop at the age of two to three [20]. Furthermore, progeria symptoms include prominent eyes, a high-pitched voice, wrinkled skin, conductive hearing loss, underdeveloped earlobes, and malnourished fingernails and toenails [21]. Although there are a great number of different disorders, movement and mental development of HGPS patients are satisfactory, and the incidence of tumors does not increase [22]. The early deaths of most HGPS cases are caused by the acceleration of atherosclerosis of the carotid and coronary arteries [23].

Meanwhile, cardiovascular diseases, including angina, congestive heart failure, myocardial infarction and stroke, occur simultaneously, leading to a short life expectancy of 14.7 years. The incidence of the disease is about one in eight million, and this rare incidence exists in many countries without noticeable ethnic differences. So far, there are still 166 HGPS children living in 51 different countries [24].

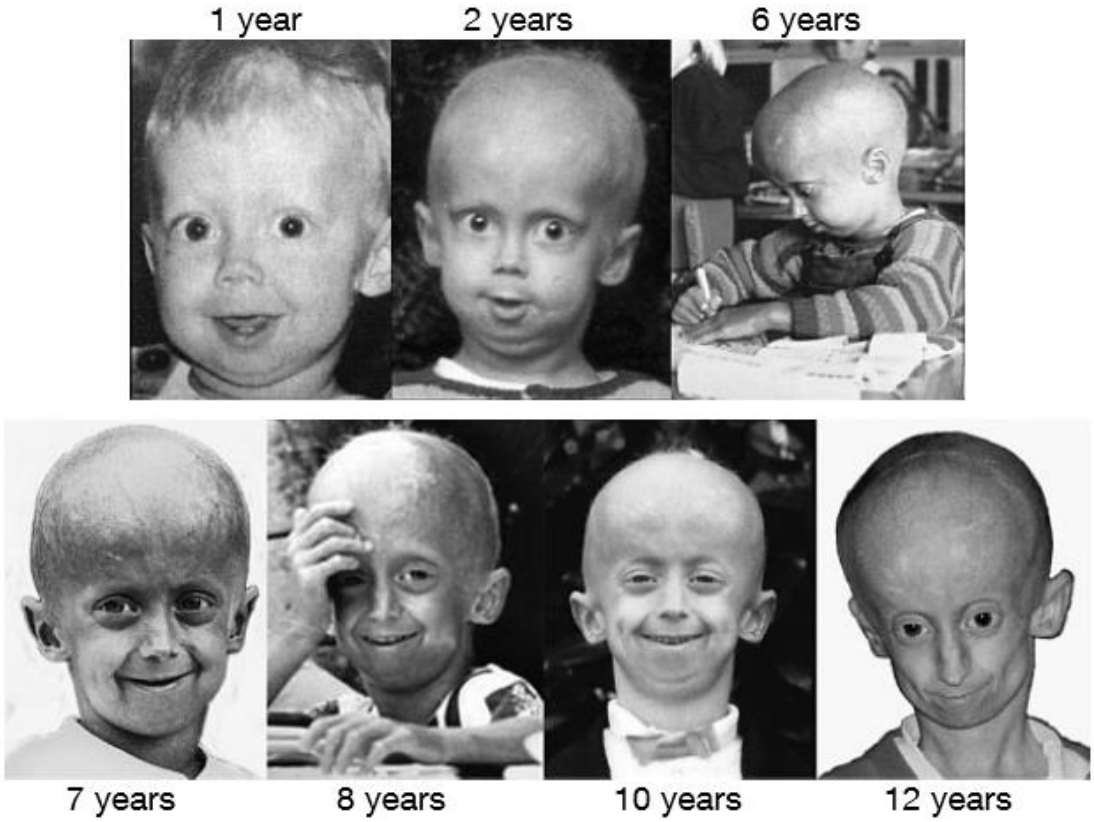

**Figure 1: The disease development process of a Dutch HGPS patient.** At the age of one year, the child showed no typical HGPS symptoms. Various symptoms began to appear from 12 months to 24 months, including hair loss, arthritis and lipodystrophy symptoms, which can easily be observed from the figure. [Modified from Hennekam, 2006[18]]

## 1.3. The nuclear lamin protein

In 2003, Eriksson identified the generation of HGPS to some mutations in the lamin A gene with the epigenetics development. Since then, laminopathies caused by LMNA mutation or its most general encoded isoform, prelamin A, have been catching more people's attention [25]. These LMNA-linked laminopathies are associated with a variety of pathologies such as premature ageing, lipodystrophies, muscular dystrophies and bone connective tissue diseases [26].

Lamins are also acknowledged as nuclear lamins. They are fibrous proteins in the V-type intermediate filament, which is essential for the stability of the cell's nuclear structure. Also, lamins are involved in a variety of transcriptional regulation, including DNA replication, RNA transcription and chromatin organization [27]. Lamin proteins interact with internal nuclear membrane proteins to form a nuclear fibre layer inside the nuclear membrane. Lamins have elasticity and mechanical sensitivity, so they can feed back external mechanical pressure signals to cells to participate in gene regulation. Lamins also engage in the decomposition and reformation of the nuclear envelope during the relocation of nuclear pores, mitosis and programmed cell death [28].

Lamins are mainly composed of three intermediate filaments: N-terminal domains, central α-helical rod domains and C-terminal domains. The median α-helical rod domain is surrounded by spherical N- and C-terminal fields, with the head located at the shorter N-terminal, and the tail situated at the longer C-terminal. As the head structure of the lamin is entirely

consistent, the type of lamin depends on the composition of the tail area. Still, all C-terminal domains include a nuclear localization sequence (NLS) [29].

Lamins contain two main categories, A-type and B-type. When cells differentiate, the LMNA gene is activated to express A-type lamins. Due to different cleavage sites, the LMNA gene produces two isoforms, lamin A and lamin C. Compared to lamin C, which is created directly by the gene, lamin A production involves a precursor called prelamin A. Lamin C is similar in structure to prelamin A except for the carboxyl terminus because prelamin A contains two more extra exons than lamin C [30].

Moreover, six unique amino acid residues only exist in lamin C, and prelamin A includes 98 residues not seen in other isoforms. Within the individual residues in prelamin A, there is a cysteine-aliphatic amino acid-aliphatic amino acid-any amino acid (CAAX) (C= cysteine, A= aliphatic amino acid, X= variable) motif, leading prelamin A to undergo a range of posttranslational changes and become mature lamin A. Briefly, these procedures are the farnesylation of the carboxy-terminal cysteine followed by the endoproteolysis to loosen the terminal amino acid. Carboxymethylation of the farnesyl cysteine and the zinc metalloproteinase eliminates the last 15 residues. As the first modification step, the prelamin A farnesylation is essential for the lamin A maturation progress. Although lamin C is an isoform of lamin A, it does not require posttranslational modifications during the development of maturation [31].

Lamin B is expressed in almost every cell and has multiple isoforms, the most common of which are lamin B1 and lamin B2, being generated by two independent genes: LMNB1 and LMNB2, respectively. By carrying a CAAX motif at the carboxyl terminus, type B lamins are similar to prelamin A at triggering the same posttranslational modification sequence. Differing from prelamin A, type B lamins do not possess the last cleavage step involving zinc metalloproteinase. The regions of introns and exons in B-type lamins are maintained among A-type lamins, but the A-type lamins contain a more significant variation, indicating that B-type lamins are the common ancestor of these lamin types [32]. Related research in the ageing area also shows that cell ageing often accompanies the loss of lamin B [33].

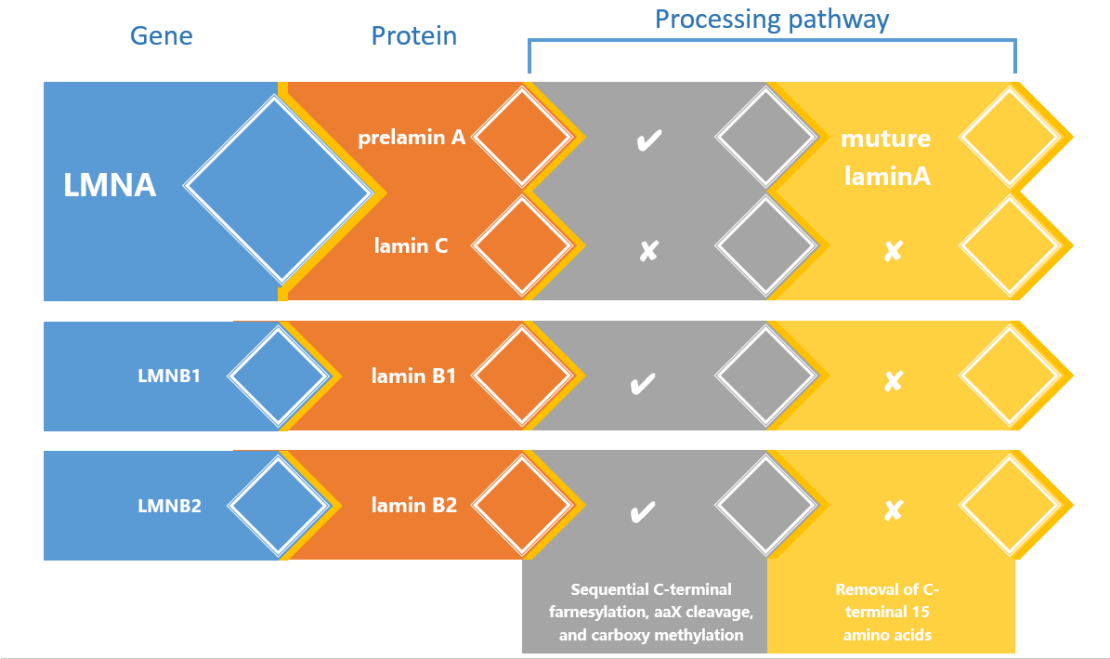


**Figure 2: The processing pathway of major A-type and B-type lamins in humans.** Prelamin A, lamin B1 and lamin B2 all carry a carboxyl-terminal CAAX motif modified by farnesylation. (For human beings, the CAAX motif means the CSIM in prelamin A, CAIM in lamin B1 and CYVM in lamin B2. C is cysteine, S is serine, I is isoleucine acid, M is methionine, A is alanine, Y is tyrosine and V is valine). The next process is the proteolysis of the aaX residues and carboxymethylation at the C-terminal end of lamin A, B1 and B2. However, only prelamin A shares a further process to eliminate the carboxy-terminal 15 amino acids, including the farnesylated and carboxymethylated cysteine, to generate mature lamin A.

As mentioned above, the posttranslational modifications of carboxy-terminal CAAX are highly required during the maturation procedure of lamin A, B1 and B2. In prelamin A, it is Cys-Ser-Ile-Met. There are three sequential steps for the enzymatic modification of the CAAX motif. First, the cysteine of the CAAX motif is farnesylated by farnesyltransferase modification. In the next modification process, the last 15 C-terminal amino acids (-AAX) of prelamin A are cleavaged, and the farnesyl is removed, with the help of the enzyme ZMPSTE24 (the zinc metalloprotease-farnesylation-protein convertase associated with the STE24 homolog in yeast FACE1). Then, the isopentenyl cysteine carboxyl group is methyl esterified with the

carboxyl-terminal cysteine methyltransferase (ICMT) [34].

At last, the other 15 amino acids at the C-terminal are removed after the canalization of ZMPSTE24 on the second proteolytic cleavage. After these three modification steps, the matured lamin A, lacking carboxy-terminal farnesyl and carboxymethyl, is produced. In this process, all of the enzymes needed to modify the carboxyl terminus of lamins are located in the inner core membrane and endoplasmic reticulum membrane. Prelamin A finishes the prelamin A translation process in the cytoplasm and then processes the modification in the nucleus [35]. In HGPS, a new hidden splice site is stimulated by the G608G mutation, and it deletes nucleotides on the prelamin A mRNA. As a result, the following important recognition site for the ZMPSTE24 enzyme (RSYLLG) does not exist at the translated prelamin A. As ZMPSTE24 is not able to cleavage the right place, the lamin A is permanently farnesylated and carboxy-methylated after the modification process. This truncated lamin A protein produced in HGPS is referred to as progerin (farnesylated prelamin AΔ50, lamin AΔ50) [36]. Progerin can lead to altered gene expressions, defective proteostasis, mitochondrial dysfunction, DNA damage and oxidative stress, which induce cells to start premature senescence [37].

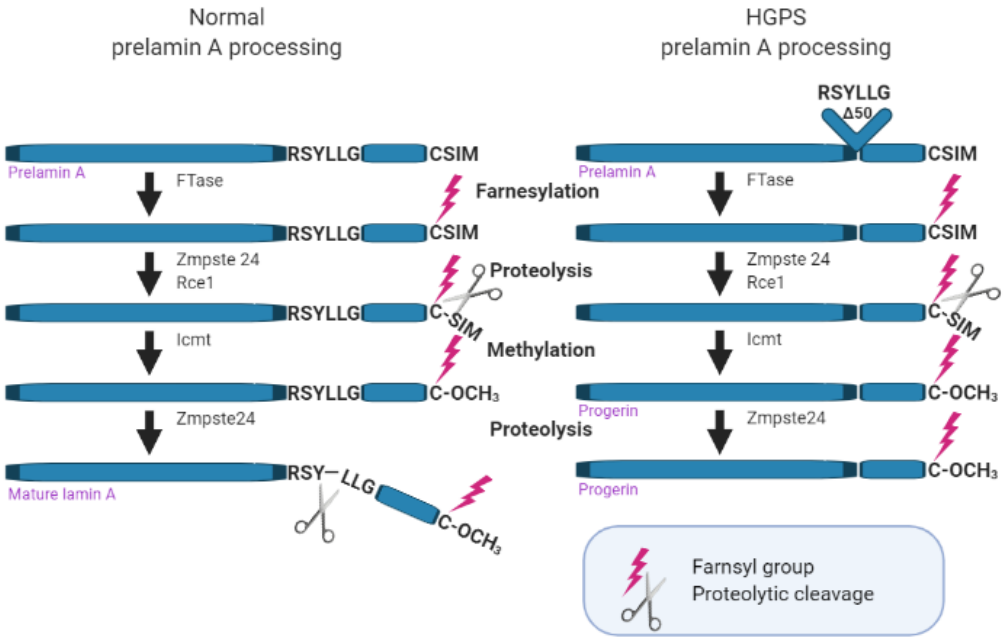


**Figure 3: The posttranslational processing of prelamin A.** The posttranslational processing of normal prelamin

A is depicted on the left side, and the prelamin AΔ50 in HGPS is shown on the right side. However, the loss of the recognition site RSYLLG for ZMPSTE24 in HGPS cells ultimately prevents the occurrence of the final proteolytic cleavage and then further leads to permanent farnesylation and carboxymethylation of lamin AΔ50, called progerin.

## 1.4. Lamin protein family and genetic diseases

In the cell structure, the nucleus and cytoplasm are separated by the nuclear envelope, resulting in two different parts, namely the outer nuclear membrane (ONM) and the inner nuclear membrane (INM), and perinuclear space (PNS) separates these two sections. There are many nuclear pore complexes (NPC) on the nuclear membrane to connect the cytoplasm and nucleus, and their presence can help large molecules enter and exit the nucleus [38]. The outer nuclear membrane contains endoplasmic reticulum (ER) proteins and ribosomes. In contrast, the inner nuclear membrane has its whole group of membrane proteins; most of these proteins combine with the nuclear lamina underlying the INM. A-type and B-type lamins and nuclear lamin-associated proteins build up the filamentous meshwork of the nuclear lamins. These nuclear lamins have a significant function for anchoring nuclear envelope transmembrane (NET) proteins such as lamin B receptor (LBR), MAN1, emerin and lamin-associated polypeptide 1/2. These proteins are crucial for the peripheral chromatin organization and the control of gene expression [39].

In recent years, with increasing understanding of lamins' major interaction networks, lamins have been found to play an essential function in various human diseases (laminopathies), including premature ageing syndrome and other conditions affecting muscle, fat, bone and neuronal tissue.

In addition to the HGPS we are studying in this research, many other diseases involve lamin changes. For example, mandibuloacral dysplasia type A (MADA) is caused by the mutation of

lamin A/C (LMNA) genes [40]; mandibuloacral dysplasia type B (MADB) is caused by the mutations of the zinc metalloproteinase (ZMPSTE24) gene [41]. Restrictive dermopathy (RD) is caused by a loss of the gene ZMPSTE24 or a mutation in the LMNA gene [42]; heterozygous mutations cause Malouf syndrome in the lamin A/C gene [43]. All of the patients suffering from the diseases mentioned above have four typical phenotypes, namely, vascular disease, lipodystrophy, alopecia and arthritis.

Therefore, these four conditions are likely to have a common defective molecular mechanism. Other studies have shown that these four phenotypes are simultaneously displayed in the lamin-related diseases and partly occur in different conditions. For example, vascular diseases, especially atherosclerosis, lipodystrophy and alopecia, are some of the principal phenotypes that describe Werner's syndrome, which is another progeroid syndrome [44]. Whipple disease usually shows arthritis, vascular disease and lipodystrophy simultaneously [45]. Lipodystrophic conditions with loss of adipocytes are always associated with alopecia [46]. Arthritis patients are also regularly suffer from alopecia [47]. Patients with severe androgenetic alopecia (AGA) possess a higher risk of subclinical atherosclerosis, and early-onset AGA alone could be an independent risk factor for cardiovascular disease [48]. Both congenital generalized lipodystrophy patients and HIV-associated lipodystrophy syndrome patients present accelerated atherosclerosis rising from a notably disordered metabolic milieu [49]. Cardiovascular disease is an essential part of rheumatoid arthritis (RA) morbidity and mortality, and it influences RA patients independent of conventional risk factors [50]. Alopecia is also a typical symptom of a cerebral vascular disease like cerebral autosomal recessive arteriopathy with subcortical infarcts and leukoencephalopathy (CARASIL) [51]. Lipodystrophical children often develop other autoimmune disorders such as RA [52]. Juvenile dermatomyositis patients seldom hold lipodystrophy and arthritis [53]. Long-term sequelae of chikungunya virus disease are associated with arthritis and alopecia [54]. More importantly, these four conditions also often more or less affect the life of a typical elder, although not necessarily all of the phenotypes – usually two to three of them at the same time [55]. All of these results indicate that these four typical HGPS phenotypes may share a common

defective molecular mechanism. Therefore, the molecular mechanism of each disease should be understood first.

**Table 1: Diseases have more than one phenotype out of those four conditions (vascular disease, lipodystrophy, alopecia and arthritis).** The literature shows that many progeroid syndromes have all four phenotypes at the same time. Meanwhile, many other diseases also have several of those four phenotypes.

| Disease name | Vascular disease | Arthritis | Alopecia | Lipodystrophy |
|---|---|---|---|---|
| Progeroid syndromes: | | | | |
| Hutchinson–Gilford progeria syndrome | ✓ | ✓ | ✓ | ✓ |
| Mandibuloacral dysplasia type A | ✓ | ✓ | ✓ | ✓ |
| Mandibuloacral dysplasia type B | ✓ | ✓ | ✓ | ✓ |
| Restrictive dermopathy | ✓ | ✓ | ✓ | ✓ |
| Malouf syndrome | ✓ | ✓ | ✓ | ✓ |
| Werner's syndrome | ✓ | ✓ | ✓ | ✓ |
| Other diseases: | | | | |
| Whipple disease | ✓ | ✓ | ✗ | ✓ |
| Lipodystrophic conditions | ✗ | ✗ | ✓ | ✓ |
| Arthritis | ✗ | ✓ | ✓ | ✗ |
| Androgenetic alopecia | ✓ | ✗ | ✓ | ✗ |
| Generalized lipodystrophy | ✓ | ✗ | ✗ | ✓ |
| HIV-associated lipodystrophy syndrome | ✓ | ✗ | ✗ | ✓ |
| Rheumatoid arthritis | ✓ | ✓ | ✗ | ✗ |
| Cerebral autosomal recessive arteriopathy with subcortical infarct | ✓ | ✗ | ✓ | ✗ |

| | | | | |
|---|---|---|---|---|
| and leukoencephalopathy | | | | |
| Lipodystrophical children | ✗ | ✓ | ✗ | ✓ |
| Juvenile dermatomyositis | ✗ | ✓ | ✗ | ✓ |
| Long-term sequelae of Chikungunya virus disease | ✗ | ✓ | ✓ | ✗ |
| Cardiovascular disease | ✓ | ✓ | ✗ | ✗ |

## 1.5. Vascular disease

### 1.5.1. Vascular disease in HGPS

Just as there are no apparent signs of senescence at first, HGPS patients are born with normal blood pressure and no symptoms of cardiovascular disease, and even the electrocardiogram pictures and blood pressure tests are normal. However, by the age of four, some patients develop a heart murmur, which is a sound produced by blood turbulence passing through a heart valve or near the heart, indicating that a particular cardiovascular disease has occurred. From four to six years of age, the patient gradually developed shortness of breath and was prone to fatigue. At the same time, blood pressure and pulse frequency increased. The electrocardiogram showed signs of damaged coronary function and expansion of the left ventricle, both at activity and rest [56].

Meanwhile, some patients also show signs of impaired coronary function, cardiac hypertrophy and earlier silent infarction. As they age, children further illustrate typical angina symptoms, such as chest pain or discomfort and extreme difficulty breathing. In most cases, the leading cause of death in patients with HGPS is an accelerated cardiovascular disease such as myocardial infarction or stroke caused by extensive atherosclerosis. After the patients' death, the researchers found decreased vascular intimal and medial diameters, smooth muscle loss, coronary artery thickening, cardiac muscle cell hypertrophy, interstitial

fibrosis, aortic valve leaflet thickening and mitral valve abnormalities, including calcification and other typical characteristics of cardiovascular disease [57].

The classic lesions of ordinary cardiovascular patients are often caused by factors such as hypercholesterolemia, smoking and early hypertension. However, HGPS patients do not have these influencing factors. In contrast, progerin is widely present in arterial walls and atherosclerotic plaques in patients with HGPS. As age increases, progerin further aggregates into a compact, rim-like structure at the nuclear envelope of vascular smooth muscle cells (VSMCs) and adventitia [58]. The accumulation of progerin may lead to nuclear defects and increase susceptibility to mechanical strain. In turn, it causes cells to die and produce an inflammatory emergency, which leads to atherosclerosis. It is not difficult to find that the pathological changes of cardiovascular disease in both elderly and HGPS patients are strictly related to the generation of inflammation.

### 1.5.2. Pathogenesis of vascular diseases

Calcification, inflammation and plaque erosion and rupture are typical features of general ageing and HGPS. In HGPS, the accumulation of minimally oxidized low-density lipoprotein (LDL) triggers the atherosclerotic plaque formation [59]. In this process, the gathering of minimally oxidized LDL causes endothelial cells (EC) to produce surface adhesion molecules, such as intercellular adhesion molecule-1 (ICAM-1), vascular cell adhesion protein-1 (VCAM-1) and very late antigen-4 (VLA-4). These proteins then increase vascular permeability, which leads to lipid and inflammatory cells becoming attached and penetrating the subendothelial space. In this space, due to the role of reactive oxygen species (ROS) and lipase, the least-oxidized LDL gets oxidized to yield highly-oxidized LDL, subsequently causing an inflammatory response. In response to this inflammation, the body releases pro-inflammatory cytokines (interleukin-6 [IL-6], C-C motif chemokine ligand 2 [CCL2] and interleukin-1 beta [IL-1β]) via a monocyte from the blood into the subendothelial space. Tumor necrosis factor (TNF) receptor-associated factor 1 (TRAF1) plays a critical role here to recruit the monocyte to the

vessel wall. Subsequently, the inflammatory environment gets established; the macrophages become differentiated and then swallow and digest these highly oxidized LDLs to produce foam cells with the assistance of complement component 3 (C3), gathering to form plaque. As the volume of plaque increases, the arterial wall becomes thicker and harder. In this process, the inflammatory factors TNFa and interferon-gamma (IFNG) also play a vital role because they mediate the cluster of differentiation 36 (CD36) and the cluster of differentiation 68 (CD68) of macrophages to recognize the process of oxidized aggregated LDL [60].

In addition to the cytokines directly involved in cardiovascular disease, many other proteins play an important role in this process. Peroxisome proliferator-activated receptor gamma (PPARG) can regulate a variety of homeostasis functions related to vascular pathologies [61]. First, it affects insulin signaling pathways and endothelial function through phosphoinositide 3-kinases (PI3K)/protein kinase B (Akt)/endothelial nitric oxide synthase (eNOS) or mitogen-activated protein kinase (MAPK)/endothelin-1 (ET-1). Second, regulating the renin-angiotensin system (cascade protein) gene expression slows down the development of atherosclerosis and hypertension. Third, oxidative stress is indirectly regulated by PPARG or by nuclear factor erythroid 2–related factor 2 (Nrf2). During the whole process of atherosclerosis, especially in the early stages, transforming growth factor-beta 1 (TGFB1) resists this process in various ways [62]. For example, TGFB1 can prevent the excessive accumulation of vascular smooth muscle cells (VSMCs) in the neointimal membrane and can advert plaque rupture by inciting extracellular matrix organization and tissue repair. It can also stimulate type III T helper cell function and governing T cells (cluster of differentiation 3+ (CD3+)/cluster of differentiation 25 (CD25)) to control local inflammation. The C-reactive protein (CRP) interacts with endothelium, lipoproteins, monocytes, neutrophils, and the complement system to regulate the immune system and change the acute inflammatory response to vascular injury into the chronic inflammatory response typical in atherosclerosis [63]. Insulin-like growth factor 1 (IGF-1) has several cardiovascular protective effects. It can reduce the development of atherosclerosis and improve the stability of atherosclerotic

plaques by inducing oxidative stress, apoptosis, pro-inflammatory and reduction of endothelial dysfunction. IGF-1 can also protect microvessels through endocrine and paracrine signaling pathways to delay the process of atherosclerosis and diabetic vascular disease [64]. Heme oxygenase-1 (HMOX1) is also highly involved in cardiovascular disease. It can affect atherosclerosis, intimal hyperplasia, myocardial infarction and angiogenesis. For example, its expression helps macrophages increase the protective effect of antioxidants and thus prevents the oxidation of LDL and consequently protects and reduces atherosclerosis [65].

### 1.5.3. Drugs for vascular diseases

Based on the molecular mechanism of atherosclerosis development, many drugs have been developed and used clinically to overcome the clinical mortality of atherosclerosis. For example, PPARG is a useful therapeutic target for atherosclerosis [66]. Once PPARG is stimulated, lipoprotein lipase and apolipoprotein A-V increase, and the hepatic apolipoprotein C-III decreases. These steps further reduce triglycerides in the plasma chylomicrons and very-low-density lipoprotein, which is the critical character that causes atherosclerosis, as mentioned above. As the high-density lipoprotein (HDL) is assembled by apolipoprotein A-I and apolipoprotein A-II, the activation of PPARG can increase their expressions and raise cholesterol levels in HDL, further delaying the formation of atherosclerosis by increasing HDL-mediated cholesterol efflux from macrophages. Hydroxylmethylglutaryl-coenzyme A reductase inhibitors (statins) are a selection of classic antihypertensive and lipid-lowering drugs [67]. They can lower cholesterol and stabilise atherosclerotic plaques, thereby reducing the embolism rate. The endoglin-mediated action is also involved in the reduction of cholesterol levels by statins. Endoglin (TGF-β receptor III, CD 105) is a glycoprotein that plays a regulative role in transforming growth factor–β (TGF-β) signaling, and the expression of endoglin is strongly correlated to cardiovascular system development [68]. The altered vasodilation properties, expanding expression of inflammatory cell adhesion molecules and a pro-thrombogenic states can all be caused by endothelial

dysfunction leading to atherogenesis.

## 1.6. Arthritis

### 1.6.1. Arthritis in HGPS

When looking at HGPS patients, the first things that often catch the eye are their narrow shoulders and slender chins. These features are caused by many different kinds of osteolysis phenomena, which are widely present in the clavicle, mandible, distal phalanx, visceral skull and neurocranium [18]. For example, increased osteolysis of the collarbone and upper ribs frequently causes the prominent narrow shoulders in patients. The clavicle osteolysis usually starts from the acromial end at a slow pace. The mandible osteolysis is relatively apparent, creating a smaller chin after one or two years of age. The reduction in the maxilla and mandible dimension makes the teeth crowded and even squeezed out. Concurrently, from the age of one to two years, the distal phalanx's osteolysis begins to occur [69]. Usually, this phenomenon starts from the index finger and the little finger. It gradually spreads to the toes, and suddenly, all of the fingers are affected, leading to phalanges and malnourished nails; the nearby skin becomes swollen and red. With age, the bones of the visceral skull also begin to dissolve, causing the facial bones to become thinner. The widely existing anterior fontanelle in the neurocranial bone may be manifested by osteolysis, which continually develops in childhood or adolescence. As a patient's condition continues to worsen, fractures begin to occur widely in various parts, and severe skull fractures can appear [18]. The polycentric osteolytic disease is an essential representative of RA, a systemic disease that causes progressive destruction of joints and surrounding structures.

### 1.6.2. Pathogenesis of arthritis

As a chronic inflammatory autoimmune disease, RA primarily affects the joints, causing joint swelling, functional impairment, inflammatory pain and muscle wasting. Moreover, RA is associated with an increased risk of cardiovascular disease and osteoporosis. Generally speaking, RA occurs in four typical stages: triggering, maturation, targeting and fulmination, eventually producing bone erosion, cartilage damage, proliferative synovium and systemic consequences [70]. Anti-citrullinated protein antibodies (ACPAs) occur in approximately 67% of RA patients with a more clinically severe phenotype compared to the one without ACPAs. Potential triggering sites in various parts of the body, including the lungs, mouth and gut, can be activated by multiple environmental factors. The citrullination of the self-protein drives RA, and it subsequently causes the body to produce autoantibodies against citrulline peptide. The maturation step is launched at the section of secondary lymphoid tissues or bone marrow. In this stage, self-antigens are released, causing the development of immune responses to endogenous epitopes [71].

Meanwhile, the titre of ACPA increases with breaking immunological tolerance. Consequently, major histocompatibility complex (MHC) class II-dependent T cells are stimulated by many citrullination neoantigens and, in turn, help B cells generate more ACPA, further inducing pain, inflammation and bone loss [72]. After entering the targeting phase, synovitis occurrs in the symmetric facet joints, and the joints become swollen. Leukocytes infiltrate the synovial compartment, and the synovial fluid is filled with pro-inflammatory mediators, inducing an inflammatory cascade. Fibroblast-like synoviocytes interact with cells of the innate immune system. Endothelial cells in synovial microvessels are activated to express various adhesion molecules and chemokines, thereby contributing to a wide range of angiogenesis.

At last, hyperplastic synovium, bone erosion, cartilage damage and systemic consequence all occur in the fulminant stage. At the places where the synovial membrane enters into the periosteum, bone erosion can be found due to bone resorption. Decreasing osteoblasts and increasing osteoclasts and synoviocytes lead to the damage of the subchondral bone, which

eventually ends in the degeneration of articular cartilage [73].

Several different types of cells closely cooperate in the development of RA, including synovial cells (fibroblasts, perivascular cells, and endothelial cells), dendritic cells, macrophages and other effector cells of the immune system. Cytokines such as IL-6, TNFa, interleukin 1 (IL-1) and interleukin 17 (IL-17) are produced by the macrophages and T cells inside the synovium, leading to inflammation and rheumatoid arthritis synovial fibroblast (RASF) stimulation [74]. As the critical character in maintaining the homeostasis of the synovium in healthy joints, RASF destruction is considered to be the principal reason for the pathogenesis of joint injury. The activation of RASF can significantly increase the expression of cathepsin, matrix metalloproteinase (MMP) and vacuolar ATP monophosphatase (ATPase), thereby destroying the bone matrix and bone tissue. Additionally, the activation of RASF also promotes the synthesis of degrading proteases and causes cartilage degradation [75].

### 1.6.3. Drugs for arthritis

Due to the crucial role of TNFa performed in RA clinical manifestations and the progression of bone and cartilage damage in RA, anti-TNFa drugs such as infliximab and methotrexate can significantly slow or prevent these pathological changes [76]. In addition to anti-TNFa drugs, drugs targeting IL-6, such as tocilizumab, have also been approved for the treatment of RA. IL-6 can activate the formation of T cells, B cells, macrophages and osteoclasts. Anti-IL-6 drugs can further prevent the induction of osteoclast formation caused by IL-6 and stop B cells from presenting antigens and forming antibodies and cytokines [77]. By also targeting B cell function, rituximab, a monoclonal antibody that specifically binds to the B-lymphocyte CD20 antigen shown on the surface of mature B cells and pre-B cells, has been shown to have excellent anti-RA capabilities [78].

## 1.7. Lipodystrophy

### 1.7.1. Lipodystrophy in HGPS

Lipodystrophy syndrome is a heterogeneous disease, which may come from a natural inheritance or be acquired. It is mainly manifested by the inability of the body to produce and maintain healthy adipose tissue, creating a variety of metabolic complications such as cardiovascular disease, diabetes, insulin resistance and dyslipidemia [79].

In patients with HGPS, lipodystrophy usually appears slightly from six months until it gradually becomes apparent at the age of three or four. Being a typical early symptom of HGPS patients, veins are visible on the bridge of the nose in the early stages of just having lipodystrophy. The reduction of body fat causes this phenomenon and makes the skin thinner, making the blood vessels more visible. Subsequently, the scalp veins become apparent, and in the late stages, the entire body's veins become evident; the eyes protrude due to the loss of fat around the eyes, and the facial skin becomes wrinkled and thin. In general, the patients' limbs often begin to lose fat first. Then the neurocranial, thorax and facial fats gradually disappear until the buccal fat pad and pubic fat finally disappear [80].

### 1.7.2. Pathogenesis of lipodystrophy

Lipodystrophy, characterised by the disappearance of subcutaneous adipose tissue, is often caused by increased lipolysis and apoptosis in adipocytes. Mitochondria play an essential role in the activation of fat cell apoptosis. Peroxisome proliferator-activated receptor gamma coactivator 1-alpha (PGC-1α) is a PPARG coactivator that regulates mitochondrial production. Its expression in adipose tissue of patients with lipodystrophy is significantly reduced, causing damage to the respiratory chain in mitochondria in many cells. This loss often leads to a decrease in the expression of the critical mitochondrial uncoupling protein-2 (UCP-2), which controls the production of ROS, leading to the formulation of a large amount of ROS, which

forces oxidative stress in adipose tissue. Excessive oxidative stress leads to the differentiation of damaged fat cells, produces a large number of pro-inflammatory mediators and activates apoptosis. Elevated lipolysis raises the level of non-esterified free fatty acids (FFA) in the systemic circulation [81].

The increase of FFA can induce macrophages to produce IL-6 and TNFa and other pro-inflammatory mediators, and the rise of these pro-inflammatory mediators in adipose tissue further activates lipolysis. TNFa can also induce insulin resistance and leptin (LEP) production, inhibit lipoprotein lipase (LPL) activity and adipogenesis, reduce preadipocyte differentiation and induce apoptosis in preadipocytes and adipocytes. Additionally, TNFa can influence adipocyte dedifferentiation, driving differentiated adipocytes to lose function and return to the early-stage developmental state [82]. Adipocytes are also closely related to IL-6. As an essential pro-inflammatory protein, 30% of the body's IL-6 comes from adipose tissue and mediates insulin resistance, which induces increased apoptosis and leads to the loss of subcutaneous fat [83]. Since leptin is mainly produced in adipose tissue and widely exists in circulation and cerebrospinal fluid, it can regulate appetite, increase energy expenditure and reduce weight. At the same time, leptin can also act through 5'-AMP-activated protein kinases, thereby reducing anabolic pathways (such as glucose, protein, and lipid synthesis) and enhancing catabolic pathways (lipid utilization and glucose). Monocyte chemoattractant protein-1 (MCP-1) can also cause insulin resistance. In this process, insulin-stimulated glucose uptake is significantly reduced, and adipogenic genes in adipocytes, such as β-adrenergic receptors, glucose transporter type 4 (GLUT4), PPARG and adipsin, are downgraded [84].

### 1.7.3. Drugs for lipodystrophy

In the process of finding drugs to treat lipodystrophy in different situations, researchers have found that the levels of hormones such as leptin and adiponectin secreted by adipose tissues in lipodystrophy patients are significantly reduced in the systemic circulation, leading to insulin resistance and metabolic abnormalities [85]. PPARG agonists can increase the

circulation level of leptin to reverse fat metabolism abnormalities and partially relieve fat loss [86]. Similarly, leptin can significantly improve blood glucose and lipid levels in patients with lipodystrophy [87].

## 1.8. Alopecia

### 1.8.1. Alopecia in HGPS

HGPS children are born with healthy hair like other children, with no difference in hair color and texture. However, between six months and two years, their hair begins to fall out, and then their eyelashes and eyebrows gradually disappear. The body hairs on the axillae, chest, limbs or pubis are sparse or missing. Hair is an essential secondary sex characteristic. The absence of new hair growth, the loss of original hair and the lightened color of remaining hair all show abnormal hair follicle lesions in HGPS patients [18].

### 1.8.2. Pathogenesis of alopecia

The growth cycle of human hair follicles often has four growth stages: long growth period (anagen), short transition period (catagen), short resting phase (telogen) and hair loss (exogen) [88]. At the end of the resting stage, hair drops out, new hair begins to grow in the hair follicles, and the cycle starts again. In HGPS, the circulation of the hair follicle growth cycle causes alopecia due to the lymphocyte infiltration into the peribulbar space of the hair follicle in the growing phase and intrafollicular locations [89]. CD4+ and CD8+ T-cells are the leading causes of hair follicular inflammation, and many activated CD4+ T cells show up around the hair follicles. The CD8+ T cells can further penetrate the hair follicles to produce cytotoxicity and destroy hair growth. These activated cytotoxic T lymphocytes produce granzyme B, Fas ligand and TNFa molecules to trigger apoptosis in hair follicle cells, regularly

interrupt normal functions and produce pro-inflammatory cytokines, including IL-1, IFNG and IL-6.

During the pathogenesis and development of alopecia, cytokines and other molecules play an essential role in coordinating the periodic growth of hair. For the pathogenesis of alopecia, TNFa exerts a powerful and highly effective proliferation inhibitory effect [90]. Epidermal keratinocytes can produce TNFa and then, together with IL-1α and IL-1β, cause coagulation and deformation of the dermal papilla. They can also create clear vacuoles in the hair follicle matrix and cause abnormal keratinisation of the hair follicle and inner root sheath, destroying follicular melanocytes. These changes finally lead melanin granules to appear in the dermal papilla, which eventually results in malnutrition of hair follicles in the growing phase and, in turn, interferes with the normal hair growth cycle [91]. The IL-1 mentioned above is an essential inhibitor of human hair growth in vitro, and the overexpression of IL-1a in the epidermis can induce alopecia areata. In the early stage of alopecia, overexpression of IL-1β can be detected, and the alopecia may be aggravated by the lack of IL-1 receptor antagonists in patients. The serum levels of IL-1α and IL-4 in patients with local alopecia areata are notably enhanced. While the disease becomes more extensive, interleukin-2 (IL-2) and IFNG are mainly elevated, suggesting that T helper 1 (Th1) cytokines are mediated at the development of this process [92]. After the perifollicular or follicle antigen-presenting cells produce IFNG, the CD4+ Th1-mediated response induces deprivation of the skin papillary cells' ability to maintain hair growth. In this process, IFNG causes a significant increase in the monokine factor MIG, leading to the recruitment of chemokine interferon-inducible protein 10 (IP-10) by monocytes, making the Th1 response in alopecia areata persistent [93].

### 1.8.3. Drugs for alopecia

In the treatment of alopecia, corticosteroids such as triamcinolone acetonide have been used as the primary treatment in the local area of a lesion because they can inhibit the occurrence of inflammation and accelerate the recovery of damaged hair follicles. Although this drug can

cause about 57% of patients' hair to fully regrow, it can also cause side effects and skin atrophy at the treatment site, and it is easy to relapse after stopping treatment [94]. Immunotherapy is the primary method for treating alopecia today. For example, squaric acid dibutyl ester and diphenylcyclopropenone can be used as immunotherapeutic agents to treat alopecia. In the course of treatment, immunotherapeutic agents can induce antigen competition, distracting CD4+ T cells from combating hair follicles [95]. Recent studies have shown that JAK inhibitors are also promising drugs for the treatment of alopecia. Janus kinase-signal transducer and activator of transcription (JAK-STAT) inhibitors, including ruxolitinib and tofacitinib, can inhibit the downstream effects of type 1 cytokines, reduce IFNG signals, and then promote hair regeneration and reverse the formation of alopecia areata. In the experiment, three patients taking oral ruxolitinib were treated for five months and achieved almost complete hair regeneration [96].

## 1.9. The JAK-STAT pathway

### 1.9.1. The JAK-STAT pathway in general

As one of the most important signaling pathways other than the second messenger system, the JAK-STAT pathway, discovered in recent years, is an essential intracellular signaling transduction pathway regulating human development and homeostasis. This pathway can be activated by various cytokines, interferons, growth factors and related molecules so that chemical signals outside the cell can cross the cell membrane and transmit the message to the gene promoter on the DNA in the nucleus, thereby regulating DNA transcription and activity in the cell level [97].

This pleiotropic cascade can be employed to transduce several signals for development and homeostasis. JAK activation stimulates cell proliferation, differentiation, migration and division and further plays a crucial role in immune development, adipogenesis,

haematopoiesis and sexually dimorphic growth. On the contrary, abnormalities in these processes can also cause a variety of difficult diseases, including inflammatory disease, gigantism, erythrocytosis and an array of leukaemias.

### 1.9.2. The composition and mechanism of the JAK-STAT pathway

The JAK family of kinases includes four proteins: JAK1, JAK2, JAK3 and TYK2. JAKs contain a FERM (F for 4.1 protein, E for ezrin, R for radixin and M for moesin) domain, a domain related to Src homology 2 (SH2), a kinase domain and a pseudokinase domain. Among them, the kinase domain exhibits the phosphorylation site, which is crucial for the JAK activation. STATs contain a family of seven potential transcription factors that are structurally and functionally related. They are located in the cytoplasm until they are activated: STAT1, STAT2, STAT3, STAT4, STAT5a, STAT5b and STAT6. The STAT proteins contain many different functional domains, and the most conserved region is the SH2 domain. The SH2 section consists of two α-helices and one β-sheet. STATs also have transcription activation domains, which are less conserved and positioned at the C-terminal. STATs also include coiled-coil, linker, amino terminus, DNA binding domain and tyrosine activation [98].

Signals from interferons, interleukins, growth factors or other chemical messengers can bind to receptors on the cell surface to cause receptor dimerisation to activate this receptor. The activated receptor can then initiate the kinase function of JAK, leading to the phosphorylation of tyrosine residues in the region of the 'activation loop' during this process. Next, the activated tyrosine residues form a protein binding site with an SH2 domain. Subsequently, STATs attach to the phosphorylated tyrosines on the receptor by using their SH2 domains. Then, JAKs tyrosines phosphorylate the STATs, causing the dissociation of STATs from the receptor. These activated STATs form heterodimers or homodimers, in which the SH2 region of a STAT binds to the phosphorylated tyrosine of an opposite STAT. Then, the dimer translocates into the nucleus. In the nucleus, the dimer binds to DNA and originates the transcription of genes that respond to a STAT [99].

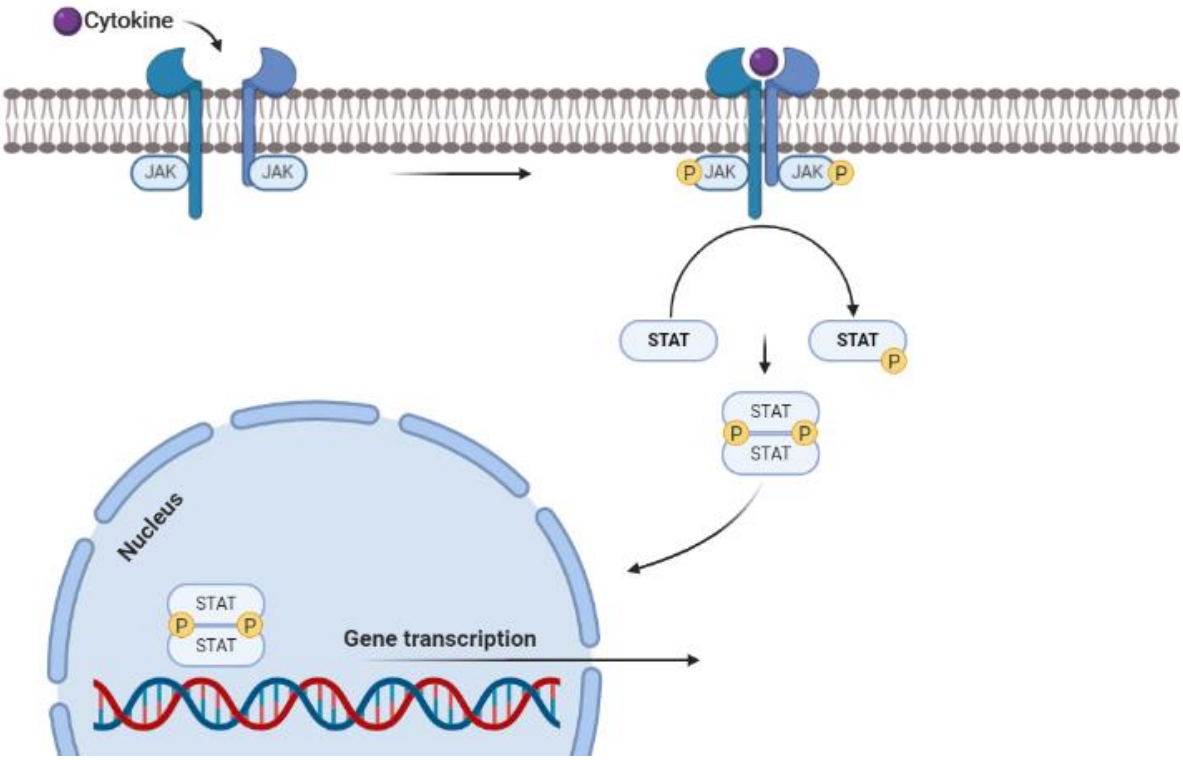


**Figure 4: The diagram of the JAK-STAT signaling pathway.** Cytokines first bind to the JAK-linked receptors, dimerising receptor subunits. This process closes together the subunits connected to JAKs. Thereby, kinases activate a series of phosphorylations that activate intracellular signaling, ultimately leading to the phosphorylation of STATs. Activated STATs dimerise and transfer to the nucleus, and then bind to DNA and regulate gene transcription.

### 1.9.3. The potential connection between the JAK-STAT pathway and HGPS

The previous research from our group found that various indicators related to the JAK-STAT signaling pathway create significant changes in HGPS patients. For example, intracellular ROS increases by over two times, and ATP production decreases by 25% [100]. Both autophagy and protease activities have different levels of reduction. The literature also shows that apoptosis increases by more than six times, and mitochondrial membrane potential increases by six

times. These results indicate that the JAK-STAT pathway function in HGPS is abnormal [101]. Since JAK-STAT inhibitors can effectively regulate the above indicators, the usage of JAK-STAT inhibitors could be a method to alleviate HGPS cellular homeostasis. Specifically, the use of JAK-STAT inhibitors can reduce the expression level of TNFa, thereby decreasing apoptosis. Similarly, overexpression of TNFa induces cells to produce large amounts of ROS and reduce ATP synthesis, and the use of JAK-STAT inhibitors can alleviate this change. The increase of STAT3 can inhibit the level of cell autophagy and produce a tendency to reduce the proteasome. The use of JAK-STAT inhibitors can well resist the above-mentioned adverse effects caused by excessive activation of STAT3. Therefore, JAK-STAT inhibitors can improve the health of HGPS cells by improving cellular homeostasis.

From a disease perspective, the JAK-STAT signaling pathway plays an essential role in the pathological process of four typical HGPS phenotypes: cardiovascular disease, lipodystrophy, arthritis and alopecia. The use of JAK-STAT inhibitors can also relieve these diseases. In cardiovascular diseases, STAT3 mediates the production of surface adhesion molecules like ICAM-1 and the generation of inflammatory cytokines such as CCL2 and IL-6 [102]. Therefore, the use of JAK-STAT inhibitors can effectively inhibit the phosphorylation of STAT3 and prevent atherosclerosis occurrence. In the synovium of an arthritis patient, TNFa, IL-6 and other cytokines play a vital role in the disease development, and the drug inflammation that inhibits JAK1, 2 and 3 has shown promising therapeutic effects [103]. In lipodystrophy, PPARG, IL-6, and TNFa are involved in critical regulatory processes to regulate the development and function of adipocytes. STAT3 can cause the loss of subcutaneous fat tissue under the stimulation of INFG [104]. Clinical trials have also shown that the use of JAK-STAT inhibitors can effectively alleviate lipodystrophy. Last, IFNG, IL-6 and TNFa can prevent healthy hair circulation and cause hair loss. The use of JAK-STAT inhibitors can prevent these cytokines from destroying the hair circulation process and stimulate the activation and proliferation of hair follicle stem cells to promote hair regeneration [105]. Therefore, since the JAK-STAT signaling pathway plays a principal role in the pathogenesis of the four main phenotypes of HGPS, this pathway is also likely to play an essential role in the pathogenesis of HGPS.

## 1.10. Current HGPS therapies

### 1.10.1. HGPS therapeutics in general

Based on the above-mentioned pathogenic mechanism for HGPS patients, a variety of drugs have been designed for different particular processes to alleviate HGPS: 1. Use genome editing techniques such as clustered, regularly interspaced, short palindromic repeats (CRISPR) to repair disease-causing mutations. 2. Prevent progerin mRNA production by using antisense oligonucleotides such as MG132 to inhibit pre-mRNA abnormal splicing. 3. Reduce the levels of isoprenylation and methylation of progerin by using farnesyl transferase inhibitors. 4. Activate cell autophagy by using rapamycin to cause progerin clearance. 5. Reduce the harmful downstream effects due to excessive aggregation of progerin by the reactivation of nuclear factor erythroid 2-related factor 2 (NRF2) [106].

### 1.10.2. The farnesyltransferase inhibitor (FTI) lonafarnib

Among these methods, the prelamin A isoprenylation and methylation inhibitor lonafarnib was the first treatment showing a positive effect under clinical practice.

As mentioned above, during the prelamin A maturation into lamin A, ZMPSTE24 removes the farnesylated carboxy terminus at the tail of prelamin A via identification of the cleavage site. However, due to the replacement of cytosine to thymine by gene mutation, ZMPSTE24 cannot cut the farnesyl group from prelamin A, resulting in the permanent farnesyl premature protein remaining anchored on the inner core membrane. When the progerin dimerises with wild-type lamins, the nuclear scaffold is negatively disrupted. A farnesyltransferase inhibitor (FTI) is a small molecule that can reversibly attach to the binding site of farnesyl transferase CAAX, so it can prevent the prelamin A farnesylation in HGPS cells. As a result, prelamin A does not gather on the nuclear rim to cause folds. This process can reduce the percentage of cells with deformed nuclei, thereby reducing the production and

toxicity of progerin and further significantly reducing nuclear blebbing [107].

The HGPS mouse model is a kind of knock-in mouse expressing non-farnesylated progerin (Lmna nHG/+). Both the HGPS mouse model and the ZMPSTE24-deficient mouse model share some common phenotypes, such as hair loss, micrognathia, osteolytic disease and osteoporosis, abnormal teeth, thinness and growth retardation. After utilizing the FTI treatment, the mouse model showed significant body weight gain at 20 weeks of age and showed increased body fat, indicating improved lipodystrophy. The mouse model also showed increased grip strength and bone integrity, indicating recovery from arthritis, effective relief of cardiovascular disease and extended lifespan, but only modestly [108].

After two years of lonafarnib treatment for HGPS patients, the results showed that HGPS children gained weight, improved vascular stiffness and reduced the prevalence of strokes and frequency of headaches. It also decreased arterial pulse wave velocity, increased bone rigidity, increased sensorineural hearing and bone mineral density and increased average lifespan by 1.6 years. Although FTI inhibits farnesyltransferases, the progerin can still be alternatively prenylated by geranylgeranyltransferase, which explains the limited helpful effects of FTI monotherapy [109]. Recently, a combination treatment of the co-substrate of farnesyltransferase and the precursor of geranylgeranyl pyrophosphate on ZMPSTE24−/− mice demonstrated positive effects on growth retardation, weight loss, lipodystrophy, hair loss and bone defects [110]. Importantly, this combination also prolonged the mice's lifespans. The clinical trial of this combination on 12 HGPS patients for 3.5 years of treatment exhibited several positive results, including weight gain and improvement of bone density with almost no side effects [111].

Although the use of FTI for HGPS has many of the above benefits, long-term use of FTI treatment can also cause serious side effects. For example, progeria mouse model results indicate that excessive aggregation of non-farnesylated prelamin A may cause lethal cardiomyopathy, anaemia, thrombocytopenia, myelosuppression and neutropenia [112].

### 1.10.3. The autophagy-activating drugs: rapamycin and sulforaphane

For a long time, autophagy has been considered to have a close relationship with degenerative disease and carcinogenesis but also to play an essential role in the cell protection of the heart, nerve, kidney and liver. Deepening of research has shown a negative correlation between autophagy and accelerated ageing. Activating the autophagy of fibroblasts in HGPS can promote the elimination of premature proteins, improve the morphological abnormalities of the nucleus, enhance histone methylation status and barrier-to-autointegration factors (BAF) and lamina-associated polypeptide 2 alpha (LAP2alpha) distribution patterns. Experimental results using rapamycin on the LMNA−/− mouse models show that this drug can improve heart and skeletal muscle function, enhance body weight and increase fat content by reversing the mammalian target of the rapamycin complex 1 (mTORC1) signal, thereby prolonging life. In clinical trials, the combined use of lonafarnib and the rapamycin derivative everolimus showed similar but more positive therapeutic effects than utilizing lonafarnib alone. However, it also showed the side effects of inhibiting fat production, myelosuppression and hyperlipidaemia [113].

Sulforaphane is an antioxidant derived from cruciferous vegetables such as broccoli, and it has been widely proven to have anti-cancer and anti-ageing effects. In an experiment treating HGPS fibroblasts, it showed an excellent ability to remove progerin by activating autophagy and further reverse the typical indicators of HPGS, such as ROS, ATP and the proteasome, by increasing the expression of proteasome system components and several heat-shock proteins and co-chaperones [100].

However, sulforaphane and lonafarnib's intermittent administration has a more apparent positive effect on the impact of saving HGPS cell homeostasis than using sulforaphane or lonafarnib alone.

### 1.10.4. Cholesterol biosynthesis pathway inhibitor: statins

Since most HGPS patients eventually die of atherosclerosis, statins, which inhibit of the cholesterol biosynthesis pathway, have recently become a choice for the treatment of HGPS patients. Statins can effectively reduce LDL cholesterol by inhibiting the production of β-hydroxy β-methylglutaryl-CoA (HMG-CoA) reductase, which performs a significant role in cholesterol production, thereby achieving the positive effect of alleviating cardiovascular disease. HMG-CoA reductase is a class of isoprenoid precursors and plays a vital role in the protein prenylation pathway to help lamin A mature. Bisphosphonate is a drug that can resist disease with enhanced bone resorption. It can reduce the synthesis of geranyl and farnesyl groups by inhibiting farnesyl pyrophosphate synthase. Combining the above two drugs in the HGPS mouse model effectively inhibited the farnesylation and geranylation of progerin and prelamin A [114].

At the same time, the weight, fat, hair loss and bone defects in HGPS mice were alleviated after administration, and the life span was also significantly extended. In subsequent clinical trials, a statin (pravastatin) and a bisphosphonate (zoledronic acid) were applied in combination with the FTI (lonafarnib) to treat HGPS patients. However, other than the increase in bone mineral density, the effectiveness was not significantly improved compared to the utilization of FTI alone, and the ability to protect from cardiovascular disease was not significantly different [115].

## 1.11. Baricitinib

### 1.11.1. Baricitinib in general

Although all of these studies have shown that FTI, rapamycin, sulforaphane, statins and bisphosphonates can reverse specific characteristics of HGPS, none can simultaneously relieve the four typical phenotypes of vascular disease, arthritis, lipodystrophy and alopecia.

Therefore, we propose that the JAK-STAT pathway also plays an essential role in the occurrence and development of HGPS. As a JAK-STAT inhibitor, baricitinib can alleviate the above four diseases at the same time; therefore, it could be a suitable candidate for the treatment of HGPS.

As an orally administered, potent, selective, reversible inhibitor of the JAK-STAT pathway, baricitinib (LY3009104, formerly INCB028050, the chemical formula is $C_{16}H_{17}N_7O_2S$, and the chemical structure is shown in Figure 5) has been applied in a variety of clinical trials. It has shown positive effects in clinical trials of atopic dermatitis, systemic lupus erythematosus, rheumatoid arthritis, alopecia areata and lipodystrophy. Baricitinib's $IC_{50}$ for JAK1, JAK2, JAK3, and TYK2 are 5.9 nM, 5.7 nM, > 400 nM, and 53 nM, respectively, showing an apparent selective inhibition of JAK1 and JAK2 [116].

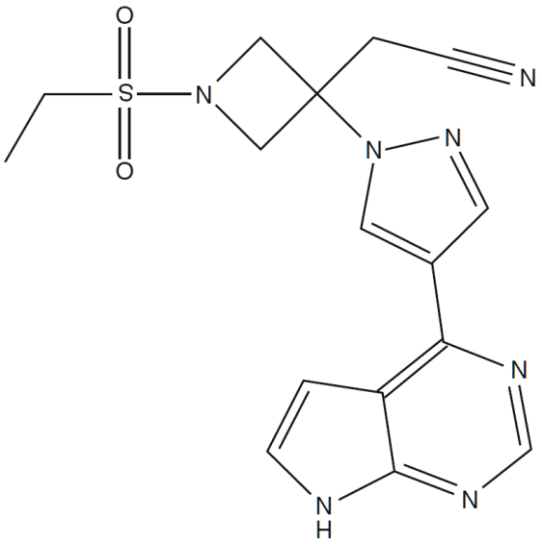


**Figure 5: The chemical structure of baricitinib.** Baricitinib is a potent and reversible inhibitor for the JAK-STAT pathway, especially for JAK1 and 2.

### 1.11.2. Baricitinib with four phenotypes

Among the many benefits of baricitinib, the first effect recognized by the market was its

excellent effect exhibited in RA. It can prevent the phosphorylation of STAT3 activated by IL-6 in T cells and subsequently inhibit the phosphorylated STAT3 from producing CCL2 and pathogenic cytokines like interleukin-22 (IL-22). In the process of using baricitinib to treat RA, a marked improvement in the disease can be seen as early as the first week of treatment. The structural joint damage can be significantly inhibited, and other related physical functions can be improved [117].

Baricitinib also showed an excellent therapeutic effect in the treatment of alopecia. In the preclinical study, the hair of alopecia model mice (C3H / HeJ) sufficiently recovered after 12 weeks of administration, which was significantly different from the control group. This result shows that CD8, NKG2D and effector memory T cells partially mediate alopecia through JAK signaling, and interferon signaling also plays a fundamental role in this process. Although the specific mechanism of baricitinib's action in alopecia has not been fully elucidated, the efficacy of the drug in the treatment of alopecia is worthy of further clinical research [118].

During the treatment of chronic atypical neutrophilic dermatosis with lipodystrophy (CANDLE), baricitinib also produced a preliminary response by inhibiting the JAK-STAT pathway within the clinical trials of 12 patients, except for one patient whose treatment effect was not noticeable. This patient developed debilitating avascular necrosis. Hence, he was withdrawn from the study, but the other 11 patients all showed a positive therapeutic effect. The average autoinflammatory diary score of these patients decreased significantly, and the symptoms of myositis and bone marrow immunosuppression improved. Specifically, platelets increased, and absolute lymphocyte counts and haemoglobin were enhanced. The treatment process can cause some common adverse reactions, such as upper respiratory tract infections and anaemia, but these adverse reactions can be successfully cured [119].

### 1.11.3. Baricitinib is more suitable for HGPS patients

As the JAK-STAT pathway is a hot topic in current research, various JAK or STAT inhibitors have been designed. Since our ultimate goal in this study is to find a JAK-STAT inhibitor that can be

used further in HGPS patients, we first narrowed the range to JAK-STAT inhibitors that have been approved by the FDA because their safety is more guaranteed. The JAK-STAT inhibitors that have been approved by the FDA are ruxolitinib, tofacitinib, oclacitinib, baricitinib and upadacitinib. A key indicator in our study, arthritis can be effectively inhibited by tofacitinib, baricitinib and upadacitinib to alleviate it in many aspects. However, for anti-alopecia, the efficacy of these drugs has made a distinct difference. Tofacitinib can help patients regenerate almost all of their hair back after six months of treatment, but all of the regrown hair is then lost after two months [120].

Similarly, ruxolitinib can regenerate 85% of the scalp hair and maintain it for 12 weeks after the administration's end before the hair falls out again. However, baricitinib can ultimately promote scalp regeneration. Therefore, baricitinib is one of the best candidates. $IC_{50}$ is the concentration of an inhibitor that reduces half of the response. The relevant $IC_{50}$ value of baricitinib (JAK1: 5.9 nM, JAK2: 5.7 nM, JAK3: > 400 nM, tyrosine kinase 2 (TYK2): 53 nM) is much lower than tofacitinib (JAK1: 112 nM, JAK2: 20 nM, JAK3: 1 nM, TYK2: - nM), showing that baricitinib is more efficient in inhibiting JAK. Therefore, we selected baricitinib as our model drug in this research [121].

Meanwhile, in terms of drug safety, patients with advance infections or hematologic, hepatic and renal disorders are more likely to have side effects during the baricitinib treatment than patients without those disorders. Typical adverse effects include an increase in the incidence of herpes zoster and a decrease in the number of neutrophils and other phagocytic cells with an increasing dose of baricitinib, which, in turn, triggers neutropenia and lymphocytopenia. Additionally, the use of baricitinib inhibits the phosphorylation of JAK2 and then prevents the signal of erythropoietin, which in turn causes anaemia. During the treatment period, although the levels of HDL, LDL, total serum cholesterol and triglycerides increased, the average HDL to LDL ratio did not change significantly, and it did not produce significant related side effects [122].

# 2. Aim of the Thesis

Hutchinson–Gilford progeria syndrome (HGPS, OMIM 176670) is a rare, disastrous paediatric disease distinguished by severe premature ageing and early death, without any existing cure [123]. HGPS patients exhibit clinical features similar to physiological ageing, including cardiovascular diseases, lipodystrophy, hair loss, progressive contracture and stiffness of joints and osteoporosis, leading to shortened life spans and early death at an average age of 14.7 years [124]. We focused on the four typically recognized conditions, namely vascular disease, arthritis, lipodystrophy and alopecia. These pathologies not only develop simultaneously in HGPS but also other progeroid syndromes, such as mandibuloacral dysplasia (MAD), restrictive dermopathy (RD), and Malouf syndrome [125,126]. This dissertation's main objective is to find a new therapeutic strategy for HGPS children based on the fact that they are suffering from these four age-related phenotypes at the same time.

**Aim 1: Identification of the signaling pathway that is deregulated in vascular disease, lipodystrophy, alopecia, and arthritis.**

To achieve this goal, we first used data mining to examine whether these four conditions might share joint defective molecular mechanisms. We conducted a text mining research of scientific literature and databases to distinguish genes altered in each of these four distinct pathologies. Seventeen unique genes were classified as changed in all four pathologies by this text mining approach. Second, we applied the several databases and bioinformatics to analyze if most of these 17 entities were interconnected and therefore belonged to converging signaling pathways. The results showed that 14 out of these 17 genes are known targets of Janus kinase (JAK)-signal transducer and activator of transcription (STAT) signaling.

**Aim 2: Identification of the JAK-STAT signaling altered in HGPS and normal cells during the replicative senescence.**

To achieve this goal, we first established an in vitro, cell-based ageing model. In this model, we no longer used the cell passage as a fixed indicator for comparison as the HGPS cells are

in a completely different ageing state than the control cell lines at the same passage because HGPS cells age faster. We were the first group in the progeria area to use the same senescence index as a feature to compare the state of the cells. We also used the other characteristics, including cell cycle, p21 and progerin level, to corroborate this method's correctness. Subsequently, we examined the expression of these 17 genes during the replicative senescence in HGPS and control cells. Based on this result, we found that 14 of the 17 genes were encoding pro-inflammatory factors and targets of the JAK-STAT signaling, and they all produced corresponding changes. Therefore, we further used Western blot to measure the expression of JAK1, JAK2, STAT1, STAT3, p-STAT1 and p-STAT3. Ultimately, our results indicated that the JAK1/2-STAT1/3 pathway is over-activated in premature cellular ageing.

**Aim 3: Correction of the JAK-STAT signaling pathway using baricitinib to delay senescence and rebalance cell homeostasis in control and HGPS cells.**

In the process of achieving this goal, we chose baricitinib to correct the JAK-STAT signaling pathway. Baricitinib is a JAK1/2 inhibitor approved by the Food and Drug Administration (FDA) and has shown significant potency in the treatment of arthritis, alopecia and lipodystrophy. The results showed that baricitinib treatment could significantly inhibit the JAK1/2-STAT1/3 signaling pathway, decrease pro-inflammatory factors, delay senescence and rebalance cell homeostasis in both senescing control and HGPS cells.

**Aim 4: Validation of baricitinib therapy's effects to delay senescence and rebalance cell homeostasis on DNA damage senescence caused by etoposide.**

To accomplish this goal, we established a senescence model caused by DNA damage [127]. Compared with the mock group, the etoposide administration significantly enhanced the cell senescence percentage, while baricitinib effectively slowed down this process. Similar to replicate senescence, the JAK1/2-STAT1/3 signaling pathway in the DNA damage senescence group was also significantly activated, increasingly producing pro-inflammatory factors. The appearance of baricitinib can alleviate the above process. Consequently, baricitinib treatment can rebalance the homeostasis of both control and HGPS cell senescence caused by DNA damage.

# 3. Materials and Methods

## 3.1. Materials

We applied the following items for the experimental procedures and cell culture.

### 3.1.1. Equipment

The equipment we applied are shown in Table 2.

**Table 2: Technical Equipment**

| Device | Manufacturer |
|---|---|
| Axio Imager D2 | Zeiss |
| Axiovert 40CFL | Zeiss |
| Balance Cp 4202 S | Sartorius |
| Biofuge fresco | Thermo Scientific |
| Certomat BS-1 | Sartorius |
| Chemi-Doc MP Imageing System | BioRad |
| FLUOstar Omega | BMG Labtech |
| HeraSafe | Thermo Scientific |
| ICycler PCR System | BioRad |
| Incubator | Binder |
| InoLab pH 720 | WTW |
| Trans-Blot® TurboT$^{M}$ Transfer System | BioRad |
| Multifuge 3S-R+ | Thermo Scientific |
| Nano Drop Spectrometer ND-1000 | PeqLab |
| StepOnePlus™ Real-Time PCR System | Applied Biosystems |

| | |
|---|---|
| Rocking platform | VWR |
| Thermomixer comfort | Eppendorf |
| Universal Hood II | BioRad |
| Vortex Genie-2 | VWR |

### 3.1.2. Consumables

The consumables we used are presented in Table 3.

**Table 3: Consumables**

| Name | Manufacturer |
|---|---|
| 3.5, 6, 10 cm tissue culture dish | Falcon |
| 4-20 % Mini-Protean TGX Precast Gel | BioRad |
| Eppendorf tubes (1.5, 2 ml) | Eppendorf |
| IPG strips | GE Healthcare |
| Luminunc 96- well plates white | Thermo Scientific |
| Membrane high-bond ECL nitrocellulose | Amersham |
| Microscope slides superfrost plus | Thermo Scientific |
| Mini Transblot filterpaper | BioRad |
| Polypropylen conical tubes (15, 50 ml) | Falcon |
| Serological pipets (1, 2, 5, 10, 25 ml) | Sarstedt |
| Superslip coverslips | Fisher Scientific |
| Tip one pipet tips (10, 20, 200, 1000 µL) | Starlab |
| Zip-tip C18 | Millipore |

### 3.1.3. Reagents

The reagents we utilized are displayed in Table 4.

**Table 4: Reagents**

| Name | Manufacturer |
|---|---|
| 0.25 % Trypsin EDTA | Invitrogen |
| 2-Mercaptoethanol | BioRad |
| Agarose ultrapure | BioRad |
| Baricitinib | Absource Diagnostics GmbH |
| Dapi Vectashield mounting medium | Vector Inc. |
| DEPC treated water | Invitrogen |
| Dimethylformamide | Merck |
| DMEM (1x) GlutaMax 4.5 g/l D-glucose+pyruvate | Gibco |
| Dodecyl sulfate sodium salt (SDS) | Merck |
| Ethanol | Roth |
| Ethidium bromide | Sigma Aldrich |
| Fetal bovine serum (FBS) | Invitrogen |
| Forskolin | Sigma Aldrich |
| D-(+)-Galactose | Sigma Aldrich |
| Gentamycin (10 mg/ml) | Invitrogen |
| Glutamine (200 mM) | Invitrogen |
| Glycine | Sigma Aldrich |
| 2x Laemmli Buffer | BioRad |
| Magnesium chloride | Sigma Aldrich |
| Methanol | Roth |
| Modified porcine trypsin protease | Promega |

| | |
|---|---|
| Penicillin-Streptomycine (5,000 U/ml) | Invitrogen |
| Phosphate-buffered saline (PBS) | Invitrogen |
| Ponceau S | Sigma Aldrich |
| Potassium chloride | Fisher Scientific |
| Precision Plus protein standards (dual color) | BioRad |
| Sodium chloride | Merck |
| Sodium hydroxide | Merck |
| SYBR Select Master Mix | Applied Biosystems |
| Sucrose | Sigma Aldrich |
| Triton X-100 | Sigma Aldrich |
| Trizma base | Sigma Aldrich |
| Tween 20 | Sigma Aldrich |

### 3.1.4. Kits

The kits we worked with are exhibited in Table 5.

**Table 5: Kits**

| Name | Manufacturer |
|---|---|
| 20S Proteasome Assay | Cayman Chemicals |
| Autophagy/Cytotoxicity Dual Staining | Cayman Chemicals |
| CellTiter-Glo Luminescent Cell Viability Assay | Promega |
| CellTox Green Cytotoxicity Assay | Promega |
| Clarity Western ECL substrate | BioRad |
| DCFDA - Cellular ROS Detection Assay | Abcam |

| | |
|---|---|
| Muse Cell Cycle Assay kit | MerckMillipore |
| Omniscript RT Kit | Qiagen |
| QIAshredder Kit | Qiagen |

### 3.1.5. Antibodies

The primary antibodies we employed are displayed in Table 6.

**Table 6: Primary antibodies**

| Antibody | Species | WB | IF | Supplier | Order Number |
|---|---|---|---|---|---|
| Anti-β-actin | Mouse | 1:5000 | - | Sigma-Aldrich | A1978 |
| Anti-JAK1 | Rabbit | 1:1000 | - | Cell Signaling | 3332 |
| Anti-JAK2 | Rabbit | 1:1000 | - | Cell Signaling | 3230 |
| Anti-lamin A/C | Rabbit | 1:10000 | - | Santa Cruz | 20681 |
| Anti-lamin A/C | Mouse | - | 1:100 | Invitrogen | 3-1000 |
| Anti-P21 | Rabbit | 1:1000 | | Invitrogen | 5-14949 |
| anti-progerin | Rabbit | 0.1µg/mL | 1µg/mL | Home made | - |
| Anti-P-STAT1 | Rabbit | 1:1000 | - | Cell Signaling | 9167 |
| Anti-P-STAT3 | Rabbit | 1:1000 | - | Cell Signaling | 9145 |
| Anti-STAT1 | Rabbit | 1:1000 | - | Cell Signaling | 14994 |
| Anti-STAT3 | Mouse | 1:1000 | - | Cell Signaling | 9139 |

The secondary antibodies we employed are displayed in Table 7.

**Table 7: Secondary antibodies**

| Antibody | Species | Dilution | Supplier | Order |
|---|---|---|---|---|

| | | | | Number |
|---|---|---|---|---|
| α -mouse-Alexa Fluor 488 | donkey | 1:750 | Invitrogen | A21202 |
| α -rabbit- Alexa Fluor 555 | donkey | 1:750 | Invitrogen | A31572 |
| α -mouse-HRP | goat | 1:5000 | Jackson ImmunoResearch | 115-035-003 |
| α -rabbit-HRP | goat | 1:5000 | Jackson ImmunoResearch | 111-035-003 |

### 3.1.6. DNA oligonucleotides

The DNA oligonucleotides we used for the real-time, quantitative PCR analysis are presented in Table 8.

**Table 8: DNA oligonucleotides for real-time, quantitative PCR**

| Primer | Target Gene | Product size(bp) | Melting Temp | Info |
|---|---|---|---|---|
| FW:5'-AATGGCGAGATCCCCTTGA-3' | JAK1 | 66 | 62.9℃ | [128] |
| REV:5'-GCACCGGCTTTCATAGAATCTCT-3' | | | 63.0℃ | |
| FW:5'-TGATTTTGTGCACGGATGGA-3' | JAK2 | 72 | 63.4℃ | [128] |
| REV:5'-ACTGCCATCCCAAGACATTCTT-3' | | | 62.1℃ | |
| FW:5'-GCCTGGAGTGGCATGAGAA-3' | JAK3 | 55 | 62.4℃ | [129] |
| REV:5'-CCCCGGTAAATCTTGGTGAA-3' | | | 62.0℃ | |
| FW:5'-GGGACCGTGGGCAGGAGCTA-3' | TYK2 | 116 | 69.0℃ | [128] |
| REV:5'-GTGCGTGTGGGAGACCTGGC-3' | | | 68.7℃ | |
| FW:5'-TTCAGAGCTCGTTTGTGGTG-3' | STAT | 419 | 60.0℃ | [130] |
| REV:5'-AGAGGTCGTCTCGAGGTCAA-3' | 1 | | 60.0℃ | |
| FW:5'-CCAAGGCTACCATGCTATTC-3' | STAT | 336 | 57.3℃ | [131] |

| | | | | |
|---|---|---|---|---|
| REV:5’-GCTGGTCTTTCAGTTGGCTG-3’ | 2 | | 61.0℃ | |
| FW:5’-CAGGAGGGCAGTTTGAGTCC-3’ | STAT | 218 | 62.1℃ | [132] |
| REV:5’-CAAAGATAGCAGAAGTAGGAGA-3’ | 3 | | 53.4℃ | |
| FW:5’-CCTGACATTCCCAAAGACAAAGC-3’ | STAT | 203 | 64.2℃ | [133] |
| REV:5’-TCTCTCAACACCGCATACACAC-3’ | 4 | | 61.2℃ | |
| FW:5’-TTACTGAAGATCAAGCTGGGG-3’ | STAT | 104 | 59.3℃ | [134] |
| REV:5’-TCATTGTACAGAATGTGCCGG-3’ | 5A | | 61.9℃ | |
| FW:5’-CATTTTCCCATTGAGGTGCG-3’ | STAT | 103 | 63.6℃ | [134] |
| REV:5’-GGGTGGCCTTAATGTTCTCC-3’ | 5B | | 60.7℃ | |
| FW:5’-CCTTGGAGAACAGCATTCCTGG-3’ | STAT | 116 | 65.3℃ | [135] |
| REV:5’-GCACTTCTCCTCTGTGACAGAC-3’ | 6 | | 59.1℃ | |
| FW:5’-GAGCCAGGAGTGGACTATGTGTA-3’ | C3 | 85 | 60.6℃ | [136] |
| REV:5’-CAATGGCCATGATGTACTCG-3’ | | | 59.9℃ | |
| FW:5’-AGCATGAAAGTCTCTGCCGC-3’ | CCL2 | 93 | 62.9℃ | [137] |
| REV:5’-GGCATTGATTGCATCTGGCTG-3’ | | | 66.0℃ | |
| FW:5’-CTTTTGGCCAGACAGACATG-3’ | CRP | 130 | 59.3℃ | [138] |
| REV:5’-GTGTAGAAGTGGAGGCACA-3’ | | | 54.5℃ | |
| FW:5’-CTGGCCGTGGCTCTCTTG-3’ | CXC | 69 | 63.2℃ | [137] |
| REV:5’-CCTTGGCAAAACTGCACCTT-3’ | L8 | | 62.5℃ | |
| FW:5’-TGAAGGACATGGCTTAGAAGTG-3’ | FAS | 118 | 59.4℃ | [139] |
| REV:5’-GGTGCAAGGGTCACAGTGTT-3’ | | | 61.0℃ | |
| FW:5’-ACTGCGTTCCTGCTCAACATC-3’ | HMO | 75 | 62.7℃ | [140] |
| REV:5’-GCTCTGGTCCTTGGTGTCATG-3’ | X1 | | 63.0℃ | |
| FW:5’-ATGCCCAGACATCTGTGTCC-3’ | ICAM | 112 | 61.0℃ | [141] |
| REV:5’-GGGGTCTCTATGCCCAACAA-3’ | -1 | | 62.2℃ | |
| FW:5’-GTCCAACGCAAAGCAATACATG-3’ | IFN- | 81 | 62.6℃ | [142] |
| REV:5’-CCTTTTTCGCTTCCCTGTTTTAG-3’ | G | | 62.4℃ | |

| | | | | |
|---|---|---|---|---|
| FW:5’-GGCACAATTACTGCTCCAAAGAC-3’ | IGF-1 | 121 | 62.2℃ | [143] |
| REV:5’-CAAGGCCCTTTCTCCCCAC-3’ | | | 64.1℃ | |
| FW:5’-ATCGCTTCCTCTCGCAACAA-3’ | IL-18 | 64 | 63.3℃ | [144] |
| REV:5’-CTTCTACTGGTTCAGCAGCCATCT-3’ | | | 63.3℃ | |
| FW:5’-AACAGCCTCACAGAGCAGAAGAC-3’ | IL-4 | 74 | 62.4℃ | [142] |
| REV:5’-GTGTTCTTGGAGGCAGCAAAG-3’ | | | 62.2℃ | |
| FW:5’-GGTACATCCTCGACGGCATCT-3’ | IL-6 | 81 | 63.6℃ | [145] |
| REV:5’-GTGCCTCTTTGCTGCTTTCAC-3’ | | | 62.4℃ | |
| FW:5’-TCCCCTCTTGACCCATCTC-3’ | LEP | 110 | 60.0℃ | [146] |
| REV:5’-GGGAACCTTGTTCTGGTCAT-3’ | | | 58.8℃ | |
| FW:5’-TGATTTTGTGCACGGATGGA-3’ | PPA | 105 | 55.4℃ | [147] |
| REV:5’-ACTGCCATCCCAAGACATTCTT-3’ | RG | | 54.6℃ | |
| FW:5’-CCCAGCATCTGCAAAGCTC-3’ | TGF | 101 | 62.1℃ | [148] |
| REV:5’-GTCAATGTACAGCTGCCGCA-3’ | B1 | | 63.4℃ | |
| FW:5’-TCAGATCATCTTCTCGAACCCC-3’ | TNFa | 134 | 62.7℃ | [149] |
| REV:5’-ATCTCTCAGCTCCACGCCAT-3’ | | | 62.3℃ | |
| FW:5’-CATGAGAGGGGAGTATGATG-3’ | TRAF | 181 | 55.4℃ | [150] |
| REV:5’-GAAGAAGAGTGGGCATCCAC-3’ | 1 | | 59.7℃ | |
| FW:5’-CTCTGCTCCTCCTGTTCGAC-3’ | GAP | 144 | 60.1℃ | [151] |
| REV:5’-TTAAAAGCAGCCCTGGTGAC-3’ | DH | | 60.2℃ | |

### 3.1.7. Cell culture media

We prepared the subsequent media under sterile circumstances according to the recipes below.

**Table 9: Cell culture medium.** Fibroblast growth medium containing high glucose.

| Fibroblast growth medium containing high glucose | |
|---|---|
| DMEM (high glucose) | 500 mL |
| FBS | 75 mL (15 %) |
| Gentamicin | 2.5 mL (0.5 %) |
| Penicillin-Streptomycin | 5 mL (1 %) |
| Glutamine | 5 mL (1 %) |

**Table 10: Cell culture medium for baricitinib treatment.** Fibroblast growth medium containing high glucose and baricitinib.

| Fibroblast growth medium containing high glucose and Baricitinib (X µM) | |
|---|---|
| Baricitinib (10 mM) | 50 X µL |
| DMEM (high glucose) | 500 mL |
| FBS | 75 mL (15 %) |
| Gentamicin | 2.5 mL (0.5 %) |
| Penicillin-Streptomycin | 5 mL (1 %) |
| Glutamine | 5 mL (1 %) |

**Table 11: Cell culture freezing medium.** The cell culture freezing medium was a complete cryopreservation medium for mammalian cell cultures.

| Freezing medium | |
|---|---|
| FBS | 9 mL |
| DMSO | 1 mL |

### 3.1.8. Buffers

**Table 12: 10x TBS buffer.** 10x TBS buffer was used to prepare TBS or TBS-Tween.

| 10x TBS buffer | |
|---|---|
| Trizma | 60.55g |
| Sodium chloride | 87.66 g |
| Milli-Q water | Add 1 L |

**Table 13: TBS buffer**

| 1x TBS buffer | |
|---|---|
| 10x TBS buffer | 100 mL |
| Milli-Q water | Add 1 L |

**Table 14: 1x TBS-T or 1x PBS-T buffer**

| 1x TBS-T or 1x PBS-T buffer | |
|---|---|
| 10x TBS buffer/ 10x PBS | 100 mL |
| Milli-Q water | Add 1 L |
| Tween 20 | 500 µL |

**Table 15: Blocking buffer for immunofluorescence**

| Blocking buffer for immunofluorescence | |
|---|---|
| FBS | 7.5 mL (15 %) |
| Tween | 20 150 µL |
| PBS | Add 50 mL |

**Table 16: Lysis buffer for nuclei preparation.** The Lysis buffer was used for nuclei preparation to make the Western blot samples.

| Lysis buffer for nuclei preparation | |
|---|---|
| FBS | 7.5 mL (15 %) |
| Tween | 20 150 µL |

| | |
|---|---|
| PBS | Add 50 mL |

**Table 17: 10x SDS gel running buffer.** A 10x SDS gel running buffer was diluted and then used for the Western blot research.

| 10x SDS gel running buffer | |
|---|---|
| Glycine | 144 g (1.92 M) |
| Trizma | 30 g (0.248 M) |
| SDS | 10 g (1 %) |
| Milli-Q water | Add 1 L |

**Table 18: Western blot transfer buffer.** A western blot transfer buffer was used in the transfer process of the Western blot.

| Western blot transfer buffer | |
|---|---|
| Glycine | 11.3 g (150 mM) |
| Trizma | 2.42 g (20 mM) |
| MeOH | 200 mL (20 %) |
| SDS | 1 g (0.1 %) |
| Milli-Q water | Add 1 L |

**Table 19: Sample Laemmli buffer.** A sample Laemmli buffer was used in the sample preparation process of the Western blot.

| Sample Laemmli buffer | |
|---|---|
| 2x Laemmli buffer | 950 µL |
| 2-Mercaptoethanol | 50 µL |
| Proteinase inhibitor cocktail | 10 µL |
| 200 mM PMSF | 5 µL |

**Table 20: Blocking buffer for Western blot.**

| Blocking buffer for western blot | |
|---|---|
| Milk powder (non-fat) | 0.6 g |
| Tween-20 | 150 µL |
| PBS buffer | Add 50 mL |

## 3.2. Text mining study

As the introduction shows, these four diseases have many associated genes. The proteins expressed by these genes affect the occurrence and development of the disease in varying degrees. To better comprehensively collect all relevant genes, we designed a semi-automated and straightforward method to mine the *PubMed* database. *PubMed* is a free search engine mainly involved in life sciences and biomedicine. So far, *PubMed* has collected more than 30 million scientific documents, covering most papers since 1966. The earliest article even dates back to 1809.

The usage of *PubMed* is also effortless, and the website can be logged into directly through https://www.ncbi.nlm.nih.gov/. When we needed to query the relationship between a specific gene and a particular disease, we only needed to enter both into the search box and see if any paper reported the two words simultaneously. For example, when entering IL-6 and alopecia into the search box at the same time, there were 45 items and specifically related documents. In this study, when the result was 0, it meant that the particular gene and disease must not be related. However, when the item number was higher than 0, it did not necessarily mean that the gene and disease had a special relationship. A follow-up validation was also required. Since the latest version of the HGNC Human Genome Database from 1 January 2019 lists a total of 19,194 protein-coding genes, manually inputting so many genes plus diseases into the search box is not only time-consuming but also error-prone [152]. Since we only

needed the item data in the first round of screening, we did not need other specific details from papers. We used the R language to help this process. For example, using the search query function in RISmed can quickly provide the item value of two keywords, including the gene and the disease. The RISmed package (https://cran.r-project.org/web/packages/RISmed/index.html) allowed us to easily extract the bibliographic content of the National Center for Biotechnology Information (NCBI) database [153]. Computers are good at repetitive operations; using the R language, we repeated this operation to get all the matching genes and item values after the disease.

Results were removed when the item value equaled 0 using Excel, so the remaining genes were more likely to be connected with the disease. We then used the 'pubmed.mineR' package (https://cran.r-project.org/web/packages/pubmed.mineR/) to download the corresponding abstract [154]. The newly created database took the abstracts of all papers that contained one of these four diseases and the specific genes associated with the disease. We assumed that the main results of the article are usually placed in the abstract; therefore, analyzing the abstract can significantly reduce the difficulty of the data search. Some papers in the bioinformatics field focus on algorithms to perform semantic recognition to achieve the purpose of reading literature efficiently. However, in a sentence such as, 'In this article, we detected the expression of three genes, A, B and C, in the disease, but only the C gene performed a statistical difference, while the A and B genes did not change significantly', the A and B genes appear, but these two genes are not related to the disease. Another example is, 'It is well known that A gene has always been one of the main causes of X disease. In this article, we will mainly study whether the A gene also plays an important role in Y disease.' Although the A gene and Y disease appear in the same sentence, there is not necessarily an obvious connection between them.

Biological information researchers often need to analyze many diseases and genetic models, so accuracy is not the most important thing. In our research, exactitude was paramount, even though we used a lot of bioinformatics to speed up our screening. In pursuit of correctness, we detected each document manually before summarizing and listing all genes related to

various diseases.

## 3.3. Identification of the signaling pathways

Genes were listed in an Excel table to determine the list of genes simultaneously associated with all four conditions after discovering the genes related to each of the four diseases. At first, we listed the genes related to the four phenotypes in an Excel table. It depicted lipodystrophy in column A, alopecia in column B, vascular disease in column C and arthritis in column D. To determine whether the gene in column A also existed in column B, we used the Excel VLOOKUP function, which can find and retrieve data in specific columns. For example, we put '= VLOOKUP (A2, B: B, 1, FALSE)' in the free column F to extract genes shared in both lipodystrophy and alopecia. If the gene involved in lipodystrophy disorders in column A2 also appeared in column B, the result would be the name of the gene. Otherwise, #N/A would be displayed. By simply replicating this process, all genes related to lipodystrophy and alopecia could be obtained.

Next, the genes associated with two phenotypes at the same time could also be distinguished. We used the VLOOKUP function again by applying '= VLOOKUP (F2, C: C, 1, FALSE)' to simultaneously identify genes shared with lipodystrophy, alopecia and vascular disease. F2 represents the genes that co-occur with lipodystrophy and alopecia, and column C contains all of the genes related to vascular diseases. Similarly, we identified genes involved in three different genes next. Last, the VLOOKUP function was applied for the last time to classify genes involved in lipodystrophy, alopecia and vascular disease that also appeared in the arthritis column. Excel quickly summarized the number of genes in each column.

The visualization of overlapping datasets is an increasingly important part of showing the relationship between genes and phenotypes. We depicted a Venn diagram to envision the results through R's ‘VennDiagram’ package. The instructions about the VennDiagram package

use are at https://cran.r-project.org/web/packages/VennDiagram/ [155]. The overlapping part of the Venn diagram showed the genes we needed to find because these genes were related to all four diseases at the same time.

## 3.4. STRING analysis

Since 17 critical genes related to these four diseases were discovered, and most of them were related to chronic inflammation and functionally related to each other, we developed a protein–protein communication network using STRING analysis. STRING (a search tool for retrieving interacting genes/proteins) is a classic biological database and network resource that can check known and predicted protein–protein interactions [156]. The STRING database contains numerous sources, including experimental data, computational prediction methods and public text sets. To have a system-level understanding of the protein–protein interaction network, we specifically used the STRING analysis website (https://string-db.org/). After logging into the website, we selected the multiple proteins section then typed the names of the 17 genes into the 'Protein Name' blank. Next, we chose Homo sapiens as the organism to continue the network.

## 3.5. Identification of the signaling pathway

After confirming that these 17 essential genes were closely connected, we examined the regulators and targets of those corresponding proteins to determine whether a particular signaling pathway regulated most of them. We used the following databases to address this question: TRRUST version 2 (http://www.grnpedia.org/trrust/) [157], TfactS (http://www.tfacts.org/) [158] and Regulatory Circuits (http://regulatorycircuits.org/) [159].

Humans-TRRUST (Transcription Regulation Relationship Revealed by Sentence-Based Text Mining) is a reference transcription factor–target interaction database formed by sentence-based text mining and subsequent manual curation. Similar to TRRUST, TfactS is also a website dedicated to predicting the regulation of transcription factors based on the up- and down-regulated gene lists generated by transcriptomics experiments. However, the regulatory circuits are more focused on mapping disturbed molecular circuits that underlie complex diseases. The website covers nearly 400 human cell types and tissue-specific gene regulation networks.

After collecting and summarizing all the data about regulators and targets from these websites, we curated all reference materials and data. The results displayed that the nuclear factor kappa-light-chain-enhancer of activated B-cells (NF-κB) and JAK-STAT pathways were highly related to these 17 essential genes. NF-κB has already been studied for HGPS, and there was no research about JAK-STAT in HGPS. Therefore, we selected the JAK-STAT pathway as the main pathway for research, and then we established again the gene list regulated by the JAK-STAT pathway using the database mentioned above. We eliminated aliases and duplications using Excel.

## 3.6. Cell culture and drug treatments

The HGPS dermal fibroblasts used in this study were obtained from the Progeria Research Foundation Cell and Tissue Bank (http://www.progeriaresearch.org). Four different fibroblast strains initially derived from HGPS patients were used: HGADFN003 (2-year-old male), HGADFN127 (3-year-old female), HGADFN164 (4-year-old female) and HGADFN188 (2-year-old female). Young skin fibroblasts for controls were obtained from Coriell Medical Research Institute (Camden, New Jersey). The following five different control strains were used: GM01651C (13-year-old female), GM01652C (11-year-old female), GM01582B (11-year-old

female), GM00323B (11-year-old male) and GM03349C (10-year-old male).

All controls and HGPS fibroblasts were cultured in a 10 cm cell culture dish in the same incubator's fibroblast growth medium. Since fibroblasts need an appropriate pH (7.0–7.7) to maintain cell function, 5% gaseous carbon dioxide and carbonate-based cell culture mediums were used cooperatively to create this condition. Therefore, we placed the cell culture dishes in a humidified incubator with 5% carbon dioxide ($CO_2$) at 37°C. All cell-related operations were performed using sterile techniques. After eight hours, the cells were attached to the Petri dish, and the medium was changed every other day. During growth, cells were passaged by splitting to maintain the logarithmic growth phase until reaching 80% confluence to avoid contact inhibition. To divide the cells, after removing the old medium, the cells were washed with phosphate-buffered saline (PBS), and then 1.5 mL of 0.25% trypsin was added to the cells and incubated for two to three minutes. Once the cells were rounded up, they would rise and float under the microscope, and 6.5 mL of fresh medium was added to the floating cells to inactivate the trypsin. The cells were then centrifuged at 1000 rpm for five minutes in a clinical centrifuge. After centrifugation, the medium was removed, and the cells were seeded in 8 mL of fibroblast growth medium at a suitable concentration according to research needs.

According to the instructions from Absource Diagnostics GmbH, baricitinib was prepared in dimethyl sulfoxide (DMSO) to store at −20 °C. For the experiments related to drug evaluation, the drug-containing mediums were freshly made before each treatment by diluting baricitinib into the culture medium to produce the corresponding concentration (mainly 1 μM). To avoid the interference by DMSO, the mock-treated group was cultured in parallel with the medium containing precisely the same amount of DMSO.

For etoposide treatment, cells were treated with or without 1 μM baricitinib for two days to inhibit the JAK-STAT pathway. Then, three different mediums (etoposide−/baricitinib−, etoposide+/baricitinib−, etoposide+/baricitinib+) were added to the corresponding groups for six days. The medium was refreshed every two days, and the DMSO concentration was adjusted to be equal in different groups. Next, the cells were cultured with or without

baricitinib under specified conditions for four days.

## 3.7. Determination of cumulative population doubling

Cell membrane-permeable DNA stains (such as Hoechst 33258 and Hoechst 33342) can penetrate the cell membrane and bind adenine and thymine in the DNA to stain all cells with a nucleus. Since debris and non-nucleated cells cannot be stained, the total number of cells, including living cells and non-viable cells, can be determined [160]. Other dyes (such as propidium iodide) only stain cells that are damaged, about to die or dead. Although the Muse™ Count and Viability Assay may not use the same reagents internally, combining two reagents with the same function can distinguish dead cells, dying cells or non-nucleated cells from live cells. Therefore, the accurate number of cells can be obtained.

Cumulative population doubling (CPD) is a standard method for tracking the growth status of HGPS cells. Cells were seeded in triplicate at a density of $1.5 \times 10^5$ cells per 10 cm dish and counted every four days.

We used the following formula to determine the doubling of the total population after measuring the cell number:

n = 3.32 (log cells harvested − log cells seeded) + x,

Where n = the final CPD number at the end of a given subculture and x = the former CPD as described previously [100].

## 3.8. Senescence-associated β-galactosidase assay

After healthy cells divide actively in a cell culture many times, they enter an irreversible growth stagnation stage called replication senescence. The morphology of senescent cells

can be manifested as cell enlargement and flattening, but it not accurate enough to distinguish the senescent cells. β-galactosidase, like p16Ink4A, is an ideal cell ageing biomarker that has been proposed by Dimri since 1995. He found that the cleavage of the chromogenic substrate X-gal by galactosidase can produce detectable blue stains. When cells age, the expression of endogenous β-galactosidase increases sharply and then accumulates in the lysosome. Therefore, β-galactosidase activity at a pH of 6.0 can be regarded as an essential feature of senescent cells [161].

According to the senescence-associated beta-galactosidase (SA-β-gal) senescence staining kit, (CS0030-1KT, Sigma-Aldrich, St. Louis, MO, USA) the medium was first removed from the cells, and then the cells were washed twice with PBS and then fixed with fixing buffer. After incubation with the fixation buffer for six to seven minutes, the cells were rinsed three times with PBS and then incubated with freshly prepared staining mixture for 12 hours at 37°C without $CO_2$. During this incubation, the plate needed to be sealed to prevent drying and $CO_2$ that may change pH. We used Image J's Cell Counter plugin to count blue cells and total cells (including staining and non-staining cells). To obtain an accurate percentage of senescent cells, we counted 1000 cells in each passage for each sample three times.

## 3.9. Cell cytotoxicity

Cell cytotoxicity remains one of the most critical indicators for evaluating the ability of drugs to kill living cells. Before starting drug treatment, cytotoxicity is usually required to obtain an appropriate therapeutic concentration. Drug-induced cytotoxic mechanisms can range from cell membrane disintegration and protein synthesis restriction to the irreversible binding to receptors, leading to necrosis (unexpected cell death) or apoptosis (programmed cell death) [162].

Therefore, membrane integrity has become the most apparent indicator for identifying

whether a cultured cell is alive or dead because non-viable cells lose membrane integrity and allow an impermeable molecular transfer. The CellTox™ Green Cytotoxicity Assay Kit (Promega, Madison, WI, USA) counts the non-permeable nucleic acid binding dyes that accumulate in dead cells in the culture so that fluorescence signals can be detected by a microplate reader (FLUOstar Omega, BMG Labtech, Germany) or microscope (Carl Zeiss, Oberkochen, Germany).

According to the experimental protocol, we seeded a density of 6000 cells per well into 96-well plates; then, the plates were incubated with several concentrations of baricitinib (0, 0.25, 0.5, 1, 2, 4 uM) for 24 hours and 48 hours. Since DMSO was the baricitinib solvent, we added a corresponding amount of DMSO to ensure that the DMSO's final concentration was equal in all groups. According to the endpoint method, a CellTox™ green reagent was diluted 500-fold into the buffer. Then, 100 µL of the final reagent was added to the wells, and the plates were gently mixed for one minute on an orbital shaker (500-700 rpm). To facilitate the binding process between the dye and DNA, we incubated the plate at room temperature protected from light for 15 minutes. We measured the fluorescence at an excitation wavelength of 485–500 nm and an emission wavelength of 520–530 nm.

## 3.10. Cell cycle analysis

The cell cycle, also known as the cell division cycle, is an essential property that can cause its DNA to duplicate; the cytoplasm and organelles divide, resulting in two daughter cells. Since the cell cycle determines the repair of genetic damage and prevents uncontrolled cell division, the regulation of the cell cycle is crucial for cell survival. The Muse™ Cell Cycle Kit was employed to quantify the percentage of cells in the G0/G1, S, and G2/M phases of the cell cycle on the Muse™ analyser.

Premixed reagents were used in the Muse™ Cell Cycle analysis. Propidium iodide (PI) in this

assay is a nuclear DNA intercalating dye that distinguishes cells at different stages of the cell cycle based on different DNA content. At the same time, RNase A in the assay was used to enhance the specificity of DNA staining. The resting cells at the G0/G1 phase had two copies of each chromosome, which could be stained with the PI described above. Once a cell begins to circulate and enter into the S phase, chromosomal DNA is synthesized, so the fluorescence intensity of PI continues to increase in this process until the cell enters the G2/M phase, and finally all chromosomal DNA doubles, showing the highest fluorescence intensity. Eventually, the G2/M phase of the cells shows strong fluorescence, twice which of the G0/G1 phase, before it finally divides into two cells [163].

After trypsin digestion, we transferred all cells from different groups to 12×75 mm polystyrene test tubes and counted to maintain $1 \times 10^6$ cells in each test tube. We centrifuged all test tubes at 300 × g for five minutes, then removed the supernatant to form a visible cell pellet. We added 1 mL of PBS to each tube, then pipetted several times or gently vortexed to mix. Then, all tubes were centrifuged again at 300 × g for five minutes, and the supernatant was removed without disturbing the cell pellet. Subsequently, 50 µL of PBS was added to each test tube, pipetting several times or vortexing gently to mix. The re-suspended cells were then added drop-wise to a test tube containing 1 mL of 70% ethanol, which was taken out from the −20°C refrigerator. The tubes were capped and frozen at −20°C for four hours, and then the staining protocol was performed. Each group of 200 µL ethanol-fixed cells was transferred to a 12×75 mm polystyrene test tube, and the final cell concentration was close to $1 \times 10^6$ cells/mL. After centrifuging and washing the cells twice with PBS, all the cell pellets of different groups were separately re-suspended in 200 µL Muse™ Cell Cycle reagent. After incubation at room temperature in the dark for 30 minutes, we transferred the cell suspension sample to a 1.5 mL microcentrifuge tube for the Muse™ Cell Analyser.

## 3.11. Measurement of proteasome activity in fibroblasts

The ubiquitin-proteasome system (UPS) plays a vital role in regulating of a variety of cellular processes because it degrades a wide range of protein substrates with excellent specificity in the cytoplasm of eukaryotic cells. UPS can control protein quality, signal transduction and cell cycle by selectively destroying proteins with abnormal conformations and short-lived regulatory proteins. From archaebacteria to yeast to humans, almost all organisms conservatively possess the 20S proteasome. However, compared to archaebacteria, which only has the 20S proteasome, the additional 19S particles bind to the 20S proteasome to form a 26S proteasome holoenzyme in eukaryotes. The 20S proteasome is the catalytic core of the proteasome complex, which is responsible for the activity of trypsin-like peptidase, chymotrypsin-like peptidase and peptidyl glutamate peptide hydrolysing peptidase. As a result, the 20S proteasome is responsible for the breakdown of the essential proteins involved with apoptosis, DNA repair, endocytosis and cell cycle control [164].

We first treated the cells in the logarithmic phase with drugs or vehicles according to the experimental design, then collected and counted them using the Muse™ Count and Viability Assay. An equal number of cells (32,000) into each well of a 96-well plate were seeded overnight to attach to the well. All groups were in triplicate. To break the cells and release the 20S proteasome to a more stable environment, 100 µL of freshly made lysis buffer was added to each well after removing the old culture medium.

The cells were next incubated with lysis buffer at 37°C while shaking. The 96-well plate was centrifuged at 1000 × g for ten minutes. 90 µL of supernatant was transferred to the corresponding new wells in the black 96-well plate, and 10 µL of 7-amino-4-methylcoumarin (AMC)-conjugated chymotrypsin substrate (2.5 µmol) was added to each well in the black 96-well plate. After incubating for one hour at 37 °C, the black 96-well plate was measured with a FLUOstar Omega fluorescence reader (excitation = 360 nm; emission = 480 nm).

## 3.12. Measurement of autophagy activity in fibroblasts

Autophagy is a critical cellular process that removes unnecessary dysfunctional components, allowing lysosomes to degrade and recycle cellular components in an orderly manner. Dysregulation of autophagy has been detected in cancer, infection and ageing. Well-functioning autophagy is necessary for survival, differentiation, development and homeostasis. In HGPS-related research, autophagy is an indispensable feature because it prevents the accumulation of damaged organelles and misfolded proteins such as progerin. In the process of autophagy, the cell components are separated by a double membrane. Then, the autophagosome and lysosome are fused to form an autolysosome, thereby degrading the cellular material.

Cayman's Autophagy/Cytotoxicity Double Staining Kit (Cayman Chemical Company, Ann Arbor, MI, USA) uses an auto-fluorescent substance, monodansylcadaverine (MDC), to detect autophagic vacuoles in cultured cells. MDC can incorporate into multilamellar bodies through both the ion trapping mechanism and the interaction with membrane lipids [165].

After treating the cells with drugs or mock for the desired period, the cells were harvested and seeded in triplicate with an equal number of cells (32,000) in 96-well plates. After incubating overnight at 37 °C to attach the cells, the plates were centrifuged at 400 × g for five minutes at room temperature, and the supernatants were removed. According to the assay protocol, 100 µL of the freshly prepared staining solution was added to each well and incubated at 37°C for ten minutes. Next, the plate was centrifuged at 400 × g for five minutes at room temperature, and the cells were washed three times with an assay buffer. Last, the fluorescence implicating the autophagic vacuole intensities were measured using an excitation wavelength of 355 nm and an emission wavelength of 520 nm.

## 3.13. Measurement of reactive oxygen species in fibroblasts

The daily oxygen metabolism process always produces reactive oxygen species (ROS), mainly in the form of superoxide and hydroperoxyl radicals, which are its natural by-products. The mitochondrial electron transport chain, including complex I (nicotinamide adenine dinucleotide (NADH) dehydrogenase ubiquinone-ubiquinol reductase) and complex III (ubiquinol-cytochrome C reductase), are the primary source of cellular ROS. When the high mitochondrial membrane potential slows down the electron transport rate, these two complexes produce ROS. The optimal level of ROS is essential for the signaling pathway because the increased production overwhelms the cell's antioxidant capacity.

After treating the cells with drugs or mock for the required time, the cells were harvested and seeded in triplicate in equal amounts (32,000) into 96-well plates, allowing the cells to attach to the wells overnight. After the cells were washed with 1x PBS, 25 µM of 2', 7'-dichlorofluorescein diacetate (DCFDA) was added and incubated at 37 °C for 45 minutes. After removing the old reagents, the cells were washed with 1x PBS and switched to 100 µL of 1x buffer solution. Subsequently, the fluorescence of 96-well plate samples was measured at an excitation wavelength of 485 nm and an emission wavelength of 520 nm. We repeated all measurements in at least three independent experiments.

## 3.14. Measurement of ATP in fibroblasts

Adenosine triphosphate (ATP) is a nucleoside triphosphate, mainly composed of a nitrogenous base (adenine), the sugar ribose and the triphosphate. ATP can be used as a ‘molecular currency’ for energy transfer in cells to store and transfer chemical energy. A variety of different cells can produce ATP. The three main pathways for eukaryotic cells to produce ATP are glycolysis, citric acid cycle/oxidative phosphorylation and β-oxidation. In

glycolysis, glucose and glycerol are metabolized to pyruvate, which causes two adenosine diphosphates (ADPs) to generate two ATPs and simultaneously produces two equivalents of NADH. The citric acid cycle is the primary way for cells to formulate ATP, mainly occurring in the mitochondria. In this process, pyruvate is oxidized by the pyruvate dehydrogenase complex to acetyl, which is completely oxidized to carbon dioxide through the citric acid cycle. Beta-oxidation is the process by which fatty acids are converted into acetyl-CoA with the presence of air and various coenzyme factors and enzymes and can also produce multiple ATP. ATP can not only participate in signaling transduction by acting as a substrate for kinases but also be converted into a second messenger cyclic adenosine monophosphate (AMP) as a substrate for adenylate cyclase, which, in turn, triggers calcium signals by releasing calcium from cells. ATP can also participate in DNA and RNA, protein synthesis, extracellular signal transduction and nerve transmission.

This reagent mainly produces a stable luminescence signal through the reaction of heat-stable luciferase. The half-life of this luminescence signal is longer than five hours. Luciferase can catalyse beetle luciferin, ATP and oxygen in the presence of $Mg^{2+}$ to generate oxyluciferin, AMP, pyrophosphate, $CO_2$ and Light. By measuring the fluorescence production, the ATP content can be quantitatively measured [166].

The CellTiter-Glo Luminous Cell Viability Kit measures the intracellular ATP in fibroblasts by combining the reagents with the cultured cells in a serum supplement medium. Before harvesting, the cells were treated with drugs or mock for the required time. Equal amounts of 32000 cells were triplicate-seeded in 96-well plates and allowed to attach to the wells in the corresponding medium at 37°C overnight. The next day, the plates were equilibrated at room temperature for 90 minutes, and then, the old medium was removed. Later, 100 µL of CellTiter-Glo reagent was added to each well of the plate and mixed on an orbital shaker for two minutes. At the same time, the ATP standard was added to fresh wells in triplicates. The plates were then incubated at room temperature in the dark for 10 minutes and measured for each well's luminescence intensity.

## 3.15. Gene expression analysis

### 3.15.1. The extraction of RNA

Cells from all different groups were collected after the designed period and counted using the Muse™ Count and Viability Assay. Before RNA isolation with the RNeasy Mini Kit, equal numbers of cells (300,000) were washed with PBS twice. 350 µL of RLT buffer containing freshly prepared β-mercaptoethanol was added to the cells for disruption. The QIAshredder spin column used to collect the solution was centrifuged at 13000 rpm for two minutes. An equal volume (350 µl) of 70% ethanol was added to each homogeneous lysate to produce 700 µL of unpurified RNA solution, which was then transferred to an RNeasy spin column for centrifugation.

After that, 700 µL of wash buffer one was added to each GeneJET RNA purification column, and these columns were centrifuged at 12000 × g for one minute. The flow-through was subsequently discarded, and the collection tube was reused to be fixed on the purification column again. Then, 600 µL of wash buffer two was added to each of the GeneJET RNA purification columns and centrifuged at 12000 × g for one minute. The effluent from each tube was then discarded, and the purification column was placed back into the collection tube. Next, 250 µL of wash buffer two was added to each column, and the column was centrifuged at 12000 × g for two minutes. Since the RNA was attached to the film, 100 µL of nuclease-free water was added to the centre of each membrane of the GeneJET RNA purification column. Then, the RNA was eluted after centrifugation at 12000 × g for one minute. Finally, the RNA could be stored at −80°C before use.

### 3.15.2. The synthesis of cDNA

A NanoDrop 1000 spectrophotometer was used to monitor the concentration and characteristics of nucleic acid samples. The absorbance of the sample at 260 nm (A260) and

the absorbance of the sample at 280 nm (A280) could be estimated. Therefore, the purity of RNA and DNA could be determined using the absorbance ratio of the sample at 260 and 280 nm. A ratio close to 2.0 indicated that the RNA quality was satisfactory, and a rate close to 1.8 suggested that the DNA quality was sufficient [167].

To measure the concentration of RNA, the 'nucleic acid' application module was selected, and then 'RNA' was selected as the sample type. After adjusting the NanoDrop with diethylpyrocarbonate (DEPC) water using 'Blank' and 'Re-blank' to have a stable baseline, we added 1 µL of aqueous nucleic acid sample to measure the concentration. We used a high-capacity cDNA reverse transcription kit (Thermo Fisher Scientific Inc., Waltham, MA, USA.). A total of 2000 ng RNA per group was reverse-transcribed into cDNA. Briefly, 2 µg RNA, 2 µL 10 mM dNTP mix, 2 µL 10x reaction buffer, 2 µL oligo-dT primers, 1 µL reverse transcriptase and 1 µL RNAse inhibitor were mixed on an ice pack to keep the temperature low. Since each sample contained a different concentration, 2 µg RNA required different volumes of aqueous nucleic acid. Therefore, it needed to be filled with various amounts of DEPC water to produce a total value of 20 µL. The mixture tube was then placed in a 37°C thermal cycler for one hour to synthesise cDNA, assuming a final cDNA concentration of 50 ng/µL.

### 3.15.3. The validation of primers

Since Kary Mullis first developed polymerase chain reaction (PCR) in 1983, it has been regarded as a laboratory technique for amplifying, identifying and quantifying targeted DNA molecules. Typically, there are two procedures for determining the target DNA for quantification. The first one uses absolute copy number, and the other uses relative copy number normalized to housekeeping genes. Non-specific fluorescent dyes (usually SYBR green) do not present as fluorescent without binding to DNA.

However, once the dye intercalates with any double-stranded DNA, a detectable fluorescence appears, making the target gene detectable. Compared with traditional PCR that can only be detected at the end, real-time PCR can vividly depict the entire DNA amplification process

after each cycle [168].

The primers were curated from the literature and verified with the UCSC (the University of California and Santa Cruz) Genome Browser (https://genome.ucsc.edu/cgi-bin/hgPcr). The in silico PCR option was selected on the tool list. Subsequently, we decided the human type as the genome, chose December 2013 (GRCh38 / hg38) as the assembly, selected the genome assembly as the target and selected the maximum product size as 4000. Later, we chose the minimum perfect match as 15, selected the minimum good match as 15 and filled the blanks of 'Forward' and 'Reverse' primers according to the primers we obtained from references before submitting the search. All validated primers and their corresponding genes were displayed in the primer list [169].

### 3.15.4. Reverse transcription PCR

To verify reverse transcription PCR (RT-PCR) and find the optimal primer conditions, we used temperature gradient PCR to screen the appropriate reaction conditions. For this method, we used the Qiagen Taq DNA Polymerase Kit for the PCR process. For this, we added 2 µL 10x mixed buffer, 2 µL 25 mM $MgCl_2$, 0.4 µL 10 mM dNTP, 0.1 µL Taq polymerase, 1 µL of 1 µM forward primer, 1 µL of 1 µM reverse primer and 2 µL cDNA in a suitable tube for the PCR machine. Then, we filled the tube with DEPC water to a final volume of 20 µL. We performed the reaction immediately using a thermal cycler after mixture and centrifuge. We selected the reaction steps as follows (Table 21).

**Table 21: Temperature gradient PCR.** Temperature gradient PCR was used to test the most suitable temperature for the RT-PCR by applying a temperature gradient.

| Reverse transcription PCR | | |
|---|---|---|
| Cycles | Time | Temperature |

| | | |
|---|---|---|
| 1x | 15 min | 95 °C |
| | 10 sec | 95 °C |
| 50x | 45 sec | Tm (primer specific) |
| | 30 sec | 60 °C |
| 1x | 10 min | 60 °C. |

In the operation of temperature gradient PCR, we used the Tm value given in the literature with 4 °C variation as the temperature range. We adjusted the temperature until obtaining a stable single band that met the requirements. The best amplification signal designated the best Tm as the experimental temperature of the subsequent RT-PCR.

We used a 1.5% agarose gel electrophoresis to analyze the PCR products. The composition of the agarose solution was 1.5% agarose, 0.4% EtBr and 1x TBE buffer. A microwave was used to heat the liquid to a complete solution and remove air bubbles. We poured the solution into the mould to let it solidify. Subsequently, by adding 6 µl Orange G to the 20 µL reaction sample, a sample for loading was prepared. After the gel was formed, we added the electrophoresis solution to the electrophoresis. The comb was carefully pulled out, and 12 µL of the sample was added to each lane. Meanwhile, the 100 bp marker was loaded. Subsequently, the gel system was operated at 180 V until the loading front reached the end of the gel.

### 3.15.5. Real-time PCR

We performed the real-time PCR using the PowerUp™ SYBR™ Green Master Mix (Applied Biosystems™, Thermo Fisher Scientific Inc., Waltham, MA, USA) in the StepOnePlus™ Real-Time PCR System (Thermo Fisher Scientific Inc., Waltham, MA, USA). After performing a series of tests on different amounts of cDNA and different concentrations of primers, we selected the optimal detection conditions as follows.

We added 5 µL of PowerUp™ SYBR™ Green Master Mix (2X), 300 nM forward primer, 300 nM

reverse primer and 10 ng cDNA to each well, then DEPC water was used to fill to yield a 10 µL of the reaction system. Therefore, 10 µL was set as the total volume of the 96-well plate. We covered the sealing plate with an optical adhesive. The components in the 96-well plate were then mixed thoroughly on a vortex machine for two minutes and centrifuged at 1200 × g for five minutes to spin down the contents and remove air bubbles.

We next placed the reaction plate was placed in a real-time PCR instrument to perform the real-time PCR reaction. Based on the primer Tm, we set the thermal cycle conditions: type of experiment, standard curve; reagents, SYBR™ Green reagent; reporter, SYBR™; quencher, none; passive reference dye, ROX™; melt curve ramp increment, continuous; reaction volume, 10 µL.

**Table 22: Real-time PCR.** Real-time PCR was used to measure the expression level of the target genes.

| Standard Cycling Mode (Primer Tm ≥ 60℃) | | | |
|---|---|---|---|
| Step | Temperature | Duration | Cycles |
| UDG Activation | 50 °C | 2 min | Hold |
| AmpliTaq® Fast DNA Polymerase, UP Activation | 95 °C | 2 min | Hold |
| Denature | 95 °C | 15 sec | 40 |
| Anneal/Extend | 60 °C | 1 min | |

The amplified signals were all controlled to be perceived between cycles of 10 and 30 to avoid spurious signals. We did all experiments in at least three replicates, and we used glyceraldehyde 3-phosphate dehydrogenase (GAPDH) as an endogenous control for comparison. The $2^{(\Delta\Delta CT)}$ method was used to calculate relative changes in gene expression. The expression folds were calculated by comparing the levels in the HGPS to control cells [170].

## 3.16. Western blot analysis

### 3.16.1. Sample collection for the Western blot

The control and HGPS cell culture dishes from different research groups were placed on ice, and all cells were washed with 4°C PBS in a cold room. After aspirating the PBS, we added various amounts of 4°C lysis buffers to the culture dishes according to the number of cells. For example, 1 mL per $10^7$ cells and 0.5 mL per $5 \times 10^6$ cells. Subsequently, a cold plastic scraper was used to scrape off the adhered cells from the Petri dishes, and then the cells were gently transferred to a pre-chilled microcentrifuge tube. The tubes were vigorously vortexed for five minutes and centrifuged at 12000 rpm in a microcentrifuge at 4°C for five minutes to develop the cell pellets. We aspirated the supernatant from each group and replaced it with a fresh test tube. All operations were kept on ice, and the tubes were gently removed from the centrifuge to avoid resuspending the cell pellets.

### 3.16.2. Protein quantification by Bradford analysis

The Bradford assay is a classic method for determining the protein concentration in a solution by measuring the change in absorbance of Coomassie Blue G reagent. Coomassie Blue has different colors under different states of charge. When the pH is lower than 0, the dye shows red and has an absorption peak at a wavelength of 465 nm because all three nitrogen atoms carried by the dye present as positively charged. Due to the low p$K_a$, the dye exhibits a total charge of +1 at a pH of 1 and appears green, with maximum absorption at 620 nm. When the pH value increases to 2, the dye becomes bright blue, and the maximum absorption is 595 nm. Under acidic conditions, the protein's base amino acids (such as arginine, lysine, and histidine) can non-covalently bind to the dye to form a complex and produce a blue color by stabilizing the negatively charged anion. After binding to this protein, the dye changes from reddish-brown to bright blue (absorption maximum is equal to 595nm) [171].

Bradford reagent was bought directly from Bio-Rad. The standards were prepared by diluting the bovine serum albumin (BSA) stock solution (1 mg/mL) to generate a standard curve from 0 mg/mL to 1 mg/mL. Therefore, we used the amounts of BSA and buffer, as shown in Table 23.

**Table 23: The preparation of the standards for protein quantification.** Standards were used to make a standard curve for protein quantification.

| The preparation of the standards for protein quantification | | |
|---|---|---|
| Sample | BSA amount [µL] | Buffer amount [µL] |
| Sample #1 (0.0 mg/ml) | 0 | 30 |
| Sample #2 (0.2 mg/ml) | 6 | 24 |
| Sample #3 (0.4 mg/ml) | 12 | 18 |
| Sample #4 (0.6 mg/ml) | 18 | 12 |
| Sample #5 (0.8 mg/ml) | 24 | 6 |
| Sample #6 (1.0 mg/ml) | 30 | 0 |

Similar to the protein samples, the standards were put in 96-well plates at 10 µL per well in triplicate. Subsequently, a 200 µL Bradford reagent was added to each well using a multi-channel pipette. After incubation for five minutes in the dark, the plate was measured at 595 nm with a microplate reader. Based on the standard curve and the date of the protein sample, the protein sample concentration could be calculated and adjusted to make it consistent.

### 3.16.3. SDS-PAGE

Electrophoresis analysis of proteins is a standard method for drug-related research, and it can separate different proteins based on molecular weight. Polyacrylamide gel, also known as sodium dodecyl sulphate-polyacrylamide gel electrophoresis (SDS-PAGE), is the most

common gel electrophoresis system for protein separation.

Polyacrylamide gels can be obtained by hydrating of acrylamide to create pores with different sizes because increasing the concentration of acrylamide causes a decreasing pore size after polymerization. With these pores, small molecules move faster than large molecules because small molecules can enter the pores and smoothly pass through the gel while large molecules are trapped at the pores. SDS molecules are negatively charged at pH 8.3. When performing electrophoresis, SDS can bind to proteins to denature them. By destroying the secondary, tertiary and quaternary structures, the denatured proteins all become negatively charged linear polypeptide chains with approximately one SDS molecule per two amino acids. Because they have a uniform mass-to-charge ratio, each protein obtains a negative charge through SDS. Eventually, the negatively charged protein can pass through the gel with different mobility under the electric field. The movement of a protein or the distance travelled by a protein is inversely proportional to the molecular weight's logarithm. Therefore, the protein can be separated according to molecular weight and then stained with Ponceau S to make it visible or detectable for antibody detection. To make it easier to monitor the running process and determine the molecular weight of the target protein, we added the visible protein mixture marker to the empty well for comparison. Pre-made gels were purchased from Bio-Rad at a concentrations of 4–20%. Homemade gels were prepared as shown in Table 24 and were polymerized for 20 minutes before use, respectively.

**Table 24: The preparation of the SDS gels.** SDS gels were prepared to have a better separation for the target proteins.

| **Running gel (percent depending on molecular weight of protein):** | | | | | |
|---|---|---|---|---|---|
| | | <70 kDa | 40-70 kDa | 20-40 kDa | |
| | 7% | 8% | 10% | 12% | 15% |
| $H_2O$ | 7.6mL | 6.8mL | 5.6mL | 4.2mL | 2.2mL |
| 30% Acrylamid | 4.6mL | 5.4mL | 6.6mL | 8.0mL | 10mL |
| 1 M Tris-HCl pH 8.8 | 7.4mL | 7.4mL | 7.4mL | 7.4mL | 7.4mL |

| | | | | | |
|---|---|---|---|---|---|
| 10% SDS | 200µL | 200µL | 200µL | 200µL | 200µL |
| Ammonlumpersulfate | 160µL | 160µL | 160µL | 160µL | 160µL |
| TEMED | 20µL | 20µL | 20µL | 20µL | 20µL |

| **Stacking gel** | | | | | |
|---|---|---|---|---|---|
| | 4% | 5% | 6% | 7% | 8% |
| $H_2O$ | 4.4mL | 4.3mL | 4.1mL | 3.8mL | 3.7mL |
| 30% Acrylamid | 0.8mL | 1.0mL | 1.2mL | 1.5mL | 1.6mL |
| 1 M Tris-HCl pH 8.8 | 750µL | 750µL | 750µL | 750µL | 750µL |
| 10% SDS | 60µL | 60µL | 60µL | 60µL | 60µL |
| Phenol Red | 20µL | 20µL | 20µL | 20µL | 20µL |
| Ammonlumpersulfate | 30µL | 30µL | 30µL | 30µL | 30µL |
| TEMED | 6µL | 6µL | 6µL | 6µL | 6µL |

For the gel preparation process, we mixed the $H_2O$, 30% acrylamide, 1 M Tris-HCl pH 8.8 and 10% SDS. Next, we quickly added the ammonium persulfate and tetramethylethylenediamine (TEMED) just before pipetting the solution to the top of the assembled gel electrophoresis apparatus chamber. Around 200 µL of isopropanol was added to the top of the gel to maintain a smooth liquid level, and we let the gel polymerise around 20 min. Once the polymerization was finished, we removed the isopropanol and added the stacking gel. Finally, a clean comb was inserted between glasses into the stacking solution, carefully removing trapped air bubbles before placing the gel in a vertical position at room temperature.

Before being added to the gel wells (20 µL per well), each sample was vortexed three times for 30 seconds and heated at 99°C for three minutes to completely denature the proteins that were present in each sample. After the device was installed, we loaded the marker and each sample in turn to each well. Based on the molecular weight of the target protein, we ran the gel at a constant voltage of 120 V for a variable time until the dye front ran out of the gels, but usually one hour and 45 minutes.

After the SDS gel electrophoresis was completed, we removed the gel from the cassette and then washed the gel with double-distilled $H_2O$ ($ddH_2O$) and equilibrated it in transfer buffer

for 10 minutes. Then we used the Trans-Blot® Turbo™ Transfer System (Bio-Rad) to transfer the protein separated in the gel to the nitrocellulose membrane at 25 V for 30 minutes. Before this process, the fiber pads, filter papers and nitrocellulose membranes were equilibrated in pre-cooled transfer buffer at 4°C overnight. At the end of the electroblotting process, the nitrocellulose membrane was washed with $ddH_2O$ before the next step [172].

### 3.16.4. Image scanning and data analysis

To verify the transfer efficiency, Ponceau S was added to the film for five minutes while shaking. After removing stains, the membrane was washed three times with PBST. Then, the membrane was blocked in 5% non-fat milk for four hours. Subsequently, the membrane was incubated overnight at 4°C with the primary antibodies we wanted to detect. The primary antibodies are anti-JAK1 (catalog number 3332, Cell Signaling, Danfoss, Massachusetts, USA, 1/1000), anti-JAK2 (catalog number 3230, CellSignaling, 1/1000), anti-STAT1 (catalog number 14994, CellSignaling, 1/1000), anti-P-STAT1 (catalog number 9167, Cell Signaling, 1/1000), anti-STAT3 (catalog number 9139, cell signal transduction, 1/1000), anti-P-STAT3 (catalog number 9145, cell signaling, 1/1000), anti-P21 (catalog number MA5-14949, Invitrogen, Carlsbad, California), United States (1/1000), anti-beta Actin (Sigma-Aldrich, 1/5000), anti-presenile protein (rabbit monoclonal Ab, 0.1 μg / mL) and anti-lamin A / C (catalog number sc-20681, Santa Cruz Biotechnology, Deke, USA Dallas, Sas., 1 / 10,000). After incubation, the membrane was washed three times with TBST and then coupled with the corresponding secondary antibody conjugated with horseradish peroxidase (Jackson ImmunoResearch Laboratories, West Grove, Pennsylvania, USA). After incubation, the membrane was washed twice with PBST for five minutes each time and then with PBS for five minutes. The signal amplified on the membrane using an enhanced chemiluminescence detection system (ECL substrate; BioRad) was then visualized and measured for optical density by ChemiDoc™ MP. While using ImageJ software (NIH) for analysis, all protein signals were quantified using β-actin for normalization.

## 3.17. Immunocytochemistry

Immunohistochemistry is an experimental technique that uses the specific binding reaction between antigens and antibodies in immunological principles to detect the presence of target antigens in cells or tissues. By binding fluorescent or colorable chemicals to an antibody, this method can be used not only to measure the amount of antigen expression but also to observe the antigen's position.

To prepare for immunocytochemistry, the coverslips were sterilized with 70% ethanol and washed three times with PBS. Mock-treated or drug-treated HGPS and control fibroblasts were grown directly on coverslips for experiments. After completing the drug treatment schedule, we washed the cells three times with PBS and then fixed the cells in ice-cold methanol at −20°C for 10 minutes. Subsequently, the dish was blocked with 5% FBS in PBS for 30 minutes at room temperature and then incubated with the primary antibody for two hours at room temperature. The following primary antibodies used were: anti-presenilin (1 µg / mL), anti-ciliary protein A / C (catalog number MA3-1000, Invitrogen, Carlsbad, California, USA, 1/100). After washing the coverslip three times with PBST, the secondary antibody was added and incubated for one hour. The secondary antibodies used were affinity-purified Alexa Fluor 488 donkey immunoglobulin G (IgG) antibody (Molecular Probes, Eugene, OR, USA) and Cy3-bound IgG antibody (Jackson ImmunoResearch). After washing three times with PBST, the coverslip was carefully dried with absorbent paper to absorb the solution on the side of the coverslip to avoid touching the cells. The coverslips were then counterstained with DAPI Vectashield mounting medium before observation. Images were collected at the same exposure time to compare the brightness of the cells using an Axioplan fluorescence microscope (Carl Zeiss, Oberkochen, Germany) [100].

## 3.18. Statistical analysis

Among all the different characteristics of HGPS and control fibroblasts with or without treatment, a student's test (⋆ $p$ <0.05, ⋆⋆ $p$ <0.01, ⋆⋆⋆ $p$ <0.001, n ≥ 3) was used for the corresponding analysis. Data with p-values below 0.05 were estimated to be statistically significant in our study. Data were expressed as mean ± standard deviation (mean ± SD) to show differences and details. In order to calculate the data and draw the graph, we used version 6.01 of the prism (GraphPad, San Diego, California, United States) [100].

# 4. Results

## 4.1. The identification of genes altered in vascular disease, arthritis, alopecia and lipodystrophy.

In drug research, understanding the connection between genes and disease is crucial because it can provide some candidate gene–disease associations before conducting large-scale research. Although HGPS babies do not have apparent phenotypes during childbirth and early infancy, four typical phenotypes – alopecia, lipodystrophy, arthritis and vascular disease – tend to rise at 12 to 24 months after birth. Therefore, we suggest that several genes are affected under all four conditions. Thus, a data mining method was established to identify those genes. In our text mining process, based on the scientific literature on *PubMed* (http://www.pubmed.gov), we used a keyword search to check the related genes. As mentioned in 'Materials and Methods', we attempted to match all genes in the human genome from the Human Gene Nomenclature Committee (HGNC) to each of these four diseases [152]. There were 2843 genes identified as associated with at least one of the four targeted conditions. Among these genes, there were 157 genes related to alopecia, 67 genes related to lipodystrophy, 1049 genes related to arthritis and 1560 genes related to vascular diseases.

As shown in the Figure 6, a Venn diagram was generated to obtain genes that changed simultaneously under all four conditions. According to the Venn diagram, the association between 17 genes and all four diseases was found simultaneously, which indicates that these 17 genes may be dysregulated in HGPS. Specifically, they are complement 3 (C3), chemokine (C-C motif) ligand 2 (CCL2/MPC1), C-reactive protein (CRP), C-X-C motif chemokine ligand 8 (CXCL8/IL8), cell surface death receptor (FAS), heme oxygenase 1 (HMOX1), intercellular adhesion molecule 1 (ICAM-1), insulin-like growth factor 1 (IGF-1), interleukin 18 (IL-18), interleukin 4 (IL-4), interleukin 6 (IL-6), interferon-gamma (IFNG), peroxisome proliferator-

activated receptor gamma (PPARG), transforming growth factor-beta 1 (TGFB1), tumor necrosis factor-alpha (TNFa ), leptin (LEP) and TNF receptor-associated factor 1 (TRAF1).

Most data scientists who have higher requirements for database capacity or improved statistical models when processing large amounts of data always have a tolerable false discovery rate. To validate the data mining process and avoid any false discovery, we further carefully curated the text mining derivative publications to determine the expression patterns of 17 genes in each of the four diseases. Table 25 represents the function and predicted expression pattern of each of the 17 genes associated with the four disorders. According to the table, HMOX1, IGF-1 and PPARG are down-regulated while CCL2, CXCL8, CRP, FAS, ICAM-1, IL-6, IL-18, TGFB1, TNFa and TRAF1 are up-regulated under these four conditions. However, C3, LEP and IL-4 decreased in lipodystrophy but increased in the other three diseases. IFNG is elevated in arthritis and reduced in the other three conditions.

By carefully examining these 17 genes, we see that most of them encode known cytokines, including the pro-inflammatory component CRP, CCL2/MCP1, CXL8/IL8, IL-6, IFNG and TNFa. These factors are classified as age-related secretory phenotypes that develop in most age-related diseases. In addition to generating permanent cell cycle arrest and resistance to cell death signals in senescent cells, the cells also produce a bio-active secretome, recognized as the senescence-associated secretory phenotype (SASP). Therefore, the results of text mining indicate that there may be a common molecular mechanism in all four cases: chronic inflammation. The inflammatory process is an essential immune defense system in living organisms. When pathogens, allergens and toxins enter the body, short-term acute inflammation occurs immediately. Usually, immune cells, endogenous anti-inflammatory agents and tissue remodeling processes are closely coordinated in various defense processes. This acute inflammation is resolved by eliminating pathogens, removing the infecting cells and repairing damaged tissues, returning to cellular homeostasis. However, when the acute inflammatory response cannot be resolved and continues to exist, the cell assembles more defense components to produce a long-term, unresolved immune response – chronic inflammation. In normal ageing, people can often be observed with an imbalanced immune

response [173].

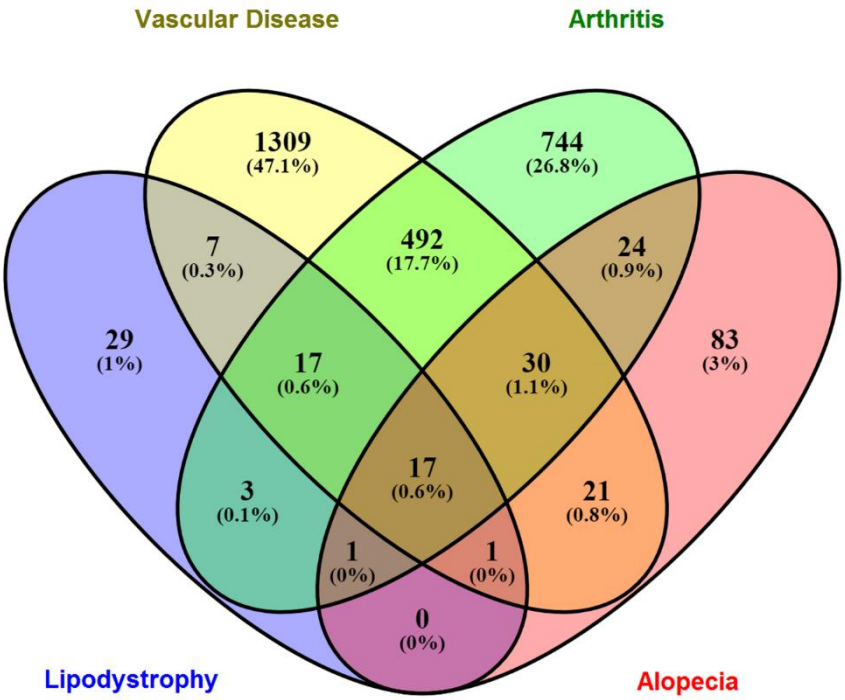


**Figure 6: The Venn diagram of the related genes.** The Venn diagram describes 2778 genes related to the four diseases identified by text mining.

**Table 25: Differential regulation of genes simultaneously altered in vascular disease (VD), arthritis (AR), lipodystrophy (LD) and alopecia (AL) derived from text mining.** According to curated literature, the level of expression (↑ = overexpressed; ↓ = downregulated) in each disease is indicated.

| **Gene** (swiss-prot gene ID) | | **Expression** | **Function** |
|---|---|---|---|
| ***FAS*** (receptor) ID: 355 | **VD** | ↑[174] | FAS-mediated apoptosis regulates apoptotic death of VSMCs during atherogenesis, and FAS overexpression determines the amount of tissue mass in the diseased vessels [175]. |
| | **AR** | ↑[176] | RA patients' monocytes and macrophages present in the synovial fluid are resistant to FAS-mediated killing, leading to the persistence of inflammatory monocytes and macrophages, perpetuating joint inflammation [177]. |
| | **LD** | ↑[178] | Regulates apoptosis in the adipose tissue [178]. |
| | **AL** | ↑[179] | The FAS/FASL system has a costimulatory role in the early phase of the disease process and induces apoptosis in FAS-expressing cells of the hair follicles by FASL-expressing cells of the perifollicular infiltrate, resulting in hair loss [179]. |
| ***PPARG*** (receptor) ID: 5468 | **VD** | ↓[180] | Protects endothelium, regulates the differentiation of adipocytes and lipid metabolism, inhibits proliferation and the migration of smooth muscle cells and reduces inflammatory chemokines [180]. |
| | **AR** | ↓[181] | Inhibits major signaling inflammation pathways and |

| | | | |
|---|---|---|---|
| | | | reduces the synthesis of cartilage catabolic factors responsible for articular cartilage degradation [182]. |
| | **LD** | ↓[183] | Essential in the differentiation of adipocytes [184]. |
| | **AL** | ↓[185] | Required for the maintenance of a functional epithelial stem cell compartment in murine hair follicles [186]. |
| ***CCL2*** (chemokine) ID: 6347 | **VD** | ↑[187] | Recruits macrophages and monocytes to the vessel wall [188]. |
| | **AR** | ↑[189] | Mediator of the migration of monocytes, macrophages and T cells. These are directly involved in the induction and perpetuation of synovitis and subsequent joint destruction [189]. |
| | **LD** | ↑[190] | Recruits macrophages to adipose tissue and induces an inflammatory response [191]. |
| | **AL** | ↑[192] | Recruits T lymphocytes and monocytes in the acute inflammatory condition and may also be an important mediator in chronic inflammation [193]. |
| ***TGFB1*** (growth factor) ID: 7040 | **VD** | ↑[194] | There is a link between increased levels of circulating TGFB and hypertension, a cardiovascular risk factor that contributes to the development of organ damage such as renal sclerosis, stroke and coronary heart disease [195]. |
| | **AR** | ↑[196] | TGFB1 has been reported to have important roles in unresolved inflammation, immune suppression, fibrosing processes and angiogenesis [197]. |
| | **LD** | ↑[198] | Potent inhibitor of adipocyte differentiation [198]. |
| | **AL** | ↑[199] | Influences the epithelial cell growth and modulates androgen receptor transactivation and androgen |

| | | | |
|---|---|---|---|
| | | | sensitivity in dermal papilla cells [199]. |
| ***CXCL8*** (Chemokine) ID: 3576 | **VD** | ↑[200] | Stimulates the adhesion of monocytes to endothelial cells and has a role in plaque destabilisation [201,202]. |
| | **AR** | ↑[203] | Induces synovial inflammation, regulates leukocyte adhesion molecule expression and it is a mediator of angiogenesis [204]. |
| | **LD** | ↑[205] | Major regulator of adipose tissue metabolism. Its overexpression in subcutaneous adipose tissue may be associated with wasting processes that lead to atrophy [205,206]. |
| | **AL** | ↑[207] | Plays a role in perturbing keratinocyte differentiation in the alopecia areata follicle [208]. |
| ***ICAM-1*** (adhesion molecule) ID: 3383 | **VD** | ↑[209] | Key molecule in atherogenesis when circulating monocytes adhere to the endothelium and subsequently transmigrate into the intima [210]. |
| | **AR** | ↑[211] | Promotes leukocyte adhesion to endothelial cells and synovial fibroblasts and promotes leukocyte migration [212]. |
| | **LD** | ↑[213] | UNKNOWN |
| | **AL** | ↑[214] | Together with IFNG mediates T cell trafficking in the skin [215]. |
| ***CRP*** (pentraxin) ID: 1401 | **VD** | ↑[216] | Directly influences complement activation, apoptosis, vascular cell activation, monocyte recruitment, lipid accumulation and thrombosis. Associated with the formation and progression of atherosclerotic lesions [217,218]. |
| | **AR** | ↑[219] | Plays a role in the bony destructive process through the |

| | | | |
|---|---|---|---|
| | | | induction of the receptor activator of nuclear factor kappa-B ligand expression and direct differentiation of osteoclast precursors into mature osteoclasts [220]. |
| | **LD** | ↑[221] | Its levels are strongly associated with adipose tissue mass [222]. |
| | **AL** | ↑[223] | UNKNOWN |
| ***C3*** (Chemokine) ID: 718 | **VD** | ↑[224] | Essential in the maturation of atherosclerotic lesions beyond the foam cell stage [225]. |
| | **AR** | ↑[226] | Contributes to inflammation and tissue injury. Has a role in the induction and progression of the disease [226]. |
| | **LD** | ↓[227] | Excessive consumption of C3 in the alternative complement pathway leads to an increased expression of Factor D. Lipodystrophy and tissue destruction are more significant in tissues where Factor D expression is increased [228,229]. |
| | **AL** | ↑[230] | C3 deposition reflects the morphological state of hair follicles in each stage of the hair cycle, suggesting a relationship between the hair cycle and C3 deposition [231]. |
| ***TRAF1*** (tumor necrose factor associated) ID: 7185 | **VD** | ↑[232] | Involved in monocyte recruitment to the vessel wall [233]. |
| | **AR** | ↑[234] | Plays a crucial role in the pathogenesis of autoantibodies and may serve as a serologic inflammatory marker of disease activity [234]. |
| | **LD** | ↑[235,236] | UNKNOWN |

| | | | |
|---|---|---|---|
| | **AL** | ↑[237] | UNKNOWN |
| ***IL-18*** (Interleukin) ID: 7185 | **VD** | ↑[238] | Has a proatherogenic effect through stimulation of IFNG secretion. It polarises T helper 1 cells (Th1) and induces the production of inflammatory cytokines, chemokines and vascular adhesion molecules [239,240]. |
| | **AR** | ↑[241] | Promotes articular Th1 responses, acts directly on macrophages to induce pro-inflammatory cytokine production and contributes to cartilage degradation [242]. |
| | **LD** | ↑[81] | Induces apoptosis of subcutaneous adipocytes in lipoatrophic areas, and it contributes towards HIV-associated lipodystrophy syndrome (HALS) by downregulating the production of adiponectin [81,243]. |
| | **AL** | ↑[244] | Induces the production of IFNG, a factor that induces alopecia [245]. |
| ***IGF-1*** (growth factor) ID: 3479 | **VD** | ↓[64] | Reduces atherosclerosis burden and improves features of atherosclerotic plaque stability through induction of reducing of oxidative stress, cell apoptosis, pro-inflammatory signaling and endothelial dysfunction [64]. |
| | **AR** | ↓[246] | Enhances the synthesis of components such as proteoglycan and collagen in normal cartilage and blocks cytokine-stimulated cartilage degradation. It is an important regulator of the repair processes during joint diseases [247,248]. |
| | **LD** | ↓[249] | IGF-1 signaling is essential for the development and |

| | | | |
|---|---|---|---|
| | | | function of adipose tissue. The IGF-1 receptors play a role in gene expression in white adipose tissue and in the maintenance of normal serum leptin and adiponectin levels [249]. |
| | **AL** | ↓[250] | Stimulates follicular epithelial cell growth [251]. |
| ***IL-6*** (Interleukin) ID: 3569 | **VD** | ↑[252] | Plays a central role in propagating the downstream inflammatory response responsible for atherosclerosis. Contributes to both atherosclerotic plaque development and plaque destabilisation [253,254]. |
| | **AR** | ↑[255] | Contributes to the induction and maintenance of the autoimmune process through B cell modulation and Th17 cell differentiation, and it plays a role in angiogenesis by inducing intracellular adhesion molecules [256]. |
| | **LD** | ↑[257] | Leads to increased apoptosis and thus contributes to the loss of subcutaneous fat [258]. |
| | **AL** | ↑[259] | Induces a rise in immunoglobulin G which can have a key role in long-standing disease due to humoral autoimmune pathology and plays a partial role in hair growth inhibition [259,260]. |
| ***TNFA*** (tumor necrosis factor) ID: 7124 | **VD** | ↑[261] | Promotes cholesterol uptake into monocytes and macrophages and cholesteryl ester-laden cell formation from differentiating monocytes, resulting in foam cell accumulation; it is involved in the production of chemokines and in the recruitment of leucocytes during inflammatory reactions. It induces VSMC proliferation, increases adherence of leucocytes to |

| | | | |
|---|---|---|---|
| | | | endothelial cells by inducing the expression of cell adhesion molecules, stimulates apoptosis of VSMCs and can induce autophagy in plaque VSMCs [261-263]. |
| | **AR** | ↑[264] | Stimulates the production of cytokines, chemokines and prostaglandins in RA synovium and stimulates the production of matrix-degrading enzymes like MMPs. It leads to an increase of the destructive potential of RASF, induces the expression of Receptor activator of nuclear factor kappa-B ligand (RANKL) and synergises with RANKL to directly promote osteoclast differentiation. It stimulates bone loss by mobilising $CD11b^+$ osteoclast precursors from the bone marrow and by reducing bone formation by inhibiting osteoblast differentiation and function [265-267]. |
| | **LD** | ↑[268] | Stimulates lipolysis and induces insulin resistance, leptin production, suppression of lipogenesis, adipocyte dedifferentiation and apoptosis in preadipocytes and adipocytes. It impairs preadipocyte differentiation [269,270]. |
| | **AL** | ↑[271] | Causes the condensation and distortion of the dermal papilla, marked vacuolation of the hair follicle matrix, abnormal keratinisation of the follicle bulb and inner root sheath, disruption of follicular melanocytes and the presence of melanin granules within the dermal papilla, resulting in the formation of dystrophic anagen hair follicles [92,272]. |
| ***HMOX1*** | **VD** | ↓[273] | Its expression in macrophages increases antioxidant |

| | | | |
|---|---|---|---|
| (oxygenase)<br>ID: 3162 | | | protection and decreases inflammatory components of atherosclerotic lesions, having a role in the protection against atherogenesis [274]. |
| | **AR** | ↓[275] | Inhibits cartilage erosion, decreases pro-inflammatory cytokine secretion and suppresses osteoclastogenesis and bone destruction [276]. |
| | **LD** | ↓[277] | UNKNOWN |
| | **AL** | ↓[278] | Its decreased expression impairs the impairment of the protective mechanism from oxidative stress in the scalp [278]. |
| ***LEP***<br>(adipokine)<br>ID: 3952 | **VD** | ↑[279] | Leptin is an important mediator in endothelial dysfunction and neointimal hyperplasia, both key steps in the evolution of atherosclerotic vascular changes. Additionally, paracrine leptin released from perivascular adipose tissue (PVAT) has deleterious effects on the underlying endothelium and VSMCs, including coronary circulation [279]. |
| | **AR** | ↑[280] | Adipocyte-derived leptin induces pro-inflammatory cytokine released from innate and adaptive immune cells, producing an inflammatory milieu that encourages cartilage damage and RA [280]. |
| | **LD** | ↓[281] | Leptin has key roles in the regulation of energy balance, body weight, metabolism and endocrine function. Leptin levels are undetectable or very low in patients with lipodystrophy, hypothalamic amenorrhea and congenital leptin deficiency (CLD) due to mutations in the leptin gene [281]. |

| | | | |
|---|---|---|---|
| | **AL** | ↑[282] | The plasma leptin level is significantly higher in AGA subjects compared to non-AGA subjects (4.45 vs 2.76 ng/mL, P< 0.05). Leptin from the circulation might impact the development of AGA [282]. |
| ***IL-4*** (Interleukin) ID: 3565 | **VD** | ↑[283] | IL-4 can induce apoptosis of human vascular endothelial cells through the caspase-3-dependent pathway, suggesting that IL-4 can increase endothelial cell turnover by accelerated apoptosis, which may cause the dysfunction of the vascular endothelium [283]. |
| | **AR** | ↑[284] | IL-4 improves anti-inflammatory effects and suppresses several pro-inflammatory cytokines, and systemic IL-4 treatment protects the cartilage and bone destruction in established murine type II collagen-induced arthritis. IL-4 has an inhibiting effect on the degradation of proteoglycans in the articular cartilage by inhibiting the secretion of matrix metalloproteinases as well as reducing the variation in the production of proteoglycans that are visible in the course of osteoarthritis (OA) [284]. |
| | **LD** | ↓[285] | IL-4 has an important role in lipid metabolism and glucose regulation by promoting insulin sensitivity and glucose tolerance. Lower insulin sensitivity reduces uptake of fatty acids, reduces glucose transport and increases free fatty acids (FFA) in the general circulation, which can lead to lipodystrophy [285]. |
| | **AL** | ↑[286] | Alopecia development is associated with CD8+ T cell |

| | | | |
|---|---|---|---|
| | | | activation, migration into the intrafollicular region and hair follicle destruction. The disease may be adoptively transferred with T lymphocytes and is class I and not class II MHC-dependent. Pathologic T cells primarily express IFNG and IL-17 early in diseases, with dramatic increases in cytokine production and recruitment of IL-4 and IL-10 production with disease progression [286]. |
| ***IFNG*** (Interferon) ID: 3458 | **VD** | ↑[287] | IFNG, known to be a pro-inflammatory cytokine, can also display anti-inflammatory properties. It is likely that it acts in both ways in atherosclerosis. It is possible that its proatherogenic actions out-weigh its anti-atherogenic ones or vice versa. IFNG promotes foam cell formation, plaque development and a Th1-driven adaptive immune response. These effects can be attributed to an array of key genes involved in atherosclerosis that are regulated by IFNG [287]. |
| | **AR** | ↓[288] | IFNG activity associated with necroptosis suggests that IFNG may modulate necroptosis and improve RA progression by preventing or reducing inflammatory cell death [288]. |
| | **LD** | ↑[289] | Cytokines play important roles in the pathogenesis of lipodystrophy syndrome. Single nucleotide polymorphisms (SNPs) at position +874 (T/A) of the IFNG gene are related to the expression of these cytokines [290]. |
| | **AL** | ↑[291] | IFNG rapidly inhibits hair elongation in cultured human |

| | | | |
|---|---|---|---|
| | | | anagen hair follicles and induces morphological signs of catagen transformation. IFNG can also inhibit proliferation and increase apoptosis and follicular melanogenesis [291]. |

## 4.2. Identification of the signaling pathway

To support this hypothesis, a protein–protein interaction network was formed by STRING analysis, indicating that all 17 proteins are functionally connected and may play a cross-linking role in the development of these four pathological processes [292].

A closer look at the picture shows that all of these proteins are interrelated. Some proteins are directly related, like the relationship between upstream and downstream, and some of them need an intermediary to achieve relevance. Among these proteins, TNF, TGFB1, CCL2, CRP, IL-4, IL-6, IL8, ICAM-1, and IFNG are directly connected to more proteins than other candidates. This result also illustrates the critical role of the pro-inflammatory components mentioned above. The regulation of these proteins may also cause shifts in other proteins. All of these proteins are the query proteins and the first shell of interactors. For these interactions, the blue lines are from curated databases, and the laboratory determines the purple ones. Yellow is the result of text mining from the article, and black is the co-expression.

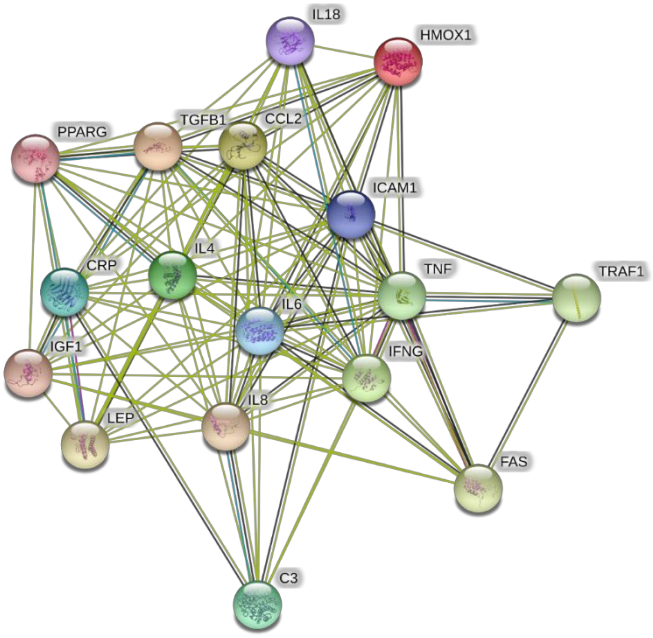


**Figure 7: The STRING analysis of the 17 related genes.** The interaction network of the 17 genes was visualised by STRING. The nodes represent proteins, and the lines symbolise functional associations between proteins. The green line indicates neighbourhood evidence; the blue line indicates co-occurrence evidence; the purple line indicates experimental proof; the light blue line indicates database evidence, and the black line indicates co-expression evidence.

Because these 17 genes are closely linked, and most of them are related to inflammation, the majority of them can be regulated through the same signaling pathway. Therefore, three databases (TRRUST version, TfactS, and Regulatory Circuit) were used to search the regulators and targets of these 17 entities. According to the results shown in Table 26, the transcription factor nuclear factor kappa-B subunit 1 (NF-κB1), RelA proto-oncogene (Rela), STAT1, STAT3, STAT5a, STAT5b and STAT6 are part of the regulatory network that can regulate many of these genes. Still, none of them can regulate all of these genes at the same time. Among all possibilities, the results support participation in the development of four pathologies through NF-κB1 and RelA in the NF-κB signaling pathway, and participation in the event of four pathologies through STAT1, STAT3, STAT5a, STAT5b and STAT6 in the JAK-STAT signaling pathway. As a classic pathway related to ageing, previous studies have shown that the

activation of NF-κB can promote ageing and age-related diseases. However, according to the literature, which summarizes all the drugs that have been used on progeria [106], the JAK-STAT pathway has not been associated with age-related diseases yet, while NF-κB is already involved in the progeria research (Table 27).

We consequently suggest that changes in the JAK-STAT pathway may mediate the four pathologies in HGPS and further HGPS itself. In summary, text mining research indicated that enhanced pro-inflammatory factors are potential common causes for four different diseases. Most of these 17 factors are related to JAK-STAT signaling, suggesting that excessive activation of JAK-STAT signaling may lead to the development of these four diseases.

**Table 26: Transcription factors that regulate most of the 17 genes identified by text mining.** We searched each of the 17 genes using the TRRUST version 2 (https://www.grnpedia.org/trrust/), TfactS (http://www.tfacts.org/) and Regulatory Circuits database (http://regulatorycircuits.org/). A total of 140 transcription factors were classified, and each transcription factor was associated with at least one of the 17 genes. The transcription factors linked to most of the 17 genes identified by direct evidence are shown.

| Gene | NF-κB1 | Rela | STAT3 | STAT1 | STAT5A | STAT5B | STAT6 |
|---|---|---|---|---|---|---|---|
| C3 | | | | | | | |
| CCL2 | √ | √ | √ | √ | | | |
| CRP | √ | √ | √ | | | | |
| CXCL8 | √ | √ | √ | √ | | | √ |
| FAS | √ | √ | √ | √ | | | |
| HMOX1 | √ | √ | √ | √ | | | |
| ICAM-1 | √ | √ | √ | √ | | | |
| IGF-1 | | | √ | | √ | √ | |
| IL-6 | √ | √ | √ | √ | √ | | |
| IL-18 | √ | √ | | | | | |

| | | | | | | | | | | |
|---|---|---|---|---|---|---|---|---|---|---|
| PPARG | √ | | | | √ | | | √ | | |
| TGFB1 | √ | | | √ | | | | | | |
| TNFA | √ | | √ | √ | | | √ | √ | | |
| TRAF1 | √ | | √ | | | | | | | |
| LEP | | | | √ | | | | | | |
| IL-4 | √ | | √ | | | | | | √ | |
| IFNG | √ | | √ | √ | √ | | √ | √ | | |

As shown above, some genes can be regulated by multiple STATs. We listed all of the genes that can be adjusted by this signaling pathway to better understand better the genes regulated by the JAK-STAT signaling pathway, as shown in Table 28. Interestingly, STAT1 and STAT3 can simultaneously regulate both cyclin-dependent kinase inhibitor 1A (CDKN1A) and tumor protein p53 (TP53). STAT5 can regulate cyclin-dependent kinase-4 inhibitor B (CDKN2B). CDKN1A encodes p21. Tumor protein 53 encodes p53, and CDKN2B encodes p14. P14, p21 and p53 are all closely related to the ageing process, and this result also suggests the importance of the JAK-STAT signaling pathway in the senescence process [293].

**Table 27: Drugs published for HGPS treatment.** Based on the literature, we summarized all of the medicines that show practical functions in the treatment of HGPS. There have been reports of using sodium salicylate, an NF-κB inhibitor, to inhibit the NF-κB signaling pathway. This result also corroborates the inference of the NF-κB signaling pathway in our data mining results. At the same time, no one has studied the role of the JAK-STAT pathway in HGPS so far, showing that our research is innovative.

| Treatment/Drug | Pathway | Target |
|---|---|---|
| All-trans retinoic acid | Autophagy | Progerin turnover |
| Antisense oligonucleotides | Access of splicingmachinery | Lamin C / prelamin A splicing &/or |

| | | |
|---|---|---|
| | | abnormal *LMNA* splicing |
| DOT1L inhibitors | Cell reprogramming | DOT1L |
| Isoprenylcysteine carboxyl methyltransferase (ICMT) knock-down = shICMT | Prelamin A processing | ICMT |
| Gene editing | CRISPR/Cas9 | LMNA sequence |
| JH4 | Progerin-lamin A/C binding | Progerin-lamin A/C binding |
| Metformin | Activation of AMPK | Hepatic gluco-neogenesis |
| Methylene blue | Mitochondrial biogenesis | Mitochondria function |
| MG132 (a proteasome inhibitor ) | Autophagy | Progerin turnover |
| Mono-aminopyrimidines | Prelamin A processing | Prelamin A farnesylation |
| N-acetyl cystine | Oxidative stress | Reactive oxygen species |
| caNRF2 | NRF2 reactivation | NRF2 |
| OSKM induction | Epigenetic remodeling | Partial cellular reprogramming |
| Pyrophosphate | Metabolism of extracellular pyrophosphate | Calcium-phosphate deposition |
| Rapamycin & analogs | Autophagy | Progerin turnover |
| Remodelin | Microtubule | NAT10 |
| Resveratrol | SIRT1 activity | SIRT1 |
| ***Sodium salicylate*** | ***NF-κB signaling*** | ***NF-κB inhibition*** |
| Stem cell transplantation | Stem cell function | Tissue regeneration |
| Sulforaphane | Autophagy | Progerin turnover |
| Telomerase | Telomere length | Telomeres [1] |

| | | |
|---|---|---|
| Vitamin D | Vitamin D receptor signaling | Vitamin D receptor |

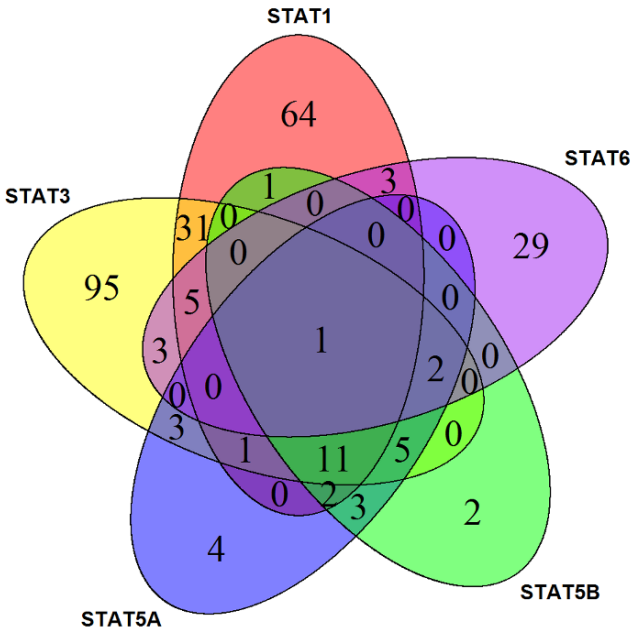


**Figure 8: Venn diagram of the STAT gene family.** The Venn diagram of the STAT family shows the number of genes regulated by different STATs, as demonstrated by the corresponding circles. Each gene was searched in the TRRUST version 2 (https://www.grnpedia.org/trrust/), TfactS (http://www.tfacts.org/) and Regulatory Circuits databases (http://regulatorycircuits.org/). Altogether, a total of 269 genes were found and curated to prevent repetitions due to aliases.

**Table 28: List of genes regulated by the JAK-STAT pathway.** Based on the literature and databases, all of the genes regulated by the JAK-STAT pathway were summarized.

| STAT1 | | STAT3 | | STAT1,3 | STAT3,5a,5b |
|---|---|---|---|---|---|
| ACAT1 | PSMB9 | AKAP12 | MDC1 | A2M | CCND1 |
| APOE | PTGFR | AKT1 | MIA2 | B3GAT3 | CCND3 |
| BAX | REV3L | BIRC5 | MICA | CCL2 | ESR2 |
| CASP4 | S100A10 | BST2 | MMP1 | CDKN1A | IGF1 |
| CCL3 | SCARB1 | CCL20 | MMP14 | CYP19A1 | OSM |

| | | | | | |
|---|---|---|---|---|---|
| CCR1 | STAT2 | CD46 | MMP2 | FAS | **STAT1,3,6** |
| CCR5 | STAT3 | CDH1 | MMP3 | FCGR1A | FOS |
| CD22 | TAP1 | CDK4 | MMP7 | FGF2 | IRF1 |
| CD40LG | TBX21 | CDKN1B | NANOG | GAST | OPRM1 |
| CD86 | TLR3 | CEBPB | NDUFA13 | HMOX1 | PTGS2 |
| CEBPD | TNFSF13B | CFB | NME1 | HSPB1 | SOCS1 |
| CEBPE | UPP1 | CFLAR | NOSTRIN | HSPCA | **STAT5a,5b** |
| CFTR | XAF1 | CHI3L1 | NR0B1 | ICAM1 | CEL |
| CIITA | **STAT6** | COPS5 | OAS1 | JAK2 | ESR1 |
| CLC | ADAM8 | CRP | OXTR | JAK3 | PAX5 |
| CSF1 | ADRA2B | CSRP1 | PAX3 | JUN | **STAT1,6** |
| CTSB | ALOX12 | CTGF | PGF | KRT17 | CD40 |
| CTSL | ALOX15 | CYR61 | PHB | MMP9 | EGR1 |
| CXCL10 | CCL17 | DDIT3 | PIAS3 | MUC4 | IL1R1 |
| CXCL9 | CCL26 | DNMT1 | POU2F1 | MYC | **STAT3,6** |
| EDN1 | CNR1 | ETV6 | PRDM1 | NOL3 | CCL11 |
| FCGR3A | COL1A1 | F2R | PTEN | NOS2A | CISH |
| FCGRT | COL1A2 | FAAH | PTPN6 | NOX5 | CXCL8 |
| FGFR3 | CYP2E1 | FASN | ROR1 | OPRM1 | **STAT1,5a,5b** |
| FOXP3 | CYSLTR1 | FGF1 | S1PR1 | REG1A | MET |
| GATA3 | DUSP1 | FGG | SAA1 | STRA13 | RNMT |
| GBP1 | EGLN3 | FGL1 | SALL4 | TIMP1 | **STAT1,3,5a,5b,6** |
| GLS | FCER2 | FLT3 | SHH | TLR2 | TNFRSF5 |
| HSP90AA1 | FOSB | GFAP | SLC9A3 | TNFRSF8 | |
| IFIT3 | HSD3B2 | HAMP | SOS1 | TP53 | |

| | | | | |
|---|---|---|---|---|
| IFNA1 | IL13 | HGF | STS | VIP |
| IFNB1 | IL24 | HIF1A | TERT | **STAT1,3,5a,5b** |
| IFNLR1 | IL4 | HP | TGFB1 | BCL6 |
| IL1B | IRF4 | HSPA4 | TNFRSF10B | EGFR |
| IL27 | ITGA2B | HSPCB | TP63 | IFNG |
| IRF7 | NCOA3 | IFNAR1 | TRH | IL2RA |
| IRF8 | ORMDL3 | IKBKE | TWIST1 | IL6ST |
| IVL | PRKCA | IL11 | TWIST2 | MUC1 |
| LTC4S | RHOA | IL1RN | TYK2 | PBF |
| LY96 | SELE | IL2 | UCP2 | PIM1 |
| MAT2A | SELP | IL21 | USP7 | PRF1 |
| MHC2TA | SIDT1 | JUNB | VDR | SEC6L1 |
| MMP13 | STAT1 | KIAA0146 | VEGFA | TIMP3 |
| MVP | **STAT5b** | KLF11 | VEGFB | **STAT3,5a** |
| NOS2 | ANGPTL4 | LBP | ZFP36 | IL10 |
| NOX1 | RARA | LCAT | **STAT5a** | BCL2 |
| NOX4 | **STAT1,5b** | LEP | CDKN2B | CCND2 |
| NR1H4 | PPARG | LGALS3BP | CSN2 | **STAT3,5a,5b,6** |
| PDCD1 | **STAT1,3,5a** | LTBP1 | SUMO1 | BCL2L1 |
| PLAU | IL6 | MCL1 | TRIP15 | TNF |

**Table 29: Genes regulated by STAT2 and other STATs simultaneously (✓ - regulated; ✖ - not regulated).**

| | STAT1 | STAT3 | STAT4 | STAT5a | STAT5b | STAT6 |
|---|---|---|---|---|---|---|
| APOE | ✓ | ✖ | ✖ | ✖ | ✖ | ✖ |
| IFIT3 | ✓ | ✖ | ✖ | ✖ | ✖ | ✖ |
| IFNA1 | ✓ | ✖ | ✖ | ✖ | ✖ | ✖ |
| IRF1 | ✓ | ✓ | ✓ | ✖ | ✖ | ✓ |
| IRF7 | ✓ | ✖ | ✖ | ✖ | ✖ | ✖ |
| NOS2 | ✓ | ✖ | ✖ | ✖ | ✖ | ✖ |
| PDCD1 | ✓ | ✖ | ✖ | ✖ | ✖ | ✖ |
| PML | ✓ | ✖ | ✖ | ✖ | ✖ | ✖ |
| PTGS2 | ✓ | ✓ | ✖ | ✖ | ✖ | ✓ |
| SCARB2 | ✖ | ✖ | ✖ | ✖ | ✖ | ✖ |

**Table 30: Genes regulated by STAT4 and other STATs simultaneously (✓ - regulated; ✖ - not regulated).**

| | STAT1 | STAT2 | STAT3 | STAT5a | STAT5b | STAT6 |
|---|---|---|---|---|---|---|
| AICDA | ✖ | ✖ | ✖ | ✖ | ✖ | ✖ |
| IFNG | ✓ | ✖ | ✓ | ✓ | ✓ | ✖ |
| IL2RA | ✓ | ✖ | ✓ | ✓ | ✓ | ✖ |
| IRF1 | ✓ | ✓ | ✓ | ✖ | ✖ | ✓ |
| MYC | ✓ | ✖ | ✓ | ✖ | ✖ | ✖ |
| NOX1 | ✓ | ✖ | ✖ | ✖ | ✖ | ✖ |
| NOX4 | ✓ | ✖ | ✖ | ✖ | ✖ | ✖ |
| PBF | ✓ | ✖ | ✓ | ✓ | ✓ | ✖ |
| PIM1 | ✓ | ✖ | ✓ | ✓ | ✓ | ✖ |

| | | | | | | |
|---|---|---|---|---|---|---|
| PRF1 | ✓ | × | ✓ | ✓ | ✓ | × |
| S100A4 | × | × | × | × | × | × |
| SOCS3 | ✓ | × | ✓ | × | × | × |
| STAT1 | - | × | × | × | × | ✓ |
| TBX21 | ✓ | × | × | × | × | × |

## 4.3. Cell-based ageing model to investigate normal and premature cellular ageing

### 4.3.1. Growth curves and cell senescence curves

We established a cell-based ageing model at the start of the research. In extensive studies, the passage number has been used as the main feature to define cell ageing status. However, for our case, this comparison is not reliable because HGPS cells and control cells have different ageing phases, and senescence states in the same passage as HGPS cells have a significantly lower growth rate than control cells, as previously reported [294]. Since the ageing of HGPS cells at the same passage is different from that of normal control cells, the proportion of senescent cells in total cells was directly used to compare the replication senescence of HGPS cells and normal cells. Therefore, an ageing model was established in vitro to track cellular lifespan. The model helped us to match the different passage numbers to the senescence ratio by comparing HGPS primary fibroblast culture and control culture at different passages. In cell culture, the loss of proliferation potential can be asynchronous. While cells still divide in later passages, cell growth inhibition may also occur in early passages. With this, we counted the growth rate and determined the percentage of senescent cells (SNS) at every passage to standardize our long-term replication senescence culture.

In this experiment, we investigated several ways to test the proportion of senescent cells, for

example, Sudan black B (SBB), beta-galactosidase (SA-β-Gal) and P21. The mechanisms of these methods are as follows: 1. Lipofuscin is an aggregate of oxidized proteins, lipids and metals, and it accumulates in ageing tissue. Sudan black B can specifically stain lipofuscin to black to mark senescence [295]. 2. The senescent cells usually become larger and express highly active beta-galactosidase at pH 6.0. This active enzyme can be detected with X-gal. This substance forms a dark blue product, 5-bromo-4-amyl blue, after cleaving β-galactoside. This blue staining is very easy to identify and quantify [296]. 3. The P21 gene is an essential member of the cyclin-dependent kinase inhibitor family discovered in recent years. It can inhibit the activity of cyclin-dependent kinase (CDKs) complex and coordinate the cell cycle, DNA replication and repair [297]. P21 is increased in senescent cells.

We conducted three parallel experiments on control fibroblasts and HGPS fibroblasts at the same time. All the experimental results showed that these three methods can adequately characterize the ageing state of cells and have good reproducibility, all of which increase with cell senescence. However, the observation of Sudan black B needs to be operated under a high-resolution, which is not conducive for large-scale counting to calculate the percentage of senescent cells to total cells. The P21 needs to be tested by Western blot, which requires higher experimental costs. At the same time, beta-galactosidase is the most classic indicator for measuring senescent cells, so we chose it to characterize the percentage of senescent cells and used P21 for validation.

As shown in Figure 9, all primary fibroblasts from different strains were initiated at passage 13, exhibiting less than 5% SNS as the percentages of all SNS were determined by beta-galactosidase assay. During the culture process of fibroblast replicative senescence, the growth rate of HGPS fibroblasts decreased after six to seven passages (corresponding to 19–20 passages) in vitro. At the same time, these cultures showed 5% to 8% SNS. However, at the same passage time (passages 19–20), the control cells maintained exponential growth, and their SNS were all below 5%. In general, the growth rate of HGPS fibroblasts and the control of fibroblasts are relatively similar when cells are young. As the fibroblast culture continues, control fibroblasts can support healthy growth for a long time before entering the

plateau phase, and then the growth rate decreases slowly. In comparison, HGPS fibroblasts not only enter the plateau phase earlier than control fibroblasts but also have a faster growth rate reduction.

HGPS cell line P003 reached 15% SNS at passages 21–22, and HGPS cell line P127 reached 15% SNS at passages 22–23, both of which were ageing faster than the control cell lines 1651C and 1652C, which achieved 15% SNS at passages 26–28 and 26–27, respectively. Similarly, P003 approached 30% SNS in passages 26–27, and P127 neared 30% SNS in passages 27–28. However, to achieve the same 30% SNS, control cells needed to be cultured until passages 36–38 for 1651C and passages 34–36 for 1652C. At the end of the culture, HGPS cells reached almost 80% SNS, while control cells had only 40% SNS. During this long-term cultivation process, the percentage of senescent cells was counted every other passage. When comparing the SNS rate from each passage, the number of HGPS cell lines was always higher than the control cell lines after 25 passages. Therefore, the senescence index of the culture was used as a critical parameter to evaluate the change relative to SNS in further studies when comparing HGPS cells with normal cells.

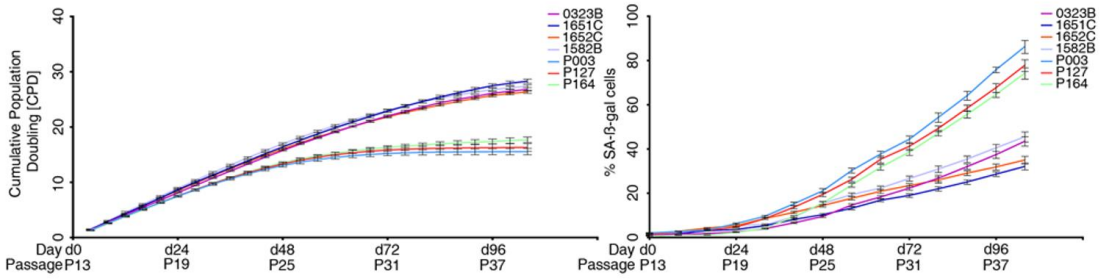


**Figure 9: Growth curves and cell senescence curves.** All cells are labelled with different colors, including four independent control cell strains (purple, blue, orange and grey) and the three HGPS cell strains (light blue, red, and turquoise). All cultures started at passage 13, with less than 5% of the percentage of SA-β-gal-positive cells in all cell strains. Proliferation rates were determined over 26 passages over 104 days. The percentage of SA-β-gal-positive cells was scored every other passage in cultures.

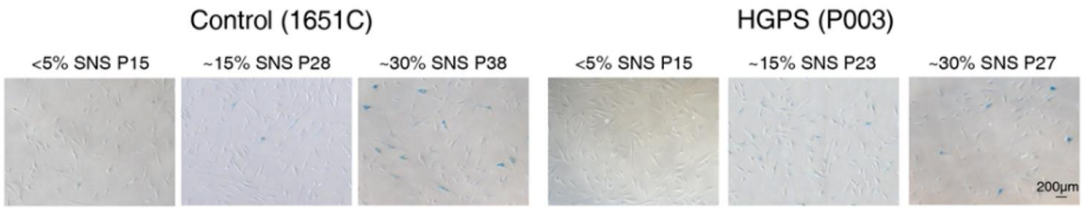


**Figure 10: The picture of SA-β-gal-positive cells.** The pictures show the cells with the SA-β-gal staining at 5%, 15% and 30% SNS. The SA-β-gal-positive cells are stained blue. Scale bar: 200 µm.

### 4.3.2. Cell cycle analysis

The cell cycle of HGPS and normal fibroblast cultures was measured while exhibiting ≤ 5% SNS and ≈ 30% SNS further to strengthen the application of the cell culture senescence index. The G1 phase is a pre-synthesis period, during which the cell mainly synthesizes RNA and ribosomes. In the S phase, DNA, histones and enzymes needed for DNA replication are synthesized. The G2 phase is the late stage of DNA synthesis. During this period, DNA synthesize ends, but the cell is still manufacturing a large amount of RNA and protein, including tubulin and protein. The M phase is a cell division phase. The cell divides from the mother cell into two daughter cells [298]. We chose young control cells as the standard because they grew well. As the number of senescent cells increased, the ratio of the G0/G1 phase increased significantly from 68.8 to 82.5, indicating that the cell's proliferative capacity decreased.

Similarly, when comparing HGPS fibroblasts with the control fibroblasts at the same 5% SNS, although the proportion of senescent cells included was the same, the reproduction ability of HGPS cells was lower than that of control cells. Similarly, when comparing 30% SNS, the proliferative capacity of HGPS cells was also lower. This result confirmed the stagnation of the G1 phase by senescent cells. The DNA damage in the senescent cells always causes irreversible p53-dependent cell cycle arrest in the G1 phase, accompanied by noticeable

morphological and biochemical changes.

The S phase is an essential period of DNA synthesis, and the reduction of the S phase is also a cardinal sign of slow cell growth, indicating that fewer cells enter S phase to synthesized DNA in preparation for cell replication [298]. When analyzing the four groups of results, when the SNS of the control cells was less than 5%, the proportion of the S phase was 22.7, the maximum among other groups. The S phase ratio of the HGPS cells at 5% SNS remained 19.3, and the control cells at 30% SNS equaled to 13.4, and the HGPS cells at 30% SNS was 5.6 as the lowest one. This confirmed that the control cell (5% SNS) had the fastest growth rate, and HGPS (5% SNS) remained similar. With the increase of the cell senescence, cell growth slowed down, and the proportion of the S phase was significantly reduced in both control cells and HGPS cells. The decrease of HGPS cells was more evident than that of control cells.

Usually, the G2/M phase ratio also decreased as cell ageing increased, indicating that fewer cells were being divided [299]. In the process of controlling cells from 5% SNS to 30% SNS, the G2/M phase decreased from 7.1 to 3.2, indicating that the growth and division rate of cells was slowing down. However, in HGPS cells, the G2/M phase did not decrease but rose from 4.2 to 8.0. This phenomenon may have been caused by DNA damage, which led the cells to stay in the G2 phase and further cause apoptosis selectively.

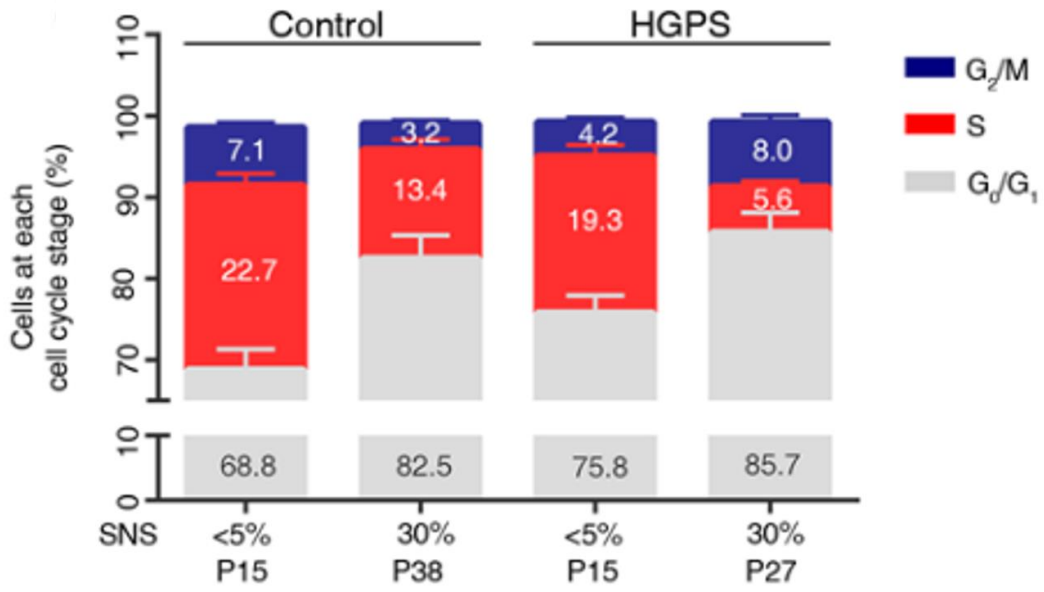

**Figure 11: Cell cycle assays.** The relative percentage of cells in the G0/G1, S and G2/M phases of the cell cycle are shown here. Cells samples are the normal (1651c) and HGPS (P003) cultures with a senescence index of < 5% and 30%. PI was used for DNA staining.

### 4.3.3. Western blot of P21 and progerin analysis.

Additionally, another classic senescence marker, namely P21, was studied to compare HGPS and control cultures at different senescence rates. P21 is cyclin-dependent kinase inhibitor 1, which can inhibit all cyclin/CDK complexes. It increases during the cell ageing process. As shown in the Figure 12, from young cells (5% SNS) to old cells (30% SNS), P21 increased by 2.9 times in 1651C, 2.4 times in 1652C, 2.8 times in P003 and 3.3 times in P127, supporting the increasing senescence index in different cell lines. However, HGPS and control cultures showed comparable p21 levels and similar SNS indexes at 5%, 15% and 30% SNS, indicating that the P21 expression was closely related to SNS index levels regardless of HGPS fibroblasts or control fibroblasts.

Progerin protein was also detected during the replicative ageing process as it accumulated and destroyed the nuclear structure of HGPS fibroblasts. According to the results of Western blotting, no progerin was probed in any passage of control cells. Still, as described in other references, a large amount of progerin accumulated in senescence HGPS cells [107]. From less than 5% SNS to about 30% SNS, the progerin level presented a 2.9-fold increase in P003 and a 3.1-fold increase in P127.

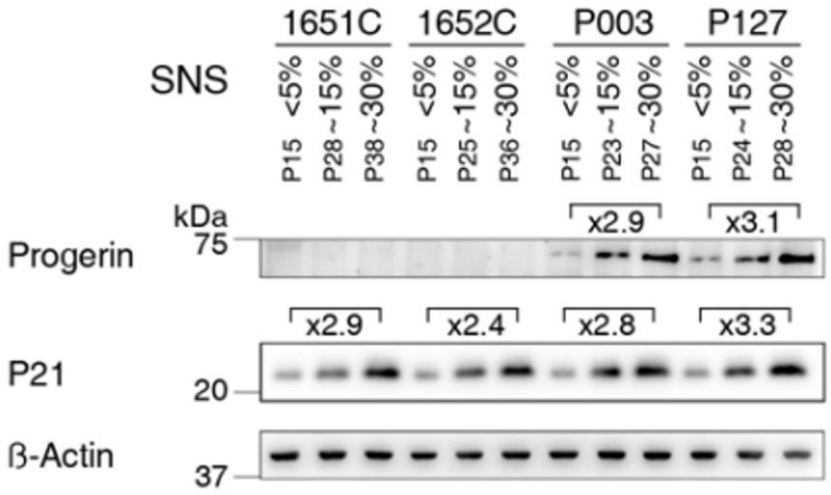


**Figure 12: The Western blot analysis of P21 and progerin.** The results exhibit the levels of p21 and progerin in control (1651c, 1652c) and HGPS (P003, P127) fibroblasts from cultures at the indicated percentages of senescence. All experiments were performed at least three times (n > 3).

## 4.4. Profiles of the 17 genes associated with vascular disease, arthritis, lipodystrophy and alopecia in the cell-based ageing model

The gene expression profiles of 17 essential genes were determined using an in vitro cell ageing model, of which the ageing rates were 5%, 15% and 30%. In normal and HGPS cultures, the direction and fold change of C3, CRP, FAS, IFNG, HMOX1, IGF-1, IL-6, IL-4, IL-18, PPARG, TGFB1, TNFa and TRAF1 expression levels are very similar regarding the comparable senescence index (Figure 13). Consistent with the text mining results, IGF-1 and PPARG decreased in both cell types of cultures at ≈ 15% and ≈ 30% SNS, and all other genes increased in both cell types of cultures at ≈ 15% and ≈ 30% SNS. The mRNA levels of CCL2/MCP1 (monocyte chemo attractant protein 1) were identified to rise at a more initial time point of 15% SNS in HGPS culture than in control cultures around 30% SNS. Compare to the control cells, HGPS cells had a higher level of ICAM-1 and CXCL8/IL-8 in cultures with around 30%

SNS. Nevertheless, the HGPS did not necessarily change more dramatically in all cases. A marked increase of LEP was found in normal cultures (≈ 30% SNS, 7.20-fold, p = 0.002) over HGPS cultures (≈ 30% SNS, 3.42-fold, p = 0.013).

To be more specific, the complement component C3-encoded protein performs a principal part in the activation of the complement system, no matter the classical or alternative complement activation pathways. Mature proteins were produced by alpha and beta subunits formed by the proteolytic process of the encoded proproteins. Well-known as the C3a allergic toxins, the C3a peptides can regulate inflammation and have antibacterial activity [300]. From young to senescent cells, C3 increased 3.2 times in 1651C, 2.2 times in 1652C, 1.9 times in P003 and 3.2 times in P127. The undifferentiated increase of C3 in HGPS cells and control cells indicates that C3 may increase with the rise of ageing, and this increase may be related to the inflammatory response.

The CRP gene-encoded protein refers to the pentaxin family. This protein can identify the host's external pathogens or broken cells and further participates in a variety of host defense-related roles. Therefore, the CPR level dramatically increases during an acute response to tissue damage, infection or other inflammatory motives [301]. CRP increased 3.0 times in 1651C, 2.1 times in 1652C, 2.2 times in P003 and 3.0 times in P127 from young to senescent cells. The simultaneous increase of CRP in HGPS cells and control cells indicates that CRP may increase with ageing. This development may be related to the acute response period of inflammatory stimuli.

The FAS-encoded protein is a constituent of the TNF receptor superfamily and carries a death domain. It plays a pivotal function in the physiological regulation of programmed death and is related to the pathogenesis of the immune system. The receptor binds to its ligand to form a cell death-inducing signaling complex, including FAS-related death domain protein (FADD), caspase-8 and caspase-10. The receptor can also activate NF-κB, MAPK3/ERK1 and MAPK8/JNK (c-Jun N-terminal kinase) signaling pathways [302]. With the increase of cell senescence, FAS increased 1.9 times in 1651C, 2.1 times in 1652C, 1.6 times in P003 and 1.8 times in P127. The rise of FAS is not related to the addition of progerin but only relevant to

ageing. Therefore, four different cell lines show almost the same fold increase. The increase in FAS may be related to increased apoptosis and inflammation in increased cell senescence. The heme oxygenase encoded by the HMOX1 gene is an essential enzyme in heme catabolism. HMOX1 can cleave heme to form biliverdin, which is then converted to bilirubin under the action of biliverdin reductase and a putative neurotransmitter like carbon monoxide. As a substrate, heme and various non-heme substances can induce heme oxygenase activity. Heme oxygenase appears in the form of two isozymes, one is inducible heme oxygenase 1, and the other is constitutive heme oxygenase 2 [303]. With ageing, HMOX1 increased 2.4 times in 1651C, 2.1 times in 1652C, 5.1 times in P003 and 7.3 times in P127, while SNS rose from 5% to 30%. However, at 5% SNS, the expression of HOMX1 in HGPS cells was much lower than that of control cells, indicating that HMOX1 may have a more direct relationship with progerin. The fold increase of HMOX1 in different SNS was higher in HGPS cells than in control cells of the same period. All of these results indicate that HMOX1 and progerin have a special relationship.

IFNG-encoded protein is a water-soluble cytokine belonging to the type II interferon class. Both the innate and adaptive immune system cells secrete this protein. When the protein is combined into a homodimer by the IFNG receptor, it triggers the cell's response to viral and microbial infections [304]. As the proportion of senescent cells increased, IFNG increased 3.4 times in 1651C, 2.9 times in 1652C, 3.3 times in P003 and 4.0 times in P127. The increase of IFNG with growing senescence may also be related to inflammation.

The protein encoded by IGF-1 is similar to insulin in structure and function and is a member of a family of proteins involved in mediating growth and development. IGF-1 is mainly produced by growth hormone to stimulate the liver; it plays an essential role in childhood growth and affects the anabolic metabolism in adults [305]. With the gradual ageing of cells, IGF-1 decreased by 70% in 1651C, 50% in 1652C, 50% in P003 and 50% in P127. Although the cell lines were different, the decreasing trend and amplitude of IGF-1 were the same, indicating that the decrease of IGF-1 was correlated with the increase in SNS, rather than the progerin level.

IL-6-encoded protein is a cytokine that plays a role in inflammation and B cell maturation. IL-6 is generated not only at the position of acute inflammation but also at the section of chronic inflammation. It is then secreted into the serum, inducing a transcriptional inflammation response through IL-6 receptor alpha. IL-6 is involved in many disease categories related to inflammation [306]. IL-6 increased 5.9 times in 1651C, 7.9 times in 1652C, 8.0 times in P003 and 8.7 times in P127 with the increasing senescence of HGPS fibroblasts and control fibroblasts. Notably, the increase of IL-6 in HGPS was slightly higher than that in control, which verifies that progerin prompts an expansion of IL-6 [306]. In HGPS, ageing is undoubtedly the cause of IL-6 increase and inflammation, but the progerin level increase is also an essential cause of the rise in IL-6.

IL-4-encoded protein is a cytokine secreted by activated type II T helper cells (Th2 cells) and is a ligand for the IL-4 receptor. The biological effects of IL-4 include stimulating the proliferation of activated B cells and T cells and differentiating CD4+ T cells into type II T helper cells. It also plays a crucial role in regulating humoral immunity and adaptive immunity. IL-4 induces the conversion of B cell antibody classes to IgE and upregulates the production of type 2 MHCs [307]. IL-4 increased 3.2 times in 1651C, 2.5 times in 1652C, 2.7 times in P003 and 3.5 times in P127 as cells entered senescence. The fold increase of IL-4 in HGPS and control cells was similar, which shows that the increase of IL-4 is closely related to ageing and has little correlation with progerin, further illustrating the immunity role in the ageing process.

IL-18-encoded protein, also known as interferon-gamma inducing factor, is a pro-inflammatory cytokine that enhances natural killer cell activity in spleen cells. It stimulates the production of IFNG in type I T helper cells. Many cell types, including hematopoietic cells and non-hematopoietic cells, have the potential to produce IL-18. IL-18 can regulate innate immunity and adaptive immunity, and its disorder can cause autoimmune or inflammatory diseases [308]. From 5% SNS to 30% SNS, IL-18 increased 4.0 times in 1651C, 3.9 times in 1652C, 4.0 times in P003 and 3.6 times in P127. These changes unrelated to progerin indicate that IL-4 increases with age and has less to do with progerin.

PPARG-encoded protein is a member of the peroxisome proliferator-activated receptor (PPAR)

subfamily of nuclear receptors involved to diabetes, atherosclerosis and cancer [309]. While cells aged from 5% SNS to 30% SNS, IL-18 decreased 50% in 1651C, 50% in 1652C, 50% in P003 and 60% in P127. This result indicates that PPARG also plays an important role in the ageing process, and it decreases with the development of ageing.

The protein transcribed by TGFB1 is a secreted ligand of the TGFB (transforming growth factor-β) superfamily. It leads to the recruitment and activation of SMAD family transcription factors that regulate gene expression after binding to the corresponding receptor. TGF-β regulates cell proliferation, differentiation and growth. It can also control the expression and activation of other growth factors (including interferon γ and tumor necrosis factor α), inducing the differentiation, chemotaxis, proliferation and activation of various immune cells [310]. As the ageing increased, TGFB1 increased 2.1 times in 1651C, 1.9 times in 1652C, 1.8 times in P003 and 1.5 times in P127. A similar increase in control and HGPS cells indicates that the rise in TGFB1 expression is directly related to ageing rather than to progerin.

The protein encoded by TNFa is a multifunctional, pro-inflammatory cytokine of the TNF superfamily. TNFa is secreted by macrophages binding to the receptor's tumor necrosis factor receptor superfamily member 1A (TNFRSF1A)/tumor necrosis factor receptor 1 (TNFR1) and tumor necrosis factor receptor superfamily member 1B (TNFRSF1B) to fulfil functions. These functions include cell proliferation, differentiation, apoptosis, lipid metabolism and blood coagulation. TNFa is associated with various autoimmune diseases and insulin resistance [311]. TNFa increased 2.1 times in 1651C, 1.9 times in 1652C, 1.8 times in P003 and 1.5 times in P127 with fibroblast senescence. This result indicates that the increase in TNFa may be closely related to ageing and inflammation.

TRAF1 protein, encoded by the TRAF1 gene, and TRAF2 protein form a heterodimeric complex, which is highly required for the activation of MAPK8/JNK and NF-κB mediated by TNFa. The protein complex built by this protein and TRAF2 also interacts with the overcome inhibitor protein (IAP), thereby mediating the antioxidant signal of the TNF receptor [312]. TRAF1 increased 2.1 times in 1651C, 1.9 times in 1652C, 1.8 times in P003 and 1.5 times in P127 while the SNS of the cell increased from 5% to 30%. The increase of TRAF1 is not highly related

to the expression of progerin but is closely associated with the development of ageing.

The protein encoded by the CCL2 gene is also known as monocyte chemoattractant protein 1 (MCP1) and small inducible cytokine A2. Belonging to the CC chemokine family, CCL2 is a small cytokine that has chemotactic activity against monocytes and basophils. However, CCL2 has no chemotactic activity on neutrophils or eosinophils. CCL2 recruits monocytes, memory T cells and dendritic cells to the site of inflammation caused by tissue damage or infection [313]. In HGPS cells, 15% SNS showed a significant increase in CCL2 levels compared to 5% SNS. In control cells, the CCL2 level at 15% SNS did not increase significantly from 5% SNS. This result indicates that the increase of CCL2 may be related not only to ageing but also the progerin level.

The ICAM-1 code generates intercellular adhesion molecule 1, also known as CD54 (Cluster of Differentiation 54). ICAM-1 is a cell surface glycoprotein expressed on endothelial cells and immune system cells. Normally, ICAM-1 binds to CD11a/CD18 or CD11b/CD18 integrins [314]. With fibroblast ageing from 5% SNS to 30%, ICAM-1 increased by 5.8 times in 1651C, 4.5 times in 1652C, 7.7 times in P003 and 6.8 times in P127. Although the stage of senescence was the same, the increase in HGPS cells was more obvious than the increase in control cells, which shows that ICAM-1 may not only be related to ageing but also increasing progerin.

The protein encoded by CXCL8/IL-8 is a member of the CXC chemokine family and the primary mediator of the inflammatory response. Macrophages and neutrophils are the primary producers of secreting CXCL8, an essential immune response medium in the innate immune system. This chemokine is also an effective angiogenesis factor. Cells show that there are many receptors on the membrane that can bind to IL-8. The most common are G protein-coupled serpentine receptors C-X-C motif chemokine receptor 1 and C-X-C motif chemokine receptor 2, and IL-8 has a stronger affinity for C-X-C motif chemokine receptor 1. [315]. With the increase of senescence, CXCL8 increased 4.3 times in 1651C, 1.7 times in 1652C, 17.4 times in P003 and 18.8 times in P127. Although control fibroblasts and HGPS fibroblasts had the same percentage of senescence, the expression of CXCL8 in HGPS cells was significantly higher than that of control cells, which indicates that the appearance of CXCL8 is not only

related to ageing but also the increase of progerin.

The protein encoded by LEP is secreted by white adipose cells and then enters the systemic circulation. This protein plays a principal role in regulating energy homeostasis. When circulating leptin binds to leptin receptors in the brain, it inhibits consumption and promotes energy expenditure. In addition, leptin is also involved in the regulation of immune and inflammatory reactions, haematopoiesis, angiogenesis, reproduction, bone formation and wound healing [316]. During the process of SNS increasing from 5% to 30%, LEP increased by 7.5 times in 1651C, 5.9 times in 1652C, 4.0 times in P003 and 3.9 times in P127. The results indicate that LEP is not only related to ageing but also the expression of progerin.

In summary, in HGPS and control cells, changes in 17 genes during replication senescence were consistent with text mining predictions. Interestingly, both control cells and HGPS cells showed similar pro-inflammatory secretory phenotypes during the replication ageing process. Although HGPS cells entered senescence earlier than normal cells, once the cells had the same ageing section, the expression of these 17 essential genes remained similar. Therefore, the increase of most genes is not necessarily directly generated by the rise of progerin, but the surge of progerin causes cells to age, and the ageing process leads to an increase in these genes. However, some of these genes are affected by both the progerin and ageing.

(a)

| Cell line | ≤ 5% SNS (0 - 5%) | ~15% SNS (13 - 17%) | ~30% SNS (28 - 32%) |
|---|---|---|---|
| 1651C | Passage ≤ 20 | Passage 26-28 | Passage 36-38 |
| 1652C | Passage ≤ 19 | Passage 26-27 | Passage 34-36 |
| P003 | Passage ≤ 18 | Passage 21-22 | Passage 26-27 |
| P127 | Passage ≤ 18 | Passage 22-23 | Passage 27-28 |

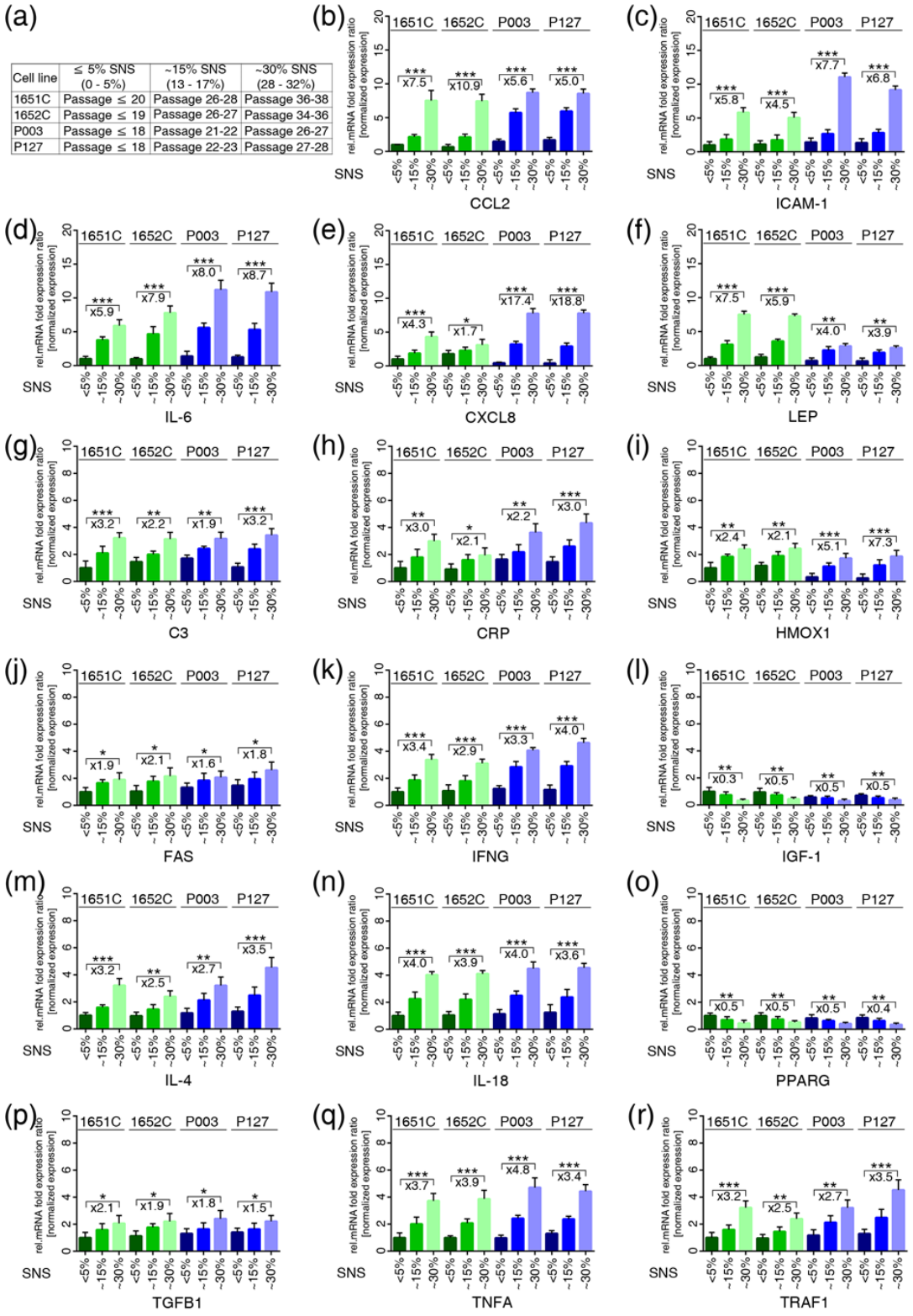


**Figure 13. Quantitative real-time PCR analysis of the 17 genes identified by text mining in normal and HGPS cells during replicative senescence.** (a) Table showing the cell strains and the percentage of the corresponding

passage of senescence (SNS). (b–r) mRNA levels of the indicated genes were determined in controls (GMO1651c, and GMO1652c) and HGPS (HGADFN003 and HGADFN127) cell strains at the indicated percentage of senescence (SNS). Relative expression was normalized to the expression of GAPDH. Graphs show the mean ± SD (★ $p$ <0.05, ★★ $p$ <0.01, ★★★ $p$ <0.001, n > 3). The mean fold changes between 5% and 30% SNS for control and HGPS are indicated.

## 4.5. Overactivation of JAK-STAT signaling during replicative senescence in normal and HGPS fibroblasts

From the 17 critical genes mentioned above, it is easy to find that the expression of inflammatory cytokines increases as the cell ageing process develops. These results correspond to the data mining predictions. According to data mining, most of these 17 genes are related to the NF-κB or JAK-STAT pathway. Therefore, the NF-κB or JAK-STAT pathway may play an essential role in the development of cell ageing. According to the reference, sodium salicylate as an NF-κB inhibitor has been studied in premature ageing cells and shows a good effect on alleviating ageing [317].

At the same time, when we examine genes related to the NF-κB or JAK-STAT pathway, none of them can regulate the C3 gene, but they can all control CCL2, CRP, CXCL8, FAS, HMOX1, ICAM-1, IL-6, PPARG, TGFB1, TNF, IL-4 and IFNG. However, the JAK-STAT pathway cannot regulate IL-18 and TRAF1, while NF-κB can manage it. NF-κB cannot regulate IGF-1 and LEP, but the JAK-STAT pathway can. Controls and HGPS cultures with similar senescence indexes had the same direction and fold change in IGF-1, IL-18 and TGFB1, indicating that the relationship between these genes and ageing is more direct, whether the ageing is caused by the progerin or not. Meanwhile, LEP is not only related to senescence but also the level of progerin. Therefore, there is reason to believe that the JAK-STAT pathway may play an indispensable role in reducing the cellular ageing of control and HGPS cells.

Subsequently, we used qPCR to study the expressions of JAKs and STATs in the JAK-STAT pathway, which is a crucial regulator of cytokine production. The mRNA expression results show that in normal cells and HGPS cells, the mRNA levels of JAK1, JAK2, STAT1 and STAT3 increased with the development of cell ageing. From 5% SNS to 30% SNS, JAK1 expression increased in various cell lines, with a 2.4-fold increase in control cells and a 2.7-fold increase in HGPS cells. Unlike JAK1, which had similar expression levels between different cell lines, the initial mRNA levels of JAK2 in each cell line were altered. For example, compared to several other control cell lines, the expression of 1582B was significantly lower than other cell lines, and the trend of 1582B was to increase first and then decrease. The changing pattern of all other cell lines was the same as the increase. The fold change of control cells and HGPS cells was 2.9 times.

Subsequently, we examined the gene expression of different STATs. Because cell lines are different, the initial expression at the young passage of each STAT is also different. For example, at 5% SNS, the control cell 0323B had a significantly higher STAT1 expression than other cell lines. At different ageing stages, the expression of STAT4 in P164 cells was substantially higher than that of other cell lines. Meanwhile, the expression of STAT4 in control cell 0323B was also significantly higher than that of other cell lines but not as high as P164. Even if the cell lines are different, most cells have a similar trend when senescence goes from 5% to 30%. For example, in control cells, STAT1 increased 5.4 times, STAT3 increased 3.8 times, STAT5A increased 2.0 times and STAT5B increased 1.9 times. In HGPS cells, STAT1 increased 5.8 times, STAT3 increased 3.5 times, STAT5A increased 1.9 times and STAT5B increased 2.0 times. JAK3, TYK2 and other STATs did not show significant changes in either cell types. Compared with previous data mining results, STAT3 is involved in the regulation of 12 genes, STAT1 is incorporated with the control of nine genes, STAT5A is related to four genes, and STAT5B is involved in the regulation of four genes, and STAT6 implicates in the provision of two genes. These findings indicate that JAK1/2-STAT1/3 signaling has a potential role in normal and HGPS cell ageing.

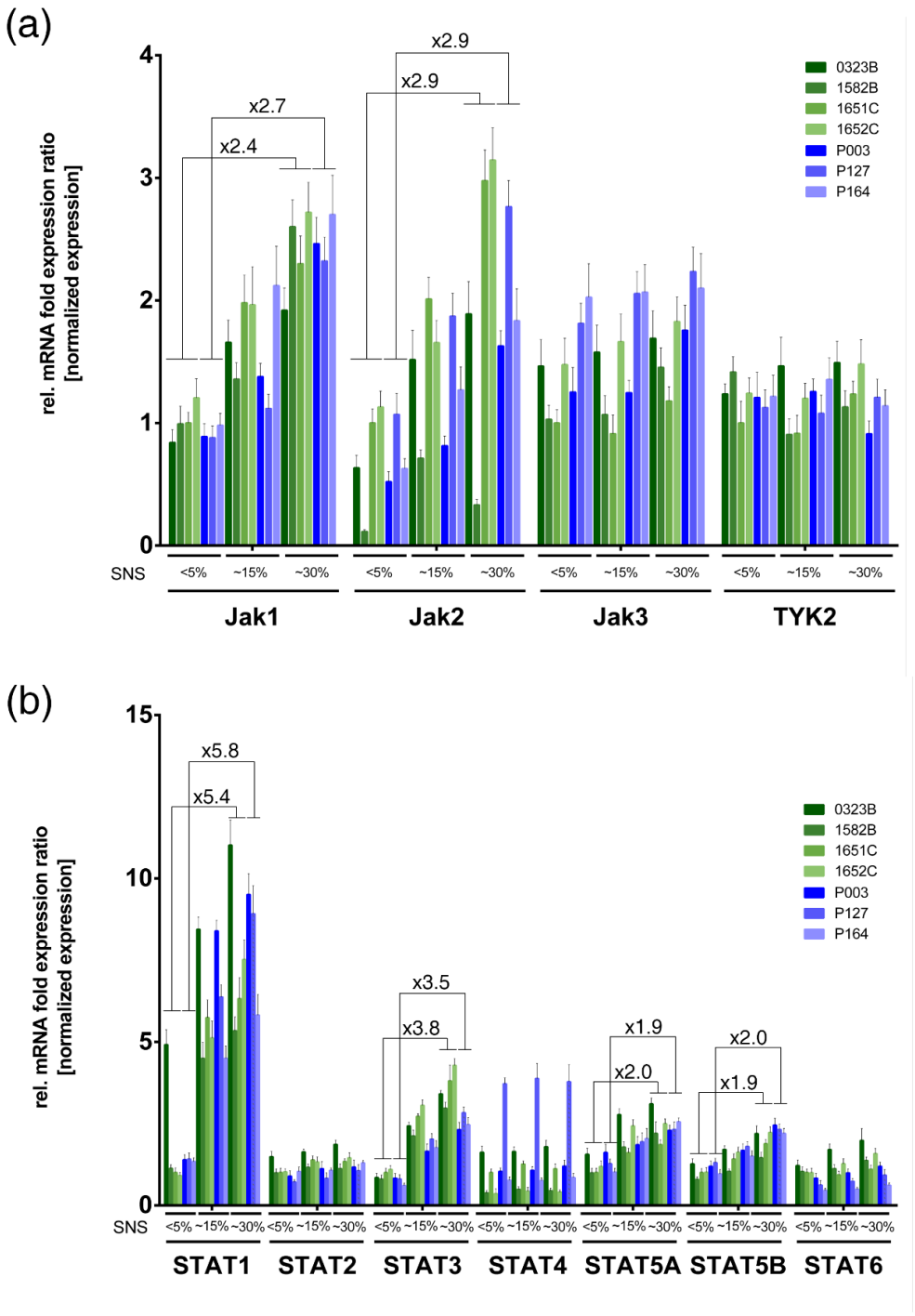


**Figure 14: Real-time PCR analysis of the JAKs and STATs gene families in control and HGPS cells.** (a) The mRNA levels of JAK1, 2, 3 and TYK2 in control (GMO1651c, GMO1652c, GMO1582B, and GMO0323B) and HGPS (HGADFN003, HGADFNP127, and HGADFNP164) cells from cultures of the indicated senescence index. (b) The mRNA levels of STAT1, 2, 3, 4, 5a, 5b and 6 in the control and HGPS cell strains like above. Relative expression

was normalized to the GAPDH expression. We only calculated the indicated fold change due to the heterogeneity in the expression levels between cell strains.

Increased gene expression is a reliable predictor of the activation of the JAK-STAT signaling pathway. However, the adequate activation of the JAK-STAT pathway not only depends on the increase of corresponding proteins but also, more importantly, the phosphorylation of the proteins. Therefore, we employed Western blot to assess JAK1, JAK2, STAT1 and STAT3 protein levels during the ageing process. The expression of JAK1 protein in young cells with less than 5% SNS varied with cell lines. For example, the expression level of JAK1 in 1651C and P127 was significantly lower than that of 1652C and P003. Therefore, the initiator level of JAK1 was irrelevant to the cell strains of control or HGPS. Specifically, during the ageing process from 5% to 30%, 1651C increased 2.3 times, 1652C decreased 20%, P003 increased 1.3 times and P127 increased 1.1 times. Accordingly, the result showed that the JAK1 level did not produce notable differences throughout replicative senescence (≈ 15%, ≈ 30% SNS). On the contrary, the protein levels of JAK2 increased with cellular ageing in control and HGPS cells. Notably, the expression of JAK2 in HGPS was also higher than that of control cells in the early cell stages. More importantly, the JAK2 protein levels of various cell lines increased when the senescence rate rose from 5% to 30%. For example, control fibroblast 1651C increased 3.9 times and 1652C increased 6.5 times. HGPS fibroblast 003C increased 3.7 times and P127 increased 5.0 times.

The activated JAK-STAT pathway requires phosphorylated STAT to perform the functions. Subsequently, we measured the expression of STAT1 and STAT3 during replicative ageing. The results showed that both STAT1 and STAT3 increased with the increasing percentage of old cells and increased whether the cells expressed progerin or not. For STAT1 expression, 1651C increased by 8.0 times, 1652C increased by 3.4 times, P003 increased by 2.0 times and P127 increased by 3.1 times. It seems that the STAT1 of the 1651C cells increased the most, but this may have been because the young 1651C cells had the lowest initial expression. For STAT3 expression, 1651C increased by 3.3 times, 1652C increased by 2.5 times, P003 increased by

1.8 times and P127 increased by 2.1 times. It is not difficult to find that the change of STAT1 protein levels is more evident than that of STAT3.

The literature shows that after the activation of JAK1/2, STAT1 is phosphorylated on tyrosine residue 701, and STAT3 is phosphorylated on tyrosine 705 [318]. Phosphorylated STATs can form heterodimers or homodimers, transfer into the nucleus and activate the transcription of its target genes, such as FAS, IL-6 and IFNG, in the 17 genes mentioned above [319]. Consequently, we further investigated the expression of p-STAT1 and p-STAT3. As the cell senescence degree increased, the expression of p-STAT1 increased by 5.3 times in 1651C, 3.7 times in 1652C, 2.7 times in P003 and 5.0 times in P127. Among them, the initial phosphorylation value of P003 cells was significantly higher than in other groups. This result corresponds to a higher STAT1 quantification of P003 cells than other groups. At the same time, the expression of p-STAT3 increased by 11.6-fold in 1651C, 3.5-fold in 1652C, 2.9-fold in P003 and 5.4-fold in P127. Among them, the initial phosphorylation value of P003 cells was significantly higher than in other groups. This result corresponds to a higher STAT3 amount of P003 cells than other groups. The rapid increase of phosphorylation in 1651C may also be related to the initial value of young cells being lower than other groups with 5% SNS.

Therefore, the above results indicate that regardless of healthy cells or HGPS cells, the phosphorylation levels of STAT1 and STAT3 increase during the cellular ageing process. Overall, the above results indicate that the JAK-STAT pathway is over-activated and is directly related to cell ageing. This association occurs in HGPS cells and control cells in different degrees.

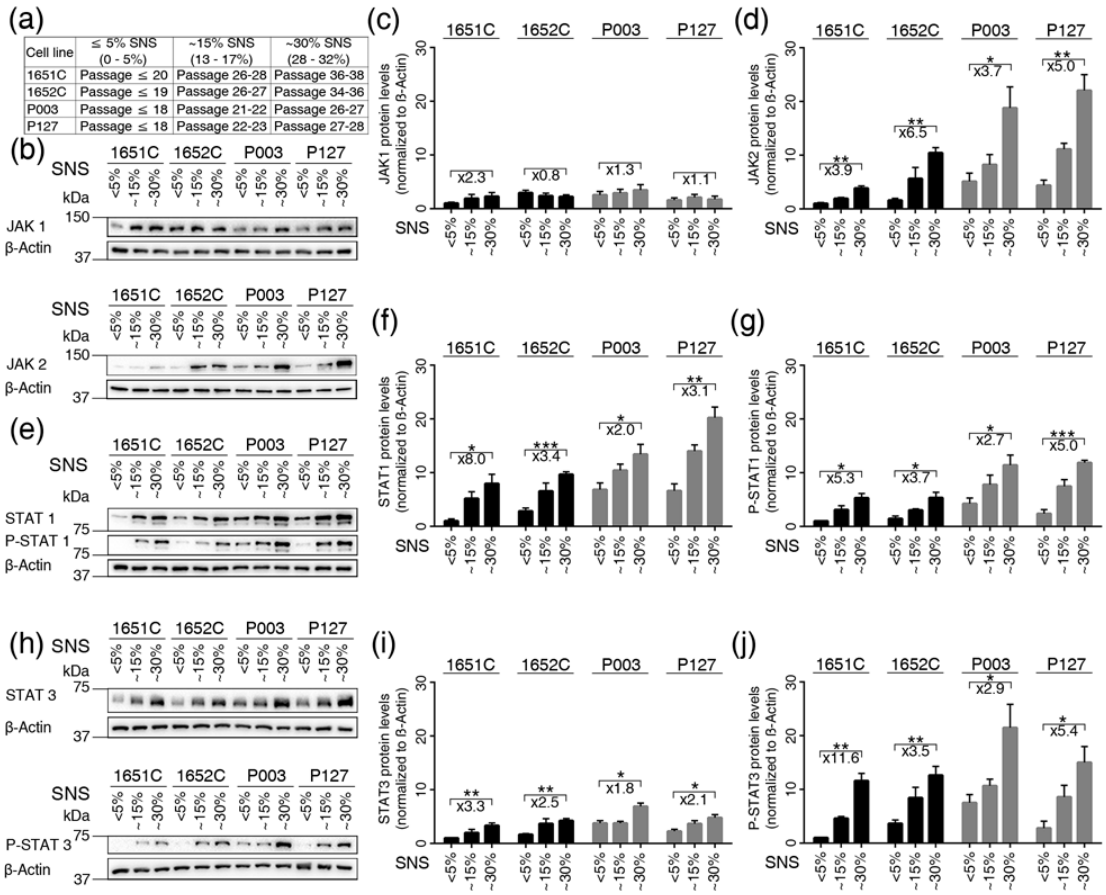


**Figure 15: Status of the JAK-STAT signaling pathway in control and HGPS cells during replicative senescence.**

(a) Table showing the cell strains and the passages corresponding percentages of senescence (SNS). (b, e , h) Representative Western blot images for JAK1/2, STAT1/3, p-STAT1 (tyr701), p-STAT3 (tyr705) and β-actin in control (GMO1651c and GMO1652c) and HGPS (HGADFN003 and HGADFN127) cell strains at the indicated percentages of senescence. (c) Quantification of JAK1, (d) JAK2, (f) STAT1, (g) p-STAT1, (i) STAT3 and (j) p-STAT3. Graphs show the mean ± SD. (★ $p$ <0.05, ★★ $p$ <0.01, ★★★ $p$ <0.001, n > 3). Fold changes between the samples with 5% and 30% senescence are indicated.

## 4.6. Baricitinib, a specific inhibitor of JAK1 and JAK2, efficiently blunts STAT1 and STAT3 activation

As cells aged, the JAK1/2-STAT1/3 pathway became getting over-activated in both control and

HGPS fibroblasts, activating most of the 17 related genes mentioned above. Then, the cytokines produced by these genes boosted the senescence of other cells around this senescent cell, leading to an overall accelerated cellular ageing. Therefore, we selected the small molecule compound baricitinib to mitigate this process. Baricitinib is a reversible inhibitor that selectively inhibits JAK1 and JAK2 kinases [320]. First, we evaluated the cytotoxicity of baricitinib on young 1651C cells. There were several reasons for choosing this cell condition for investigation: 1. From the results mentioned above, senescent cells have higher expressions of p-STAT1 and p-STAT3 than young cells. If we selected senescent cells as the experimental subjects, baricitinib would reveal the cytotoxicity and show therapeutic effects to alleviate ageing. Therefore, we decided to use young cells to assess the cytotoxicity effect of baricitinib to obtain an objective determination as the therapeutic effects prevent cell death. 2. Similarly, in the early stage (SNS <5%), the p-STAT1 and p-STAT3 of HGPS are also higher than the corresponding values of the control cells. It cannot avoid the possible therapeutic effect of baricitinib, which leads to a particular remission role of cell ageing. Therefore, the measurement of baricitinib on HPGS cells will evaluate the corrective impact of baricitinib rather than the cytotoxicity. 3. Even young HGPS cells will express a certain amount of progerin. The expression of progerin will affect the function of many signaling pathways, rather than only the JAK-STAT pathway. Therefore, we could not prevent baricitinib from affecting other signaling pathways. 4. The control fibroblast 1651C at less than 5% SNS has lower expression levels of JAK1, JAK2, STAT1, STAT3, p-STAT1 and p-STAT3 than that of the 1652C. Collectively, we chose control fibroblast 1651C (<5% SNS) as the experimental target. We used the CellTox™ Green Cytotoxicity Assay Kit to detect the cytotoxicity of baricitinib against GMO1651C in control fibroblasts. Cells were treated with different concentrations of baricitinib (Mock, 0.125 μM, 0.25 μM, 0.5 μM, 1 μM, 2 μM, and 4 μM) and incubated for 24 and 48 hours before measuring the cytotoxicity. As described from the results, the cell deaths from 0.125 μM, 0.25 μM, 0.5 μM and 1 μM baricitinib treatment all remained at about 1% after 24 hours or 48 hours, and there was no significant cells death increase over the mock group. While the concentration continued to increase, the cytotoxicity of baricitinib

presented at 2 µM. Meanwhile, the 4 µM baricitinib group displayed more potent cytotoxicity. Simultaneously, the average percentage of cell death from each group after 48 hours was slightly higher than the average rate corresponding to 24 hours, but there was no significant difference. Therefore, in future studies, we would choose 1µM baricitinib as the target concentration because it is the highest concentration that shares cytotoxicity similar to the mock group.

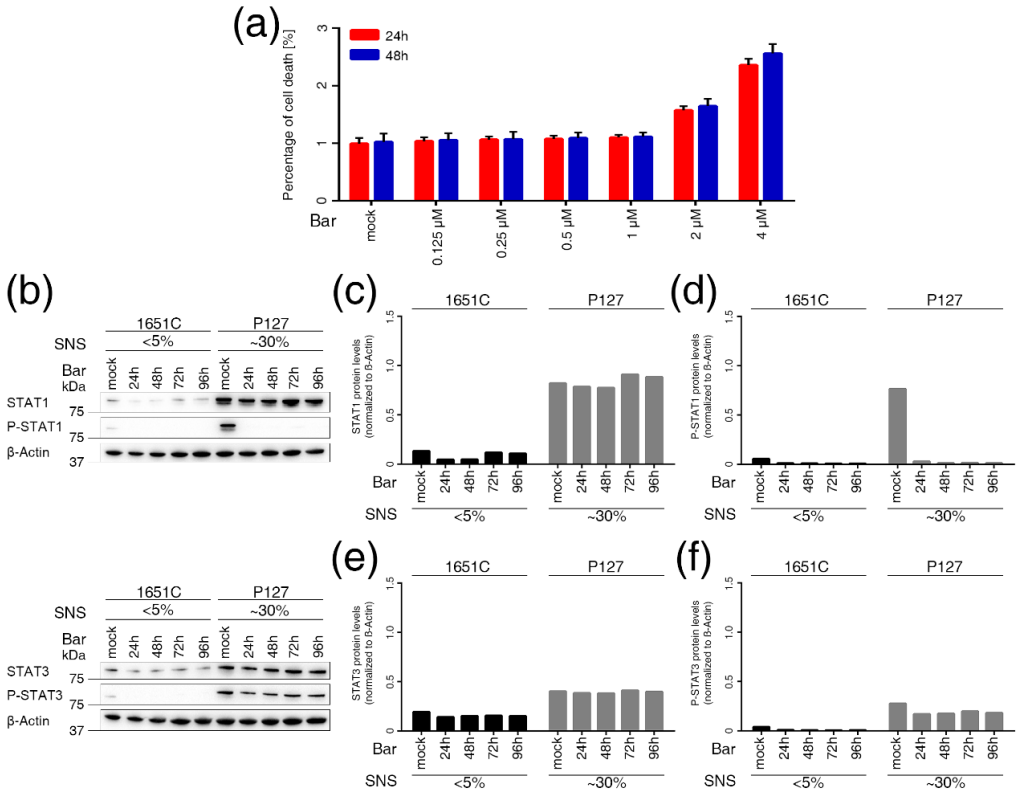


**Figure 16: Cytotoxicity and stability of baricitinib in a cell-based ageing model.** (a) Cell cytotoxicity was determined by the CellTox™ Green Cytotoxicity Assay kit in control fibroblasts GMO1651C. Cells were treated with baricitinib at different concentrations (0.125 µM, 0.25 µM, 0.5 µM, 1 µM, 2 µM, 4 µM) for 24 and 48 hours. (b) Representative Western blot images for STAT1/3, p-STAT1/3 and β-actin in the control (GMO1651) and HGPS (HGDFN127) cells at the indicated senescence index that were treated with baricitinib or DMSO for an indicated period without medium change. (c-f) Quantifications of STAT1/3 and p-STAT1/3 are shown. Graphs show the mean (n>3).

Subsequently, we verified the stableness and effectiveness of baricitinib for inhibiting the JAK-STAT pathway, or whether it can effectively inhibiting the phosphorylation of STAT1 and STAT3. The administration process lasted four days in total, without changing the medium within that time. We selected 1651C in the young state (< 5% SNS) and P127 (> 30% SNS) in the senescence phase for the experiment administration. Because the expression of p-STAT1 and p-STAT3 in 1651C (< 5% SNS) was deficient, it could be used as a control to estimate whether baricitinib can effectively inhibit the high expression of p-STAT1 and p-STAT3 in P127 (~ 30% SNS).

The experimental results showed that baricitinib has a powerful and effective inhibitory effect on p-STAT1, which can reduce the expression of p-STAT1 by 90% until 96 hours. At the same time, baricitinib also has a distinct inhibitory effect on p-STAT3, which considerably reduces the appearance of p-STAT3 until 96 hours. However, there was no significant effect on the expression of STAT1 and STAT3 treatment after baricitinib. Therefore, treating the young control fibroblasts 1651C and the senescent HGPS fibroblasts P127 with 1 μM baricitinib for 96 hours without changing the culture medium indicates that baricitinib can stably and effectively inhibit JAK1/2 and further inhibit the phosphorylation of STAT1/3. This result matches the report from the literature.

Afterwards, in order to estimate the inhibitory effect of long-term baricitinib use on the JAK-STAT pathway, we chose the control and HGPS cells with less than 5% SNS for studying the changes in the JAK-STAT signaling pathway after taking baricitinib for 30 days. The experimental results showed that JAK1 and JAK2 protein levels had a slight downward trend after baricitinib treatment, but the changes were not remarkable. After one month of treatment, the expression level of STAT3 sill remained consistent, while the protein level of STAT1 rose slightly after the treatment procedure. Among them, 1651C increased by 34%, and 1652C increased by 36%, P003 increased by 44%, while P127 increased by 20%. However, after the administration of baricitinib, the expression of p-STAT1 and p-STAT3 in control cells and HGPS cells all decreased. For p-STAT1, 1651C decreased by 68%, 1652C reduced by 67%, P003 lowered by 79% and P127 diminished by 72%. For p-STAT3, 1651C decreased by 89%,

1652C reduced by 87%, P003 declined by 93% and P127 shrank by 94%. It is clear that the p-STAT1 and p-STAT3 cells reduced in each group after baricitinib treatment. These results indicate that baricitinib treatment can effectively inhibit the JAK1/2-STAT1/3 signaling pathway in control cells and HGPS cells for long-term treatment.

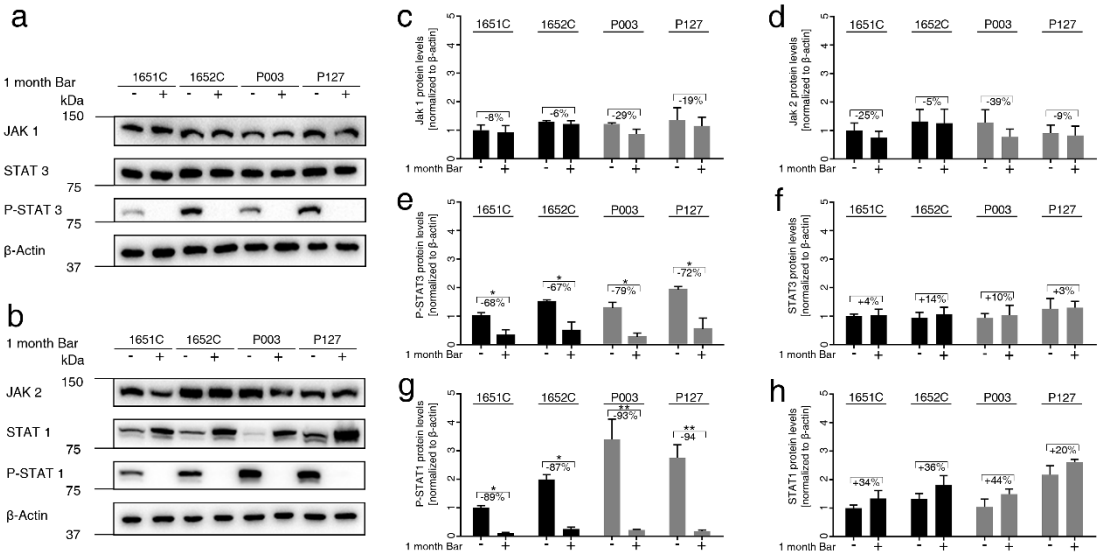


**Figure 17: Status of the JAK-STAT signaling pathway in normal and HGPS cells treated with 1 µ M baricitinib.** (a, b) Representative images of Western blots for JAK1/2, STAT1/3, p-STAT1/3 and β-actin in normal (GMO1651c, and GMO1652c) and HGPS (HGADFN003, and HGADFN127) cells treated as indicated. Cultures exhibiting <5% senescence were treated with baricitinib or DMSO for one month. (c) Quantification of JAK1, (d) JAK2, (e) p-STAT3, (f) STAT3, (g) p-STAT1 and (h) STAT1. Graphs show the mean ± SD. Protein levels were compared by two-tailed t-test (★ $p$ <0.05, ★★ $p$ <0.01, ★★★ $p$ <0.001, n > 3).

## 4.7. Inhibition of JAK1 and JAK2 ameliorates age-related cellular changes in normal and HGPS cells

The experimental outcomes revealed that during a 30-day administration period, baricitinib

could effectively inhibit the JAK1/2-STAT1/3 pathway for a long time. At the same time, the excessive activation of this signaling pathway is also closely related to ageing. Therefore, both the short-term administration of seven days and the long-term administration of 30 days of baricitinib have therapeutic effects of delaying ageing-related cell changes. To evaluate baricitinib's impact on improving the changes that occur during cellular ageing, we selected control and HGPS cultures with initial states of 5% SNS and 15% SNS, respectively. According to the previous cell senescence curve under normal circumstances, the young cells with < 5% SNS from both control and HGPS cell lines regularly reach about 15% SNS after 30 days. Therefore, this process can well characterize the baricitinib process of preventing young cells from ageing.

Meanwhile, control cell cultures starting at 15% SNS will reach about 30% SNS after 30 days, and HGPS cell cultures end at nearly 50% SNS after 30 days when beginning at 15% SNS. This process can help us to study the effect of baricitinib on senescent cells. We were reluctant to use 70% SNS cells as the research object for the senescent cells. When most cells are senescent, the apoptosis and other signal pathways of cells are also activated, which would affect our results.

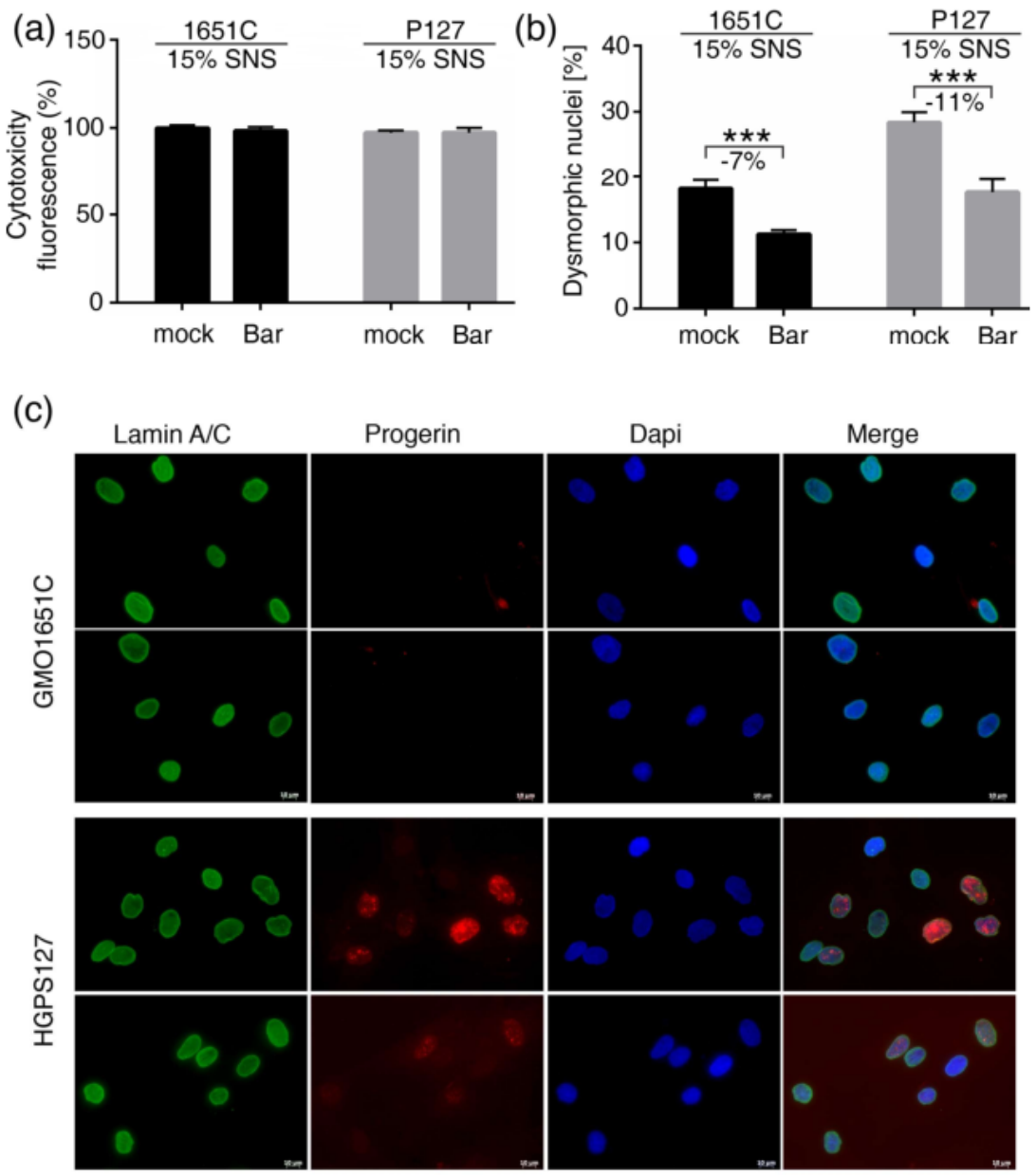


**Figure 18: Baricitinib treatment ameliorates HGPS nuclear morphology.** ( a ) Cell cytotoxicity was determined using CellTox™ green cytotoxicity assay on mock-treated or baricitinib-treated control (GMO1651C) and HGPS (HGADFN127) fibroblasts at the indicated senescence index (48 hours treatment). (b) The frequency of misshapen nuclei (dysmorphic) after 20 days of treatment with either DMSO or 1.0 µM baricitinib. An average of 1000 nuclei was examined for each condition, and each experiment was repeated three times. (c) Immunochemistry was performed on mock-treated or temsirolimus-treated control (GMO1651C) and HGPS

(HGADFN127) fibroblasts after 20 days using antibodies against the indicated proteins (lamin A/C, and progerin). Representative images are shown. Scale bar: 10 μm.

First, we tested the cytotoxicity of 1 μM baricitinib administration to 15% SNS control and HGPS cells to ensure that the experimental process was not affected by the cytotoxicity generated by baricitinib. The results showed that after treating the control cells 1651C and HGPS cells P127 for 48 hours, neither group of cells showed significant cytotoxicity, so it was suitable for the following research. The result of the population doubling after treatment showed that baricitinib treatment significantly increased the growth rate in the one-week and one-month groups. Specifically, after one week of administration, the control cells containing 5% SNS increased population doubling (PPD) by 10%, HGPS cells containing 5% SNS increased PPD by 14%. The 15% SNS control cells increased PPD by 19%, and 15% of SNS HGPS cells increased PPD by 17%. Corresponding to the one-month treatment, the 5% SNS control increased PPD by 12%, and the 5% SNS HGPS increased PPD by 22%. The 15% SNS control increased PPD by 18%, and the 15% SNS control increased PPD by 23%. Overall, these results indicate that baricitinib treatment can accelerate the growth rate of cells, showing a beneficial effect on cell growth. In each group's changes, the growth rate change of senescent cells was more significant than that of young cells. The growth rate adjustment of HGPS cells was more distinguished than that of control cells, and the growth rate improvement of long-term administration was more significant than that of short-term treatment. These results may be due to the excessive activation of the JAK-STAT pathway caused by the increasing number of senescent cells, the progerin expression in HGPS and the long-term culture leading to more replicative senescence. This result shows that whether the decrease in the growth rate is due to the normal replication senescence or the abnormal expression of progerin, the administration of baricitinib can significantly relieve this process.

In terms of slowing down cell ageing, baricitinib also shows an alleviation of the increasing senescence. We treated 5% and 15% of the control and HGPS cells with 1 μM of baricitinib for one week and one month, respectively, and then compared the percentage of cell

senescence reduction in the baricitinib to that of mock groups.

The short-term, one-week treatment results showed that the senescence of 5% SNS control cells decreased by 5%, the senescence of 15% SNS control cells lowered by 7%, and the senescence of 5% SNS HGPS cells decreased by 8%, while the senescence of 15% SNS HGPS cells reduced by 12%. Long-term, one-month treatment results showed that the senescence of 5% SNS control cells lowered by 16%, the senescence of 15% SNS control cells reduced by 19%, and the senescence of 5% SNS HGPS cells decreased by 10%, while the senescence of 15% SNS HGPS cells declined by 21%. Overall, compared with the mock-treated group, the short-term administration of baricitinib only reduced the percentage of cell ageing by a small amount. While the HGPS cells with 15% of SNS improved significantly after treatment, the changes in other groups were not noticeable. However, the long-term administration for each group displayed a significant anti-ageing effect. Furthermore, treating both control and HGPS cultures originating from 15% SNS with baricitinib for one month reduced the senescence proportion by about 20% compared to the mock treatment. The results showed that after one month of treatment, baricitinib administration improved proliferative lifespan and delayed the senescence of both the control group and HGPS cells.

To further study the therapeutic effect of baricitinib on changing cell homeostasis, we investigated classical indicators that always apply in the HGPS study, such as autophagy, proteostasis, mitochondrial function and progerin levels. Autophagy can effectively help cells degrade progerin, thereby reducing the damage of progerin to cells. The autophagy level of HGPS cells in the young state (< 5% SNS) was significantly lower than that of the corresponding control cells in the same initial state but similar to the control cells with 15% SNS. Simultaneously, in HGPS cultures exhibiting 15% SNS, the basal level of autophagy was even lower. This result is consistent with previous reports that HGPS cells have more reduced autophagy than control cells, while senescent cells are younger [37].

When we used baricitinib to treat each group of cells, the autophagy slightly increased in the short-term, one-week dosing events. The 5% SNS control cells increased by 6%, 15% SNS control cells grew by 13%, and HGPS cells with 5% SNS increased by 12%, while the 15% SNS

HGPS cells rose by 33%. The long-term, one-month administration results showed that the control cells of 5% SNS rose by 26%, the control cells of 15% SNS increased by 37%, the HGPS cells of 5% SNS improved by 41%, and the HGPS cells of 15% SNS expanded by 52%. The outcomes show that after administration, baricitinib can help each group of cells enhance autophagy, regardless of the cell senescence percentage. Nevertheless, because autophagy decreases while cells are entering senescence, the effect of baricitinib on senescent cells is prominent. For example, autophagy was significantly reduced in the cells with a high initial senescence rate, HGPS cells and cells with a long cultivation process for replication senescence. Consequently, baricitinib shows a promoted ability to alleviate autophagy in these conditions.

Afterward, we evaluated the effect of baricitinib administration on the proteasome activity of each group of cells. The initial state of 5% SNS control cells and HGPS cells was similar. Meanwhile, with the increase of culture time, the proteasome activity of the 5% SNS control group did not significantly decrease after one week or one month. On the contrary, the proteasome activity reduced considerably in the HGPS group, and it dropped more in the one-month cultivation than in one-week cultivation. For the cells beginning with 15% SNS, the control cells' proteasome activity did not reduce significantly after one week of administration. However, it dropped a decent amount after one month of treatment. At the same time, after one week or one month of culture, the activity of the proteasome in HGPS cells with 15% SNS initially was all reduced, and after one month, the decline was even more significant. These results indicate that proteasome activity decreases as cells age. However, baricitinib treatment can increase the proteasome activity of each group. Specifically, in the one-week administration group, 5% SNS control cells increased by 13%, 15% SNS control cells increased by 25%, 5% SNS HGPS cells increased by 20%, and 15% SNS HGPS cells increased by 35%. In the one-month administration group, 5% SNS control cells increased by 35%, 15% SNS control cells increased by 37%, 5% SNS HGPS cells increased by 41%, and 15% SNS HGPS cells increased by 39%. In general, each group's proteasome activity increased after the use of baricitinib, and the one-month administration group's increase was more noticeable than

in the one-week administration group. The results show that after a one-week and one-month treatment of baricitinib, the proteasome activity of normal cells and HGPS cells was all enhanced regardless of the ageing index before medication.

Like our previous report, critical indicators of mitochondrial functional ROS increased in the HGPS group and the group with a higher senescence ratio. Nevertheless, baricitinib can reduce the production of ROS in each group. For instance, with one week of baricitinib administration, 5% SNS control cells lowered by 5%, 15% SNS control cells reduced by 5%, 5% SNS HGPS cells were decreased by 8%, and 15% SNS HGPS cells decreased by 9%. After the one-month baricitinib administration, 5% SNS control cells decreased by 26%, 15% SNS control cells reduced by 29%, 5% SNS HGPS cells lowered by 34%, and 15% SNS HGPS cells decreased by 41%. The results showed that baricitinib treatment effectively reduced the level of ROS production in the one-month administration group. In contrast, the treatment effect of baricitinib was not apparent in the one-week administration group.

In addition, ATP (another essential indicator of mitochondrial function) also decreased as SNS rose. Under the same SNS, the ATP in the HGPS group was lower than that in the control group. Meanwhile, the ATP in the one-month administration group was lower than that in the one-week administration group. Baricitinib treatment significantly increased the level of ATP production in each group. Specifically, in the one-week administration group, 5% SNS control cells increased by 23%, 15% SNS control cells grew by 28%, 5% SNS HGPS cells rose by 28%, and 15% SNS HGPS cells developed by 34 %. In the one-month administration group, 5% SNS control cells increased by 20%, 15% SNS control cells increased by 25%, 5% SNS HGPS cells increased by 30%, and 15% SNS HGPS cells increased by 37%. In general, baricitinib can increase the intracellular ATP level of each group of cells, with HGPS and control fibroblasts starting at 15% SNS expanding by more than 30%, which is more prominent than others. Regardless of cell type, the increasing percentages of ATP are all similar and located between 20% and 30% after one week and one month of treatment.

Although HGPS cells are different from control cells in cell homeostasis, the fundamental separation is still the progerin expression. As autophagy can effectively degrade the progerin

expressed in HGPS, we evaluated the progerin levels of each group after baricitinib treatment [100]. The Western blot results showed that the progerin level of each group decreased to varying degrees. The results show that 5% SNS HGPS fell by 1% after a one-week treatment, 15% SNS HGPS cells decreased by 22% after a one-week treatment, 5% SNS HGPS cells reduced by 41% after a one-month treatment, and 15% SNS HGPS cells diminished by 45% after a one-month treatment. The results show that the long-term administration of baricitinib can significantly reduce the expression of progerin.

Later, to further confirm the effectiveness of baricitinib, we examined the impression of baricitinib treatment on HGPS nuclear morphology. In Figure 18, we can see the highly irregular deformation and various alterations of the HGPS nuclei, including the nuclear envelope abnormalities, nuclear envelope blebbing and invaginations. Baricitinib treatment for 20 days significantly reduced the percentage of dysmorphic nuclei in both the control group and the HGPS group. Also, using the anti-progerin antibodies indicated that more progerin proteins accumulated in the HGPS nuclei envelope in some specific areas after the mock treatment. In contrast, overall, the percentage of bright progerin-positive nuclei and the signal intensity of these nuclei in HGPS cells were reduced in the HGPS cells treated with baricitinib compared to HGPS cells treated with mock.

Overall, baricitinib effectively alleviated the HGPS morphology by lowering progerin levels. In summary, these results indicate that inhibiting the JAK1/2-STAT1/3 pathway with baricitinib can effectively restore proliferation, proteostasis and mitochondrial function, reduce progerin and improve nuclear morphology, all of which are known hallmarks of cell ageing.

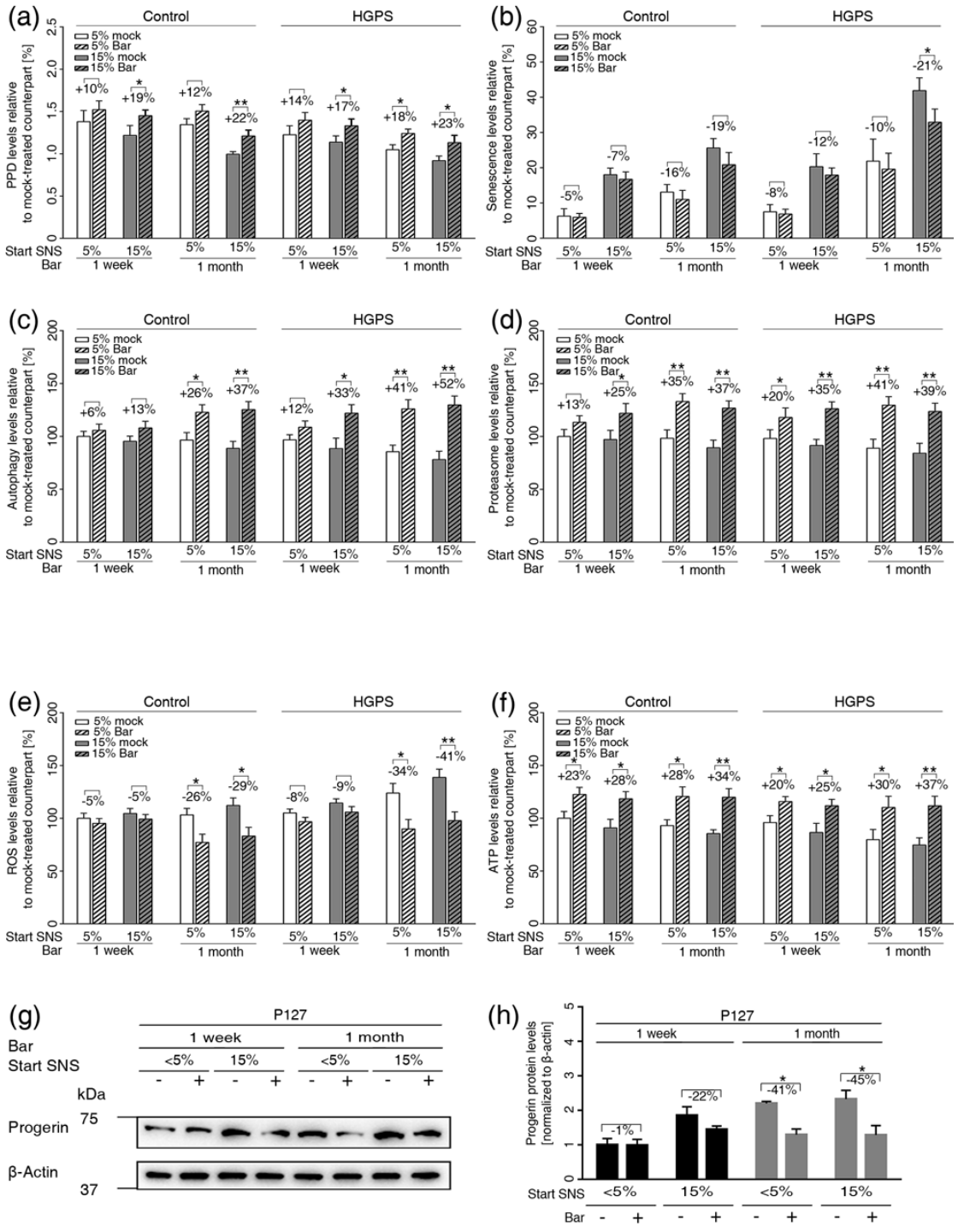


**Figure 19: Baricitinib treatment ameliorates normal and HGPS cellular functions during long-term treatment.**

(a) The graph shows the population doublings of control (GMO1651c, and GMO1652c) and HGPS (HGADFN003, and HGADFN127) cells. Baricitinib (1 µ M) or DMSO treatment was administrated for one week or one month, as indicated. The percentage of senescence (SNS) in cultures before treatment is indicated. (b) The graph shows the percentage of SA-β-gal-positive cells measured after treatment. (c) Autophagy activity was determined by

measuring MDC levels using fluorescence photometry of the same cultures as in (a). (d) Proteasome activity was determined by measuring chymotrypsin-like proteasome activity using Suc-LLVY-AMC as a substrate. (e) Intracellular ROS levels were determined by measuring oxidized dichlorofluorescein (DCF) levels using a DCFDA cellular ROS detection assay. (f) Cellular ATP levels were measured using a CellTiter-Glo Luminescence ATP Assay. (c–f) The per cent change in baricitinib-treated cells relative to mock-treated counterparts is indicated. (g) Representative images of a Western blot for progerin in HGPS (HGADFN127) cells from cultures at 5% and 15% senescence administered the mock or baricitinib treatment for one week or one month, as indicated. (h)Quantification of the progerin signal. The per cent changes between baricitinib-treated cells and mock-treated counterparts are indicated. Graphs show the mean ± SD. Comparisons were performed by two-tailed t-test (★ $p$ <0.05, ★★ $p$ <0.01, ★★★ $p$ <0.001, n > 3).

## 4.8. JAK-STAT inhibition reduces pro-inflammatory factors

The significant role of the JAK1/2-STAT1/3 pathway in the inflammation process and our previous measurement of 17 essential genes identified through text mining show that these genes increase while the percentage of senescent cells increases. Therefore, we tested whether the inhibition of JAK1/2-STAT1/3 can rebalance the expression of these 17 genes. The overexpression of these 17 genes can influence the occurrence of the related four phenotypes, including arthritis, hair loss, lipodystrophy and vascular disease. The reduction of these critical genes' expression alleviates these phenotypes in HGPS patients. Simultaneously, these 17 genes are also essential for cellular ageing, and their excessive release also causes the senescence of other cells. Accordingly, we again tested the expression levels of these 17 genes by using qPCR at the condition.

We treated both young control and HGPS cultures containing less than 5% SNS cells with 1 μM baricitinib or mock treatment for one month. Subsequently, we used the same experimental methods and conditions as the previous qPCR to measure each gene's

expression after administration. As reported above, baricitinib treatment reduces the percentage of senescent cells to total cells. It further prevents the excessive upregulation of most cytokines/chemokines known as SASPs (CCL2 / MPC1, CXCL8 / IL8, IFNG, IL-4, IL-6, IL-18, LEP, TNFA). Among them, the most significant reduction occurs in pro-inflammatory factors, such as IL-6, CXCL8 / IL8, IL-18 and CCL2/MPC1. Similarily, TGFB1, TRAF1, ICAM-1, FAS and CRP were reduced in baricitinib-treated cells. In the cells treated with baricitinib, the levels of IGF-1 and PPARG increased and, therefore, improved in both cell types (Figure 20). These results collectively indicate that baricitinib treatment reduces the expression of several SASPs, which may lead to delayed senescence of normal cells and HGPS cells.

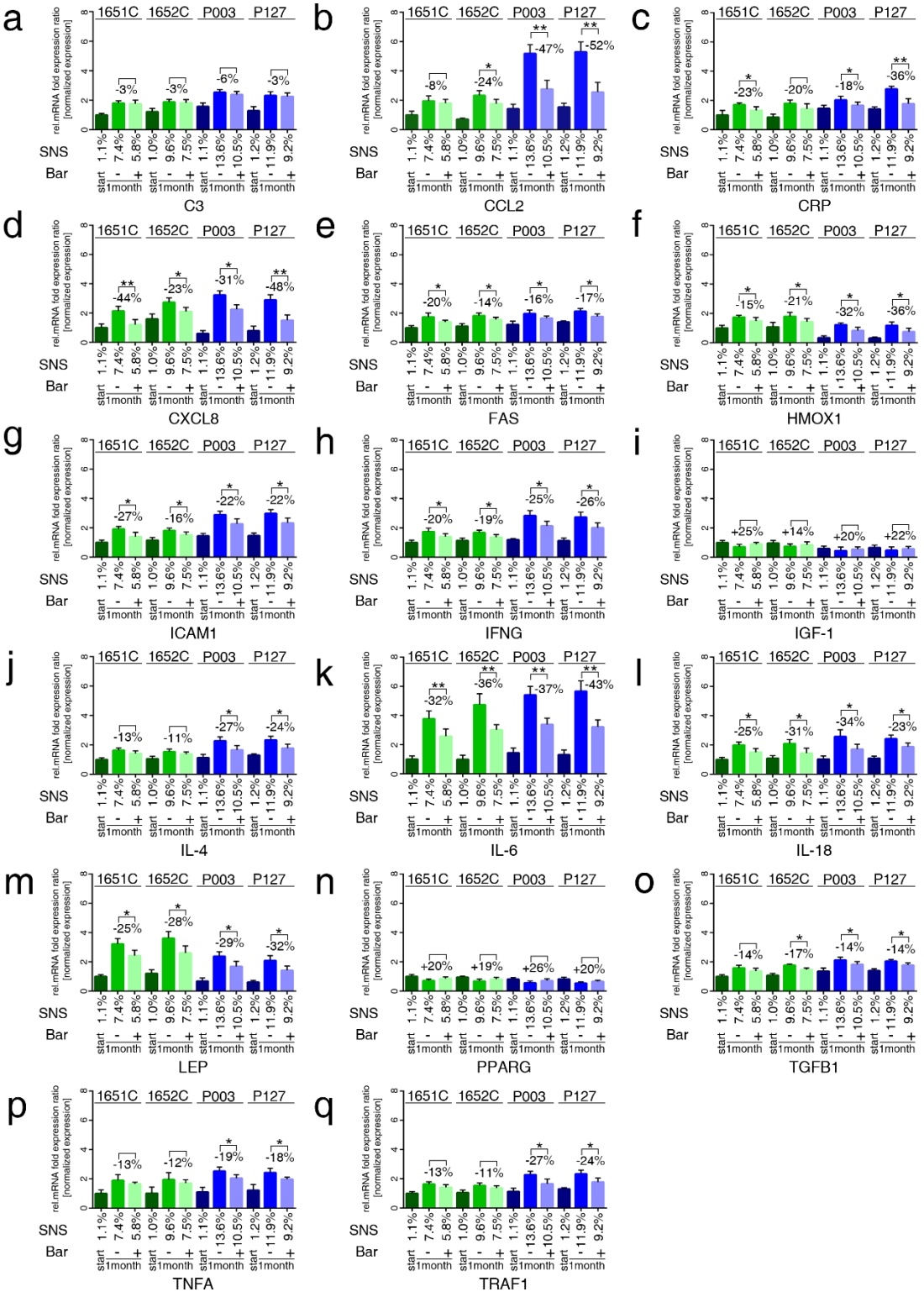


**Figure 20: Real-time PCR analysis of the 17 genes identified by text mining in normal and HGPS cells after being treated with baricitinib for one month.** (a-q) mRNA levels of indicated genes were determined in controls (GMO1651c, GMO1652c) and HGPS (HGADFN003 and HGADFN127) cell strains. The starting senescence indexes

of the culture and the senescence indexes of cultures at the end of the treatment are indicated (Start SNS). Relative expression was normalized to the expression of GAPDH. Graphs show mean ± SD (n ≥ 3). Comparisons were performed with the two-tailed t-test (★ $p$ <0.05, ★★ $p$ <0.01, ★★★ $p$ <0.001, n > 3). The per cent changes between baricitinib-treated cells and mock-treated counterparts are shown.

## 4.9. Etoposide-induced DNA damage over-activates the JAK-STAT pathway in both normal and HGPS cells

The above results indicate that the JAK1/2-STAT1/3 signaling pathway plays a vital role in the occurrence and development of replicative senescence. However, to establish a more direct link between this signaling pathway and senescence, rather than just replicative senescence, we set a classical senescence model caused by etoposide.

Etoposide is a topoisomerase inhibitor widely applied in cancer treatment. In the DNA replication process, topoisomerase II can assist the unfolding of DNA, which plays an essential role in the regular procedure of DNA replication. Etoposide can form a ternary complex with DNA and topoisomerase II, which stabilizes the complex of topoisomerase II after the DNA strand breaks. This process, in turn, hinders the operation of DNA ligase, leading to the destruction of DNA. DNA-damaged cells exhibit a sustained DNA damage response, which eventually triggers cell cycle arrest and senescence [321]. This kind of senescent cell usually has nuclear substructures with persistent DNA damage and DNA damage response proteins, namely the DNA segments with chromatin alterations reinforcing senescence (DNA-SCARS). DNA-SCARS are associated with PML nuclear bodies and the accumulation of activated p53, ATM and ATR proteins [322]. Similarly, such senescent cells exhibit similar senescence-associated secretory phenotypes, mediating the non-cell-autonomous ageing effect. Likewise, the SASP here is composed of a highly complex mixture of secreted cytokines, chemokines, growth factors and proteases [323].

As shown in Figure 21, we treated the control and the HGPS cell lines with 5 μM etoposide for six days to damage the DNA, and then we switched to the standard cell culture medium for four days in the etoposide group. For the baricitinib administration group, we used 1 μM baricitinib pre-administration for two days to execute a protective function. Then, we also administered 1 μM baricitinib during the DNA damage of etoposide for six days. In the last four days of the normal cultivation process with the standard cell culture medium, we again added 1 μM baricitinib to exert anti-ageing effects. For the mock control group, we only gave the corresponding mock treatment throughout.

After the ten days of cell culture, we used the SA-β-gal staining to probe each group for the percentage of cell senescence. The control cell line 1651C and the HGPS cell line P003 in the mock treatment group still maintained less than 1% SNS, with well-functioning growth status and regular cell morphology. The cells in the etoposide administration group had a noticeable increase in cell senescence. The percentage of senescent cells in 1651C increased to 65% SNS, while the senescence rate of P003 cells was higher, reaching 75% SNS. Meanwhile, the growth rate of cells slowed down, and the cell morphology became flat and no longer like a slender spindle. The baricitinib treatment group effectively delayed cell senescence caused by etoposide. It reduced the cell senescence in control 1651C to 57% and the cell senescence in the HGPS P003 to 63%. This result indicates that baricitinib can alleviate the process of cell ageing to a certain extent. For example, the percentage of SNS decreased by 8% in control cells and decreased by 12% in HGPS cells. Correspondingly, the expression level of the classic senescence index protein p21 also increased significantly in the etoposide administration group.

At the same time, the p21 expression level of the baricitinib administration group rose considerably. However, its increasing level was lower compared to the etoposide group, but it was still significantly higher than the mock group. This result shows that baricitinib has a decent ability to alleviate the ageing process caused by etoposide. At the same time, we also compared the expression of progerin in each group of cells. We found that the progerin levels in each group of cells were almost identical, and there was no noticeable change. This

phenomenon may be explained by the fact that the long-term overexpression of progerin can cause cell senescence. However, the short-term rapid senescence of cells does not necessarily accelerate the production of progerin. Nevertheless, the baricitinib administration group still showed a certain degree of progerin reduction. It may be related to the activation of cell autophagy by baricitinib, and the cell autophagy may have reduced the expression of progerin in the HGPS cells.

Etoposide can accelerate cellular ageing of both control and HGPS cells via DNA damage. To explore if the accelerated ageing generated by DNA damage also leads to the excessive activation of the JAK1/2-STAT1/3 pathway, we evaluated the expression status of STAT1 and STAT3. The results showed that the expressions of STAT1, p-STAT1, STAT3 and p-STAT3 in the control cell line and HGPS cell line were shallow, corresponding to the previous experimental results. However, after using etoposide to induce senescence, the expression levels of STAT1 in the HGPS group and HGPS group were significantly increased, and the expression levels of STAT3 were also considerably increased. The increase in STAT3 was slightly lower than that of STAT1. However, we then conducted a more extensive investigation of the control group and the HGPS group regarding p-STAT1 and p-STAT3. The results showed that both of them increased dramatically several times after the etoposide treatment. The change of p-STAT1 was also more significant than that of p-STAT3, in accord with results from the replicative senescence. These results all prove that etoposide significantly activates STAT1, p-STAT1, STAT3 and p-STAT3 during the ageing process of normal cells and HGPS cells, showing the connection between the JAK1/2-STAT1/3 pathway and senescence.

It can be seen that the performance of baricitinib effectively prevents the rise of p-STAT1 and p-STAT3 caused by etoposide. Related to the expression changing of p-STAT1, the 1651C reduced by 83%, the 1652C reduced by 88%, P003 reduced by 88% and the P127 reduced by 95%. Related to the expression changing of p-STAT3, the 1651C reduced by 75%, the 1652C reduced by 74%, the P003 reduced by 74% and the P127 reduced by 79%. Similar to the previous results of the baricitinib treatment group, the expression level of STAT1 did not change significantly, but the expression of STAT3 increased in both the control and the HGPS

cell lines. In the protein level change of STAT3, the 1651C increased by 35%, the 1652C rose by 36%, the P003 was enhanced by 10% and the P127 grew by 27%. Collectively, these results demonstrate that highly damaged DNA can lead to cell senescence, and it can further lead to over-activation of the JAK1/2-STAT1/3 pathway. These processes are similar to the senescence presented during replicative senescence.

We also examined the genetic changes after etoposide damaged the DNA. We already knew the role of the JAK1/2-STAT1/3 pathway in senescence caused by etoposide and understood that the activation of this signaling pathway leads to changes in the expression of those 17 essential genes. Therefore, we designed and tested the five most critical related genes. The results showed that, in contrast to the mock treatment, the expressions of CCL2/MPC1, CXCL8/IL8, IFNG, IL-6 and TNFa in the control cell and HGPS cell etoposide treatment groups were both significantly increased. They corresponded to the changes we reported above; their gene expression increased as the senescence index increased.

For example, related to the change of CCL2, 1651C decreased by 70%, 1652C reduced by 66%, P003 lowered by 57% and P127 declined by 54%. Among the changes in CXCL8, 1651C reduced by 37%, 1652C decreased by 34%, P003 lowered by 45% and P127 declined by 49%. Among the changes in IFNG, 1651C reduced by 52%, 1652C decreased by 45%, P003 reduced by 55% and P127 declined by 56%. In the IL-6 changes, 1651C declined by 32%, 1652C decreased by 36%, P003 reduced by 40% and P127 declined by 40%. In the change in TNFa, 1651C decreased by 40%, 1652C lowered by 43%, P003 declined by 45% and P127 decreased by 46%.

Taken together, these findings indicate that DNA damage-induced senescence is similar to replication induced senescence. DNA damage inducers mediate ageing through the excessive activation of JAK-STAT signaling, while baricitinib treatment can delay ageing and reduce the expression of pro-inflammatory SASP.

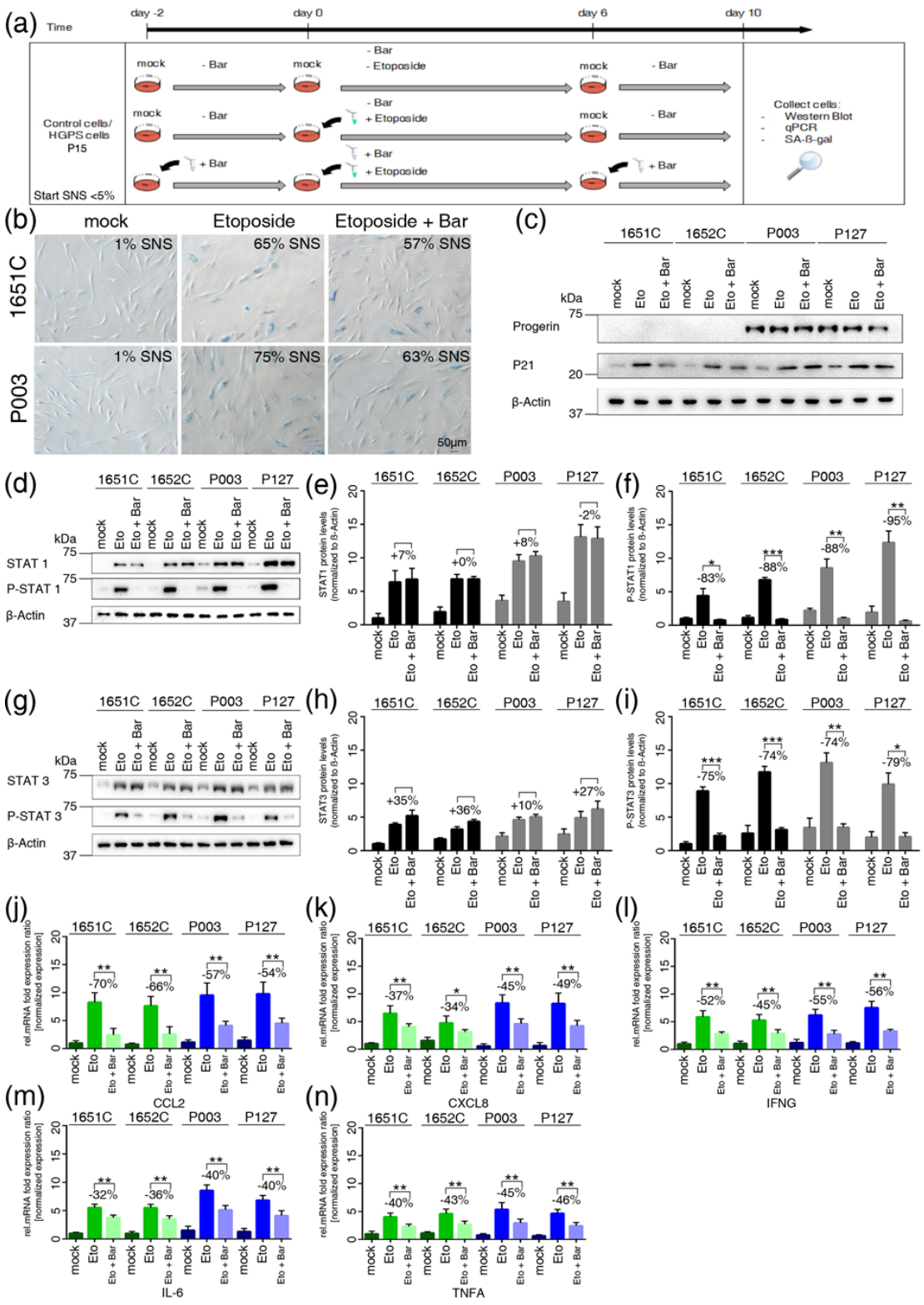


**Figure 21: Etoposide treatment activates the JAK-STAT signaling pathway in HGPS and normal cells.** (a) Schematic representation of the etoposide treatment protocol. All treatments started with cultures exhibiting

< 5% senescence. Cells were either pre-treated with or without 1 μ M baricitinib for two days and then exposed to medium with or without etoposide in the presence or absence of baricitinib for six days. Next, cells were grown for four days with or without baricitinib as indicated. (b) Representative images of SA-β-gal-positive cells in mock-, etoposide- and etoposide+ baricitinib-treated cultures (GMO1651cand HGADFN003) shown. The percentages of senescence after treatment are indicated. Scale bar: 10 μm (c) Representative images of Western blots for progerin, p21 and β-actin in normal (GMO1651c, and GMO1652c) and HGPS (HGADFN003, and HGADFN127) cells, treated as indicated. (d) and (g) Representative images of Western blots for JAK1/2, STAT1/3, p-STAT1/3 and β-actin in normal (GMO1651c, and GMO1652c) and HGPS (HGADFN003, and HGADFN127) cells, treated as indicated. (e) Quantification of STAT1, (f) p-STAT1, (h) STAT3 and (i) p-STAT3. The per cent change between etoposide- and etoposide+ baricitinib-treated cells is indicated. (j–n) Quantitative real-time PCR analysis of CCL2, CXCL8, IFNG, IL-6 and TNFa in cells, treated as indicated. Relative expression was normalized to the expression of GAPDH. Graphs show the mean ± SD. Comparisons were performed by two-tailed t-test (★ $p$ <0.05, ★★ $p$ <0.01, ★★★ $p$ <0.001, n > 3). All experiments were repeated at least three times (n > 3).

# 5. Discussion

With this study, we became the first group to use text mining in the HGPS field to identify potential molecular markers. Previous research has explored many possible ways to treat HGPS patients from multiple angles. For example, medicines like pravastatin and zoledronic can alleviate symptoms in HGPS patients. At the same time, drugs like lonafarnib or sulforaphane can reduce progerin at a molecular level. Specifically, pravastatin is a statin that can lower cholesterol and prevent cardiovascular disease. Zoledronic acid can improve osteoporosis and prevent bone fractures. Lonafarnib can prevent progerin production by inhibiting farnesyl transferase. Sulforaphane activates autophagy to degrade the expression of progerin.

We combined the molecular mechanisms behind the four most common phenotypes in the elderly and HGPS patients and then identified the commonalities and potential homogeneity of these four diseases. Finally, we found a new signaling pathway that has never been reported before. The four different pathologies associated with ageing are vascular disease, arthritis, alopecia and lipodystrophy, and the signaling pathway is the JAK1/2-STAT1/3 pathway. We found that regulating this signaling pathway can effectively relieve vascular disease, arthritis and alopecia. More importantly, we discovered that senescence is highly related to JAK1/2-STAT1/3 signaling.

We used text mining to examine genes related to these four critical diseases and found that 17 essential genes are crucial in these four diseases simultaneously. Of these 17 genes, 14 are regulated by STAT1 and STAT3 transcription factors. At the same time, these 14 inflammatory markers belong to SASP and are secreted by SNS cells [324]. Subsequently, we found that the excessive activation of the JAK1/2-STAT1/3 pathway mediated by these pro-inflammatory cytokines plays a vital role in the pathogenesis of these four diseases. We found that chronic inflammation and excessive activation of the JAK1/2-STAT1/3 pathway play a role in the development of these four ageing-related diseases and also play a role in the ageing

process of ordinary people and HGPS patients.

Increasing research has shown that there is an indispensable relationship between chronic inflammation and senescence [325]. Researchers have detected inflammatory signals not only in the blood samples of patients with vascular disease, arthritis, alopecia or lipodystrophy but also in patients with HGPS [326]. Therefore, the 17 genes we distinguished can be used as biomarkers to track and evaluate the development stage and severity of these four related diseases and HGPS.

Organisms with a vascular system often have a defensive response to inflammatory factors and local damage through inflammation, in which the plasma sample levels of pro-inflammatory factors, such as cytokines IL-6, IL8, IL-18 and TNFa, usually increase significantly. These conditions are mainly caused by the stimulation of biological tissues such as trauma, bleeding or pathogen infection[327]. In general, inflammation is the body's automatic defense response showing a beneficial effect, but persistent inflammation can also cause damage and adverse effects on tissues and organs. When this delicate balance of cytokine shifts, chronic inflammation is activated and leads to ageing and diseases related to ageing. This process is also called inflame-ageing [328].

Similarly, the accumulation of SNS in specific tissues and organs can also cause chronic inflammation by releasing SASP. In general, ageing causes inflammation, which, in turn, causes ageing, and this mutual process can occur in many different cell types. These cell types include immune cells, stem cells, smooth muscle cells, endothelial cells, fibroblasts in atherosclerotic plaques, adipocyte cells in fat tissue, keratinocytes, fibroblasts in the ageing skin and the synovial fibroblasts of arthritic joints. Therefore, the increase in the proportion of SNS of different cell types leads to the senescence of various tissue parts and then determines which age-related pathology develops. Therefore, where SNS accumulates determines which age-related pathology emerges, and SNS accumulation over time will make the condition worse.

Studies have shown that the occurrence and development of inflammation is a complex process. In addition to the JAK1/2-STAT1/3 pathway described above, NF-κB is also an

important pathway that mediates inflammation. In the classical pathway, IκB (Inhibitor of κB) binds to NF-κB/Rel to restrict the function of NF-κB. Once the pro-inflammatory factor, lipopolysaccharides, growth factor and antigen receptor activate the IκB kinase complex, the IκB protein gets phosphorylated, causing the IκB protein to be ubiquitinated and degraded by lysosomes. Subsequently, NF-κB is released and further phosphorylated before it transfers into the nucleus, thereby inducing the expression of target genes, producing cytokines such as IL-6, IL-1 α, TNFa and so on. These cytokines can further create intracellular pro-inflammatory signaling cascades. For example, these cytokines can activate the JAK-STAT pathway, showing that the occurrence of inflammation directly or indirectly activates the JAK-STAT pathway.

Meanwhile, inflammation is closely related to senescence. Therefore, in this paper, we confirmed that the JAK-STAT signaling pathway is over-activated in both control and HGPS cells using an in vitro cell level ageing model. The common four ageing-related complications always affect mesenchymal-derived tissues, including the heart, vascular vessels, skin, bone and joints. These tissues all contain resident immune cells, tissue-specific cell types and fibroblast subtypes. Although fibroblasts are highly heterogeneous, they all have similar characteristic properties. They express various cytokines that perform different functions, such as wound healing, repair, remodeling, fibrosis and stem cell maintenance. As fibroblasts are present in all tissues related to these four diseases, their increased ageing can characterize senescence's critical role in the pathological development of these diseases.

In past research, people often chose control and HGPS fibroblasts within the same passage number or with the same population doublings for comparison. The premise of this comparison is that regular cell lines always maintain a similar character after experiencing the same passage number. However, that was not valid in our case. We found in experiments that due to progerin expression, HGPS cells enter ageing earlier than control cells. Even at the same incubation time or passage number, the control cells and HGPS cells were at totally different levels of senescence.

Therefore, we cultivated primary fibroblast cultures for a long time to check normal and HGPS

fibroblasts and tested the indicators of the two cell lines under similar ageing indexes. We found that both control and HGPS cells showed similar growth rates when they were at less than 5% senescence, as well as minimal differences in autophagy levels, proteasome activity, ROS and ATP levels. When the two cell lines both grew to 15% or 30% SNS, all of these indicators had corresponding changes. The HGPS cell parameters in the same senescence index period were similar to that of control cells. These results indicate that with the increase of SNS, the growth rate, proteostasis and mitochondria function all have corresponding changes in control and HGPS cells. Our experimental results show that although these functional changes are slightly related to progerin expression, they are more associated with the senescence index.

It appears that we obtained a different experimental result from previous studies. The reason for this discrepancy might be that previous studies did not adequately consider the scoring of senescent cell levels; the same passage may be at an entirely different senescence level. We found the impact of this critical parameter because we also used passage number as an indicator to measure the state of cells in the early stage of the experiment. When we compared the control and HGPS cells at the beginning, we found that even though two different cells were in matching passage numbers, they showed inconsistent p-STAT1 and p-STAT3 levels, and this also happened in the same cell strain. When we strictly evaluated the proportion of senescent cells in these two groups of cells during the cell culture process, control and HGPS cells showed a surprising similarity of senescing at the molecular and cellular level. In addition to the cell growth rate and cell homeostasis mentioned above, this strategy also enabled control and HGPS fibroblasts to exhibit similar mRNA levels of gene encoding pro-inflammatory factors (CRP, CCL2, IL8, C3, TRAF1, IL-18, IL-6, and TNFa) and adhesion molecules ICAM-1 and CRP. This result indicates that when cultures have the same percentage of senescent cells, they express a similar SASPs. This feature has nothing to do with whether the cells are normal cells or HGPS cells. In the subsequent Western blot experiments, we observed that the phosphorylated forms of STAT1 and STAT3 presented comparable rising levels in the replicating senescence process. This result indicates that the

JAK1/2-STAT1/3 signaling pathway is over-activated during the ageing process caused by etoposide treatment, and this process occurs in both the control and HGPS cells.

In addition to telomere attrition, many other stresses can also cause the occurrence of cell senescence. We used etoposide to induce the senescence of the control and HGPS fibroblasts via DNA damage. Notably, the over-activation of the JAK1/2-STAT1/3 signaling pathway could be found in cells after injury using etoposide, like replicative senescence. In etoposide-treated control and HGPS cells, the levels of phosphorylated STAT1 and STAT3 increased abruptly in SNS, and the expression of a targeted set of inflammatory cytokines (IL-6, L8, TNFa, CCL2, IFNy) was also significantly up-regulated. Therefore, the JAK-STAT pathway's excessive activation during senescence depends on a common mechanism. Although this mechanism is always accompanied by ageing, the generation of ageing can be induced by multiple sources. It can be caused by telomere attrition or promoted by progerin expression, or it can be affected by DNA damage. No matter what kind of stress causes cell ageing, the JAK-STAT pathway can continuously release pro-inflammatory factors during the senescence process.

To prevent the release of these pro-inflammatory factors, we selected baricitinib, a similar inhibitor of JAK1 and JAK2, to repair this process. The experimental results showed that baricitinib treatment effectively prevented the activation of JAK1/2-STAT1/3 signaling pathways during the replicative senescence process and DNA damage senescence caused by etoposide. After being treated with baricitinib for one month, several ameliorations were enhanced, including improved growth rate, postponed senescence, ameliorated proteostasis and mitochondrial function, significantly attenuated pro-inflammatory marker levels in both control and HGPS cells and reduced progerin levels in the HGPS cells. Consequently, baricitinib treatment can rebalance the homeostasis of both control and HGPS fibroblasts and correct multiple hallmarks of senescence.

# 6. References


1. Manor, B.; Lipsitz, L.A. Physiologic complexity and aging: implications for physical function and rehabilitation. *Progress in neuro-psychopharmacology & biological psychiatry* **2013**, *45*, 287-293, doi:10.1016/j.pnpbp.2012.08.020.
2. Phillip, J.M.; Aifuwa, I.; Walston, J.; Wirtz, D. The Mechanobiology of Aging. *Annual review of biomedical engineering* **2015**, *17*, 113-141, doi:10.1146/annurev-bioeng-071114-040829.
3. Crimmins, E.M. Lifespan and Healthspan: Past, Present, and Promise. *The Gerontologist* **2015**, *55*, 901-911, doi:10.1093/geront/gnv130.
4. Jin, K. Modern Biological Theories of Aging. *Aging and disease* **2010**, *1*, 72-74.
5. Goldsmith, T.C. Emerging programmed aging mechanisms and their medical implications. *Medical hypotheses* **2016**, *86*, 92-96, doi:10.1016/j.mehy.2015.10.015.
6. Zinovkina, L.A.; Zinovkin, R.A. DNA Methylation, Mitochondria, and Programmed Aging. *Biochemistry. Biokhimiia* **2015**, *80*, 1571-1577, doi:10.1134/S0006297915120044.
7. Maynard, S.; Fang, E.F.; Scheibye-Knudsen, M.; Croteau, D.L.; Bohr, V.A. DNA Damage, DNA Repair, Aging, and Neurodegeneration. *Cold Spring Harbor perspectives in medicine* **2015**, *5*, doi:10.1101/cshperspect.a025130.
8. Nita, M.; Grzybowski, A. The Role of the Reactive Oxygen Species and Oxidative Stress in the Pathomechanism of the Age-Related Ocular Diseases and Other Pathologies of the Anterior and Posterior Eye Segments in Adults. *Oxidative medicine and cellular longevity* **2016**, *2016*, 3164734, doi:10.1155/2016/3164734.
9. Milholland, B.; Dong, X.; Vijg, J. "Best-Guess" MRAD Provides Robust Evidence for a Limit to Human Lifespan: Reply to de Grey (Rejuvenation Res. 2017;20:261-262). *Rejuvenation research* **2017**, *20*, 437-440, doi:10.1089/rej.2017.2008.
10. Piekarowicz, K.; Machowska, M.; Dzianisava, V.; Rzepecki, R. Hutchinson-Gilford Progeria Syndrome-Current Status and Prospects for Gene Therapy Treatment. *Cells* **2019**, *8*, doi:10.3390/cells8020088.
11. Dreesen, O.; Stewart, C.L. Accelerated aging syndromes, are they relevant to normal human aging? *Aging* **2011**, *3*, 889-895, doi:10.18632/aging.100383.
12. Lessel, D.; Kubisch, C. Hereditary Syndromes with Signs of Premature Aging. *Deutsches Arzteblatt international* **2019**, *116*, 489-496, doi:10.3238/arztebl.2019.0489.
13. Coppede, F. The epidemiology of premature aging and associated comorbidities. *Clinical interventions in aging* **2013**, *8*, 1023-1032, doi:10.2147/CIA.S37213.
14. Coutinho, H.D.; Falcao-Silva, V.S.; Goncalves, G.F.; da Nobrega, R.B. Molecular ageing in progeroid syndromes: Hutchinson-Gilford progeria syndrome as a model. *Immunity & ageing : I & A* **2009**, *6*, 4, doi:10.1186/1742-4933-6-4.
15. Pollex, R.L.; Hegele, R.A. Hutchinson-Gilford progeria syndrome. *Clinical genetics* **2004**,

*66*, 375-381, doi:10.1111/j.1399-0004.2004.00315.x.

16. Kashyap, S.; Shanker, V.; Sharma, N. Hutchinson - Gilford progeria syndrome: A rare case report. *Indian dermatology online journal* **2014**, *5*, 478-481, doi:10.4103/2229-5178.142507.
17. McKusick, V.A. The Gordon Wilson Lecture: The clinical legacy of Jonathan Hutchinson (1828-1913): syndromology and dysmorphology meet genomics. *Transactions of the American Clinical and Climatological Association* **2005**, *116*, 15-38.
18. Hennekam, R.C. Hutchinson-Gilford progeria syndrome: review of the phenotype. *American journal of medical genetics. Part A* **2006**, *140*, 2603-2624, doi:10.1002/ajmg.a.31346.
19. Kreienkamp, R.; Gonzalo, S. Metabolic Dysfunction in Hutchinson-Gilford Progeria Syndrome. *Cells* **2020**, *9*, doi:10.3390/cells9020395.
20. Rork, J.F.; Huang, J.T.; Gordon, L.B.; Kleinman, M.; Kieran, M.W.; Liang, M.G. Initial cutaneous manifestations of Hutchinson-Gilford progeria syndrome. *Pediatric dermatology* **2014**, *31*, 196-202, doi:10.1111/pde.12284.
21. Ceylan, G.; Yilmaz, N.; Senyurt, O.; Ergun Kunt, G. Implant supported prosthesis in a patient with progeria: case report. *Bosnian journal of basic medical sciences* **2009**, *9*, 210-214, doi:10.17305/bjbms.2009.2808.
22. Sinha, J.K.; Ghosh, S.; Raghunath, M. Progeria: a rare genetic premature ageing disorder. *The Indian journal of medical research* **2014**, *139*, 667-674.
23. Nabel, E.G. Cardiovascular insights from a premature aging syndrome: a translational story. *Transactions of the American Clinical and Climatological Association* **2012**, *123*, 221-225; discussion 225-226.
24. Hamczyk, M.R.; del Campo, L.; Andres, V. Aging in the Cardiovascular System: Lessons from Hutchinson-Gilford Progeria Syndrome. *Annual review of physiology* **2018**, *80*, 27-48, doi:10.1146/annurev-physiol-021317-121454.
25. Eriksson, M.; Brown, W.T.; Gordon, L.B.; Glynn, M.W.; Singer, J.; Scott, L.; Erdos, M.R.; Robbins, C.M.; Moses, T.Y.; Berglund, P., et al. Recurrent de novo point mutations in lamin A cause Hutchinson-Gilford progeria syndrome. *Nature* **2003**, *423*, 293-298, doi:10.1038/nature01629.
26. Schreiber, K.H.; Kennedy, B.K. When lamins go bad: nuclear structure and disease. *Cell* **2013**, *152*, 1365-1375, doi:10.1016/j.cell.2013.02.015.
27. Dechat, T.; Pfleghaar, K.; Sengupta, K.; Shimi, T.; Shumaker, D.K.; Solimando, L.; Goldman, R.D. Nuclear lamins: major factors in the structural organization and function of the nucleus and chromatin. *Genes & development* **2008**, *22*, 832-853, doi:10.1101/gad.1652708.
28. Hah, J.; Kim, D.H. Deciphering Nuclear Mechanobiology in Laminopathy. *Cells* **2019**, *8*, doi:10.3390/cells8030231.
29. Glass, C.A.; Glass, J.R.; Taniura, H.; Hasel, K.W.; Blevitt, J.M.; Gerace, L. The alpha-helical rod domain of human lamins A and C contains a chromatin binding site. *The EMBO journal* **1993**, *12*, 4413-4424.
30. Dittmer, T.A.; Misteli, T. The lamin protein family. *Genome biology* **2011**, *12*, 222,

doi:10.1186/gb-2011-12-5-222.

31. Young, S.G.; Fong, L.G.; Michaelis, S. Prelamin A, Zmpste24, misshapen cell nuclei, and progeria--new evidence suggesting that protein farnesylation could be important for disease pathogenesis. *Journal of lipid research* **2005**, *46*, 2531-2558, doi:10.1194/jlr.R500011-JLR200.
32. Yang, S.H.; Jung, H.J.; Coffinier, C.; Fong, L.G.; Young, S.G. Are B-type lamins essential in all mammalian cells? *Nucleus* **2011**, *2*, 562-569, doi:10.4161/nucl.2.6.18085.
33. Dreesen, O.; Ong, P.F.; Chojnowski, A.; Colman, A. The contrasting roles of lamin B1 in cellular aging and human disease. *Nucleus* **2013**, *4*, 283-290, doi:10.4161/nucl.25808.
34. Davies, B.S.; Fong, L.G.; Yang, S.H.; Coffinier, C.; Young, S.G. The posttranslational processing of prelamin A and disease. *Annual review of genomics and human genetics* **2009**, *10*, 153-174, doi:10.1146/annurev-genom-082908-150150.
35. Barrowman, J.; Hamblet, C.; Kane, M.S.; Michaelis, S. Requirements for efficient proteolytic cleavage of prelamin A by ZMPSTE24. *PloS one* **2012**, *7*, e32120, doi:10.1371/journal.pone.0032120.
36. Casasola, A.; Scalzo, D.; Nandakumar, V.; Halow, J.; Recillas-Targa, F.; Groudine, M.; Rincon-Arano, H. Prelamin A processing, accumulation and distribution in normal cells and laminopathy disorders. *Nucleus* **2016**, *7*, 84-102, doi:10.1080/19491034.2016.1150397.
37. Gabriel, D.; Gordon, L.B.; Djabali, K. Temsirolimus Partially Rescues the Hutchinson-Gilford Progeria Cellular Phenotype. *PloS one* **2016**, *11*, e0168988, doi:10.1371/journal.pone.0168988.
38. Martins, F.; Sousa, J.; Pereira, C.D.; da Cruz, E.S.O.A.B.; Rebelo, S. Nuclear envelope dysfunction and its contribution to the aging process. *Aging cell* **2020**, *19*, e13143, doi:10.1111/acel.13143.
39. Mendez-Lopez, I.; Worman, H.J. Inner nuclear membrane proteins: impact on human disease. *Chromosoma* **2012**, *121*, 153-167, doi:10.1007/s00412-012-0360-2.
40. Luo, D.Q.; Wang, X.Z.; Meng, Y.; He, D.Y.; Chen, Y.M.; Ke, Z.Y.; Yan, M.; Huang, Y.; Chen, D.F. Mandibuloacral dysplasia type A-associated progeria caused by homozygous LMNA mutation in a family from Southern China. *BMC pediatrics* **2014**, *14*, 256, doi:10.1186/1471-2431-14-256.
41. Cenni, V.; D'Apice, M.R.; Garagnani, P.; Columbaro, M.; Novelli, G.; Franceschi, C.; Lattanzi, G. Mandibuloacral dysplasia: A premature ageing disease with aspects of physiological ageing. *Ageing research reviews* **2018**, *42*, 1-13, doi:10.1016/j.arr.2017.12.001.
42. Thill, M.; Nguyen, T.D.; Wehnert, M.; Fischer, D.; Hausser, I.; Braun, S.; Jackisch, C. Restrictive dermopathy: a rare laminopathy. *Archives of gynecology and obstetrics* **2008**, *278*, 201-208, doi:10.1007/s00404-008-0676-6.
43. Silfeler, D.B.; Karateke, A.; Keskin Kurt, R.; Aldemir, O.; Bugra Nacar, A.; Baloglu, A. Malouf syndrome with hypergonadotropic hypogonadism and cardiomyopathy: two-case report and literature review. *Case reports in obstetrics and gynecology* **2014**, *2014*, 275710, doi:10.1155/2014/275710.

44. Qi, Q.; Wattis, J.A.; Byrne, H.M. Stochastic simulations of normal aging and Werner's syndrome. *Bulletin of mathematical biology* **2014**, *76*, 1241-1269, doi:10.1007/s11538-014-9952-8.
45. Sellin, J.; Beales, I.L.P. Whipple's Disease: A Well-Done Outcome to a Rare Disease. *Digestive diseases and sciences* **2019**, *64*, 9-11, doi:10.1007/s10620-018-5342-7.
46. Brown, R.J.; Araujo-Vilar, D.; Cheung, P.T.; Dunger, D.; Garg, A.; Jack, M.; Mungai, L.; Oral, E.A.; Patni, N.; Rother, K.I., et al. The Diagnosis and Management of Lipodystrophy Syndromes: A Multi-Society Practice Guideline. *The Journal of clinical endocrinology and metabolism* **2016**, *101*, 4500-4511, doi:10.1210/jc.2016-2466.
47. Ostojic, P.; Pavlov-Dolijanovic, S. Alopecia universalis in a patient with rheumatoid arthritis developed during treatment with adalimumab. *Zeitschrift fur Rheumatologie* **2018**, *77*, 412-415, doi:10.1007/s00393-018-0464-z.
48. Dogramaci, A.C.; Balci, D.D.; Balci, A.; Karazincir, S.; Savas, N.; Topaloglu, C.; Yalcin, F. Is androgenetic alopecia a risk for atherosclerosis? *Journal of the European Academy of Dermatology and Venereology : JEADV* **2009**, *23*, 673-677, doi:10.1111/j.1468-3083.2009.03137.x.
49. Bruder-Nascimento, T.; Kress, T.C.; Belin de Chantemele, E.J. Recent advances in understanding lipodystrophy: a focus on lipodystrophy-associated cardiovascular disease and potential effects of leptin therapy on cardiovascular function. *F1000Research* **2019**, *8*, doi:10.12688/f1000research.20150.1.
50. Krougly, L.B.; Fomicheva, O.A.; Karpov, Y.A.; Popkova, T.V.; Novikova, D.S.; Nasonov, E.L. [Cardiovascular Complications of Rheumatoid Arthritis: Prevalence and Pathogenesis]. *Kardiologiia* **2016**, *56*, 89-95, doi:10.18565/cardio.2016.6.89-95.
51. Fukutake, T. Cerebral autosomal recessive arteriopathy with subcortical infarcts and leukoencephalopathy (CARASIL): from discovery to gene identification. *Journal of stroke and cerebrovascular diseases : the official journal of National Stroke Association* **2011**, *20*, 85-93, doi:10.1016/j.jstrokecerebrovasdis.2010.11.008.
52. Muto, Y.; Fujimura, T.; Kakizaki, A.; Tsuchiyama, K.; Kusakari, Y.; Aiba, S. Adult-onset acquired partial lipodystrophy accompanied by rheumatoid arthritis. *Case reports in dermatology* **2015**, *7*, 70-74, doi:10.1159/000381844.
53. Pachman, L.M.; Khojah, A.M. Advances in Juvenile Dermatomyositis: Myositis Specific Antibodies Aid in Understanding Disease Heterogeneity. *The Journal of pediatrics* **2018**, *195*, 16-27, doi:10.1016/j.jpeds.2017.12.053.
54. van Aalst, M.; Nelen, C.M.; Goorhuis, A.; Stijnis, C.; Grobusch, M.P. Long-term sequelae of chikungunya virus disease: A systematic review. *Travel medicine and infectious disease* **2017**, *15*, 8-22, doi:10.1016/j.tmaid.2017.01.004.
55. Liao, K.P. Cardiovascular disease in patients with rheumatoid arthritis. *Trends in cardiovascular medicine* **2017**, *27*, 136-140, doi:10.1016/j.tcm.2016.07.006.
56. Hamczyk, M.R.; Andres, V. Accelerated atherosclerosis in HGPS. *Aging* **2018**, *10*, 2555-2556, doi:10.18632/aging.101608.
57. Prakash, A.; Gordon, L.B.; Kleinman, M.E.; Gurary, E.B.; Massaro, J.; D'Agostino, R., Sr.; Kieran, M.W.; Gerhard-Herman, M.; Smoot, L. Cardiac Abnormalities in Patients With

Hutchinson-Gilford Progeria Syndrome. *JAMA cardiology* **2018**, *3*, 326-334, doi:10.1001/jamacardio.2017.5235.

58. Hamczyk, M.R.; Andres, V. Vascular smooth muscle cell loss underpins the accelerated atherosclerosis in Hutchinson-Gilford progeria syndrome. *Nucleus* **2019**, *10*, 28-34, doi:10.1080/19491034.2019.1589359.
59. Lusis, A.J. Atherosclerosis. *Nature* **2000**, *407*, 233-241, doi:10.1038/35025203.
60. Wang, J.C.; Bennett, M. Aging and atherosclerosis: mechanisms, functional consequences, and potential therapeutics for cellular senescence. *Circulation research* **2012**, *111*, 245-259, doi:10.1161/CIRCRESAHA.111.261388.
61. Kvandova, M.; Majzunova, M.; Dovinova, I. The role of PPARgamma in cardiovascular diseases. *Physiological research* **2016**, *65*, S343-S363, doi:10.33549/physiolres.933439.
62. Toma, I.; McCaffrey, T.A. Transforming growth factor-beta and atherosclerosis: interwoven atherogenic and atheroprotective aspects. *Cell and tissue research* **2012**, *347*, 155-175, doi:10.1007/s00441-011-1189-3.
63. Galkina, E.; Ley, K. Immune and inflammatory mechanisms of atherosclerosis (*). *Annual review of immunology* **2009**, *27*, 165-197, doi:10.1146/annurev.immunol.021908.132620.
64. Higashi, Y.; Sukhanov, S.; Anwar, A.; Shai, S.Y.; Delafontaine, P. Aging, atherosclerosis, and IGF-1. *The journals of gerontology. Series A, Biological sciences and medical sciences* **2012**, *67*, 626-639, doi:10.1093/gerona/gls102.
65. Ayer, A.; Zarjou, A.; Agarwal, A.; Stocker, R. Heme Oxygenases in Cardiovascular Health and Disease. *Physiological reviews* **2016**, *96*, 1449-1508, doi:10.1152/physrev.00003.2016.
66. Huang, J.V.; Greyson, C.R.; Schwartz, G.G. PPAR-gamma as a therapeutic target in cardiovascular disease: evidence and uncertainty. *Journal of lipid research* **2012**, *53*, 1738-1754, doi:10.1194/jlr.R024505.
67. Pahan, K. Lipid-lowering drugs. *Cellular and molecular life sciences : CMLS* **2006**, *63*, 1165-1178, doi:10.1007/s00018-005-5406-7.
68. Fonsatti, E.; Del Vecchio, L.; Altomonte, M.; Sigalotti, L.; Nicotra, M.R.; Coral, S.; Natali, P.G.; Maio, M. Endoglin: An accessory component of the TGF-beta-binding receptor-complex with diagnostic, prognostic, and bioimmunotherapeutic potential in human malignancies. *Journal of cellular physiology* **2001**, *188*, 1-7, doi:10.1002/jcp.1095.
69. Domingo, D.L.; Trujillo, M.I.; Council, S.E.; Merideth, M.A.; Gordon, L.B.; Wu, T.; Introne, W.J.; Gahl, W.A.; Hart, T.C. Hutchinson-Gilford progeria syndrome: oral and craniofacial phenotypes. *Oral diseases* **2009**, *15*, 187-195, doi:10.1111/j.1601-0825.2009.01521.x.
70. Guo, Q.; Wang, Y.; Xu, D.; Nossent, J.; Pavlos, N.J.; Xu, J. Rheumatoid arthritis: pathological mechanisms and modern pharmacologic therapies. *Bone research* **2018**, *6*, 15, doi:10.1038/s41413-018-0016-9.
71. Kurowska, W.; Kuca-Warnawin, E.H.; Radzikowska, A.; Maslinski, W. The role of anti-citrullinated protein antibodies (ACPA) in the pathogenesis of rheumatoid arthritis.

*Central-European journal of immunology* **2017**, *42*, 390-398, doi:10.5114/ceji.2017.72807.

72. Smatti, M.K.; Cyprian, F.S.; Nasrallah, G.K.; Al Thani, A.A.; Almishal, R.O.; Yassine, H.M. Viruses and Autoimmunity: A Review on the Potential Interaction and Molecular Mechanisms. *Viruses* **2019**, *11*, doi:10.3390/v11080762.
73. Remy, A.; Combe, B. Repair of radiographic hip joint in juvenile rheumatoid arthritis patients treated with etanercept plus methotrexate. *Joint, bone, spine : revue du rhumatisme* **2014**, *81*, 447-449, doi:10.1016/j.jbspin.2014.03.006.
74. Lutzky, V.; Hannawi, S.; Thomas, R. Cells of the synovium in rheumatoid arthritis. Dendritic cells. *Arthritis research & therapy* **2007**, *9*, 219, doi:10.1186/ar2200.
75. Kinne, R.W.; Brauer, R.; Stuhlmuller, B.; Palombo-Kinne, E.; Burmester, G.R. Macrophages in rheumatoid arthritis. *Arthritis research* **2000**, *2*, 189-202, doi:10.1186/ar86.
76. Akhlaghi, S.; Sahebari, M.; Mahmoodi, M.; Yaseri, M.; Mansournia, M.A.; Zeraati, H. Casual effect of methotrexate+etanercept/infliximab on survival of patients with rheumatoid arthritis. *Pragmatic and observational research* **2019**, *10*, 23-28, doi:10.2147/POR.S194408.
77. Hennigan, S.; Kavanaugh, A. Interleukin-6 inhibitors in the treatment of rheumatoid arthritis. *Therapeutics and clinical risk management* **2008**, *4*, 767-775, doi:10.2147/tcrm.s3470.
78. Casan, J.M.L.; Wong, J.; Northcott, M.J.; Opat, S. Anti-CD20 monoclonal antibodies: reviewing a revolution. *Human vaccines & immunotherapeutics* **2018**, *14*, 2820-2841, doi:10.1080/21645515.2018.1508624.
79. Akinci, B.; Sahinoz, M.; Oral, E. Lipodystrophy Syndromes: Presentation and Treatment. In *Endotext*, Feingold, K.R., Anawalt, B., Boyce, A., Chrousos, G., Dungan, K., Grossman, A., Hershman, J.M., Kaltsas, G., Koch, C., Kopp, P., et al., Eds. South Dartmouth (MA), 2000.
80. esterified free fatty acidsCoppede, F. The epidemiology of premature aging and associated comorbidities. *Clinical interventions in aging* **2013**, *8*, 1023-1032, doi:10.2147/CIA.S37213.
81. Iannello, A.; Samarani, S.; Debbeche, O.; Boulassel, M.R.; Tremblay, C.; Toma, E.; Routy, J.P.; Ahmad, A. Potential role of IL-18 in the immunopathogenesis of AIDS, HIV-associated lipodystrophy and related clinical conditions. *Current HIV research* **2010**, *8*, 147-164, doi:10.2174/157016210790442713.
82. Foss-Freitas, M.C.; Ferraz, R.C.; Monteiro, L.Z.; Gomes, P.M.; Iwakura, R.; de Freitas, L.C.C.; Foss, M.C. Endoplasmic reticulum stress activation in adipose tissue induces metabolic syndrome in individuals with familial partial lipodystrophy of the Dunnigan type. *Diabetology & metabolic syndrome* **2018**, *10*, 6, doi:10.1186/s13098-017-0301-6.
83. Crujeiras, A.B.; Diaz-Lagares, A.; Carreira, M.C.; Amil, M.; Casanueva, F.F. Oxidative stress associated to dysfunctional adipose tissue: a potential link between obesity, type 2 diabetes mellitus and breast cancer. *Free radical research* **2013**, *47*, 243-256,

doi:10.3109/10715762.2013.772604.

84. Kola, B. Role of AMP-activated protein kinase in the control of appetite. *Journal of neuroendocrinology* **2008**, *20*, 942-951, doi:10.1111/j.1365-2826.2008.01745.x.
85. Stern, J.H.; Rutkowski, J.M.; Scherer, P.E. Adiponectin, Leptin, and Fatty Acids in the Maintenance of Metabolic Homeostasis through Adipose Tissue Crosstalk. *Cell metabolism* **2016**, *23*, 770-784, doi:10.1016/j.cmet.2016.04.011.
86. Caron, M.; Vigouroux, C.; Bastard, J.P.; Capeau, J. Antiretroviral-related adipocyte dysfunction and lipodystrophy in HIV-infected patients: Alteration of the PPARgamma-dependent pathways. *PPAR research* **2009**, *2009*, 507141, doi:10.1155/2009/507141.
87. Safar Zadeh, E.; Lungu, A.O.; Cochran, E.K.; Brown, R.J.; Ghany, M.G.; Heller, T.; Kleiner, D.E.; Gorden, P. The liver diseases of lipodystrophy: the long-term effect of leptin treatment. *Journal of hepatology* **2013**, *59*, 131-137, doi:10.1016/j.jhep.2013.02.007.
88. Muneeb, F.; Hardman, J.A.; Paus, R. Hair growth control by innate immunocytes: Perifollicular macrophages revisited. *Experimental dermatology* **2019**, *28*, 425-431, doi:10.1111/exd.13922.
89. Guo, H.; Cheng, Y.; Shapiro, J.; McElwee, K. The role of lymphocytes in the development and treatment of alopecia areata. *Expert review of clinical immunology* **2015**, *11*, 1335-1351, doi:10.1586/1744666X.2015.1085306.
90. Hoffmann, R.; Eicheler, W.; Huth, A.; Wenzel, E.; Happle, R. Cytokines and growth factors influence hair growth in vitro. Possible implications for the pathogenesis and treatment of alopecia areata. *Archives of dermatological research* **1996**, *288*, 153-156, doi:10.1007/BF02505825.
91. Ramadi, K.B.; Mohamed, Y.A.; Al-Sbiei, A.; Almarzooqi, S.; Bashir, G.; Al Dhanhani, A.; Sarawathiamma, D.; Qadri, S.; Yasin, J.; Nemmar, A., et al. Acute systemic exposure to silver-based nanoparticles induces hepatotoxicity and NLRP3-dependent inflammation. *Nanotoxicology* **2016**, *10*, 1061-1074, doi:10.3109/17435390.2016.1163743.
92. Gregoriou, S.; Papafragkaki, D.; Kontochristopoulos, G.; Rallis, E.; Kalogeromitros, D.; Rigopoulos, D. Cytokines and other mediators in alopecia areata. *Mediators of inflammation* **2010**, *2010*, 928030, doi:10.1155/2010/928030.
93. Freyschmidt-Paul, P.; McElwee, K.J.; Hoffmann, R.; Sundberg, J.P.; Vitacolonna, M.; Kissling, S.; Zoller, M. Interferon-gamma-deficient mice are resistant to the development of alopecia areata. *The British journal of dermatology* **2006**, *155*, 515-521, doi:10.1111/j.1365-2133.2006.07377.x.
94. Gupta, A.K.; Carviel, J.L.; Foley, K.A.; Shear, N.H.; Piraccini, B.M.; Piguet, V.; Tosti, A. Monotherapy for Alopecia Areata: A Systematic Review and Network Meta-Analysis. *Skin appendage disorders* **2019**, *5*, 331-337, doi:10.1159/000501940.
95. Strazzulla, L.C.; Wang, E.H.C.; Avila, L.; Lo Sicco, K.; Brinster, N.; Christiano, A.M.; Shapiro, J. Alopecia areata: An appraisal of new treatment approaches and overview of current therapies. *Journal of the American Academy of Dermatology* **2018**, *78*, 15-24, doi:10.1016/j.jaad.2017.04.1142.

96. Sardana, K.; Gupta, A.; Gautam, R.K. Recalcitrant alopecia areata responsive to leflunomide and anthralin-Potentially undiscovered JAK/STAT inhibitors? *Pediatric dermatology* **2018**, *35*, 856-858, doi:10.1111/pde.13688.
97. Garrido-Trigo, A.; Salas, A. Molecular structure and function of Janus kinases: implications for the development of inhibitors. *Journal of Crohn's & colitis* **2019**, 10.1093/ecco-jcc/jjz206, doi:10.1093/ecco-jcc/jjz206.
98. Ferrao, R.; Lupardus, P.J. The Janus Kinase (JAK) FERM and SH2 Domains: Bringing Specificity to JAK-Receptor Interactions. *Frontiers in endocrinology* **2017**, *8*, 71, doi:10.3389/fendo.2017.00071.
99. Babon, J.J.; Lucet, I.S.; Murphy, J.M.; Nicola, N.A.; Varghese, L.N. The molecular regulation of Janus kinase (JAK) activation. *The Biochemical journal* **2014**, *462*, 1-13, doi:10.1042/BJ20140712.
100. Gabriel, D.; Roedl, D.; Gordon, L.B.; Djabali, K. Sulforaphane enhances progerin clearance in Hutchinson-Gilford progeria fibroblasts. *Aging cell* **2015**, *14*, 78-91, doi:10.1111/acel.12300.
101. Cao, K.; Graziotto, J.J.; Blair, C.D.; Mazzulli, J.R.; Erdos, M.R.; Krainc, D.; Collins, F.S. Rapamycin reverses cellular phenotypes and enhances mutant protein clearance in Hutchinson-Gilford progeria syndrome cells. *Science translational medicine* **2011**, *3*, 89ra58, doi:10.1126/scitranslmed.3002346.
102. Wung, B.S.; Ni, C.W.; Wang, D.L. ICAM-1 induction by TNFalpha and IL-6 is mediated by distinct pathways via Rac in endothelial cells. *Journal of biomedical science* **2005**, *12*, 91-101, doi:10.1007/s11373-004-8170-z.
103. Magyari, L.; Varszegi, D.; Kovesdi, E.; Sarlos, P.; Farago, B.; Javorhazy, A.; Sumegi, K.; Banfai, Z.; Melegh, B. Interleukins and interleukin receptors in rheumatoid arthritis: Research, diagnostics and clinical implications. *World journal of orthopedics* **2014**, *5*, 516-536, doi:10.5312/wjo.v5.i4.516.
104. Ma, X.; Wang, D.; Zhao, W.; Xu, L. Deciphering the Roles of PPARgamma in Adipocytes via Dynamic Change of Transcription Complex. *Frontiers in endocrinology* **2018**, *9*, 473, doi:10.3389/fendo.2018.00473.
105. Gao, Z.; Jin, Y.Q.; Wu, W. SOCS3 treatment prevents the development of alopecia areata by inhibiting CD8+ T cell-mediated autoimmune destruction. *Oncotarget* **2017**, *8*, 33432-33443, doi:10.18632/oncotarget.16504.
106. Harhouri, K.; Frankel, D.; Bartoli, C.; Roll, P.; De Sandre-Giovannoli, A.; Levy, N. An overview of treatment strategies for Hutchinson-Gilford Progeria syndrome. *Nucleus* **2018**, *9*, 246-257, doi:10.1080/19491034.2018.1460045.
107. Gabriel, D.; Shafry, D.D.; Gordon, L.B.; Djabali, K. Intermittent treatment with farnesyltransferase inhibitor and sulforaphane improves cellular homeostasis in Hutchinson-Gilford progeria fibroblasts. *Oncotarget* **2017**, *8*, 64809-64826, doi:10.18632/oncotarget.19363.
108. Yang, S.H.; Chang, S.Y.; Ren, S.; Wang, Y.; Andres, D.A.; Spielmann, H.P.; Fong, L.G.; Young, S.G. Absence of progeria-like disease phenotypes in knock-in mice expressing a non-farnesylated version of progerin. *Human molecular genetics* **2011**, *20*, 436-444,

doi:10.1093/hmg/ddq490.

109. Gordon, L.B.; Massaro, J.; D'Agostino, R.B., Sr.; Campbell, S.E.; Brazier, J.; Brown, W.T.; Kleinman, M.E.; Kieran, M.W.; Progeria Clinical Trials, C. Impact of farnesylation inhibitors on survival in Hutchinson-Gilford progeria syndrome. *Circulation* **2014**, *130*, 27-34, doi:10.1161/CIRCULATIONAHA.113.008285.
110. Varela, I.; Pereira, S.; Ugalde, A.P.; Navarro, C.L.; Suarez, M.F.; Cau, P.; Cadinanos, J.; Osorio, F.G.; Foray, N.; Cobo, J., et al. Combined treatment with statins and aminobisphosphonates extends longevity in a mouse model of human premature aging. *Nature medicine* **2008**, *14*, 767-772, doi:10.1038/nm1786.
111. Gordon, L.B.; Kleinman, M.E.; Massaro, J.; D'Agostino, R.B., Sr.; Shappell, H.; Gerhard-Herman, M.; Smoot, L.B.; Gordon, C.M.; Cleveland, R.H.; Nazarian, A., et al. Clinical Trial of the Protein Farnesylation Inhibitors Lonafarnib, Pravastatin, and Zoledronic Acid in Children With Hutchinson-Gilford Progeria Syndrome. *Circulation* **2016**, *134*, 114-125, doi:10.1161/CIRCULATIONAHA.116.022188.
112. Adam, S.A.; Butin-Israeli, V.; Cleland, M.M.; Shimi, T.; Goldman, R.D. Disruption of lamin B1 and lamin B2 processing and localization by farnesyltransferase inhibitors. *Nucleus* **2013**, *4*, 142-150, doi:10.4161/nucl.24089.
113. Ramos, F.J.; Chen, S.C.; Garelick, M.G.; Dai, D.F.; Liao, C.Y.; Schreiber, K.H.; MacKay, V.L.; An, E.H.; Strong, R.; Ladiges, W.C., et al. Rapamycin reverses elevated mTORC1 signaling in lamin A/C-deficient mice, rescues cardiac and skeletal muscle function, and extends survival. *Science translational medicine* **2012**, *4*, 144ra103, doi:10.1126/scitranslmed.3003802.
114. Blondel, S.; Egesipe, A.L.; Picardi, P.; Jaskowiak, A.L.; Notarnicola, M.; Ragot, J.; Tournois, J.; Le Corf, A.; Brinon, B.; Poydenot, P., et al. Drug screening on Hutchinson Gilford progeria pluripotent stem cells reveals aminopyrimidines as new modulators of farnesylation. *Cell death & disease* **2016**, *7*, e2105, doi:10.1038/cddis.2015.374.
115. Clements, C.S.; Bikkul, M.U.; Ofosu, W.; Eskiw, C.; Tree, D.; Makarov, E.; Kill, I.R.; Bridger, J.M. Presence and distribution of progerin in HGPS cells is ameliorated by drugs that impact on the mevalonate and mTOR pathways. *Biogerontology* **2019**, *20*, 337-358, doi:10.1007/s10522-019-09807-4.
116. Mayence, A.; Vanden Eynde, J.J. Baricitinib: A 2018 Novel FDA-Approved Small Molecule Inhibiting Janus Kinases. *Pharmaceuticals* **2019**, *12*, doi:10.3390/ph12010037.
117. Taylor, P.C. Clinical efficacy of launched JAK inhibitors in rheumatoid arthritis. *Rheumatology* **2019**, *58*, i17-i26, doi:10.1093/rheumatology/key225.
118. Jabbari, A.; Dai, Z.; Xing, L.; Cerise, J.E.; Ramot, Y.; Berkun, Y.; Sanchez, G.A.; Goldbach-Mansky, R.; Christiano, A.M.; Clynes, R., et al. Reversal of Alopecia Areata Following Treatment With the JAK1/2 Inhibitor Baricitinib. *EBioMedicine* **2015**, *2*, 351-355, doi:10.1016/j.ebiom.2015.02.015.
119. Boyadzhiev, M.; Marinov, L.; Boyadzhiev, V.; Iotova, V.; Aksentijevich, I.; Hambleton, S. Disease course and treatment effects of a JAK inhibitor in a patient with CANDLE syndrome. *Pediatric rheumatology online journal* **2019**, *17*, 19, doi:10.1186/s12969-

019-0322-9.

120. Westhovens, R. Clinical efficacy of new JAK inhibitors under development. Just more of the same? *Rheumatology* **2019**, *58*, i27-i33, doi:10.1093/rheumatology/key256.
121. de Oliveira, A.B.; Alpalhao, M.; Filipe, P.; Maia-Silva, J. The role of Janus kinase inhibitors in the treatment of alopecia areata: A systematic review. *Dermatologic therapy* **2019**, *32*, e13053, doi:10.1111/dth.13053.
122. Kuriya, B.; Cohen, M.D.; Keystone, E. Baricitinib in rheumatoid arthritis: evidence-to-date and clinical potential. *Therapeutic advances in musculoskeletal disease* **2017**, *9*, 37-44, doi:10.1177/1759720X16687481.
123. Gordon, L.B.; Rothman, F.G.; Lopez-Otin, C.; Misteli, T. Progeria: a paradigm for translational medicine. *Cell* **2014**, *156*, 400-407, doi:10.1016/j.cell.2013.12.028.
124. Merideth, M.A.; Gordon, L.B.; Clauss, S.; Sachdev, V.; Smith, A.C.; Perry, M.B.; Brewer, C.C.; Zalewski, C.; Kim, H.J.; Solomon, B., et al. Phenotype and course of Hutchinson-Gilford progeria syndrome. *The New England journal of medicine* **2008**, *358*, 592-604, doi:10.1056/NEJMoa0706898.
125. Novelli, G.; Muchir, A.; Sangiuolo, F.; Helbling-Leclerc, A.; D'Apice, M.R.; Massart, C.; Capon, F.; Sbraccia, P.; Federici, M.; Lauro, R., et al. Mandibuloacral dysplasia is caused by a mutation in LMNA-encoding lamin A/C. *American journal of human genetics* **2002**, *71*, 426-431, doi:10.1086/341908.
126. Motegi, S.; Yokoyama, Y.; Uchiyama, A.; Ogino, S.; Takeuchi, Y.; Yamada, K.; Hattori, T.; Hashizume, H.; Ishikawa, Y.; Goto, M., et al. First Japanese case of atypical progeroid syndrome/atypical Werner syndrome with heterozygous LMNA mutation. *The Journal of dermatology* **2014**, *41*, 1047-1052, doi:10.1111/1346-8138.12657.
127. Dai, W.; Jiang, Y.; Chen, K.; Qiu, J.; Sun, J.; Zhang, W.; Zhou, X.; Huang, N.; Li, Y.; Li, W. Effect of etoposide-induced alteration of the Mdm2-Rb signaling pathway on cellular senescence in A549 lung adenocarcinoma cells. *Oncology letters* **2017**, *14*, 3935-3940, doi:10.3892/ol.2017.6684.
128. Derecka, M.; Gornicka, A.; Koralov, S.B.; Szczepanek, K.; Morgan, M.; Raje, V.; Sisler, J.; Zhang, Q.; Otero, D.; Cichy, J., et al. Tyk2 and Stat3 regulate brown adipose tissue differentiation and obesity. *Cell metabolism* **2012**, *16*, 814-824, doi:10.1016/j.cmet.2012.11.005.
129. Jacobsen, M.; Repsilber, D.; Kleinsteuber, K.; Gutschmidt, A.; Schommer-Leitner, S.; Black, G.; Walzl, G.; Kaufmann, S.H. Suppressor of cytokine signaling-3 is affected in T-cells from tuberculosisTB patients. *Clinical microbiology and infection : the official publication of the European Society of Clinical Microbiology and Infectious Diseases* **2011**, *17*, 1323-1331, doi:10.1111/j.1469-0691.2010.03326.x.
130. Chang, M.C.; Chiang, Y.C.; Ho, C.M.; Chen, Y.L.; Chen, C.A.; Cheng, W.F.; Chou, C.Y. New primers for methylation-specific polymerase chain reaction enhance specificity of detecting STAT1 methylation. *Taiwanese journal of obstetrics & gynecology* **2012**, *51*, 43-49, doi:10.1016/j.tjog.2012.01.009.
131. Hambleton, S.; Goodbourn, S.; Young, D.F.; Dickinson, P.; Mohamad, S.M.; Valappil, M.; McGovern, N.; Cant, A.J.; Hackett, S.J.; Ghazal, P., et al. STAT2 deficiency and

susceptibility to viral illness in humans. *Proceedings of the National Academy of Sciences of the United States of America* **2013**, *110*, 3053-3058, doi:10.1073/pnas.1220098110.

132. Patel, K.; Kollory, A.; Takashima, A.; Sarkar, S.; Faller, D.V.; Ghosh, S.K. MicroRNA let-7 downregulates STAT3 phosphorylation in pancreatic cancer cells by increasing SOCS3 expression. *Cancer letters* **2014**, *347*, 54-64, doi:10.1016/j.canlet.2014.01.020.
133. Liu, F.; Guo, J.; Tian, T.; Wang, H.; Dong, F.; Huang, H.; Dong, M. Placental trophoblasts shifted Th1/Th2 balance toward Th2 and inhibited Th17 immunity at fetomaternal interface. *APMIS : acta pathologica, microbiologica, et immunologica Scandinavica* **2011**, *119*, 597-604, doi:10.1111/j.1600-0463.2011.02774.x.
134. Cantu, C.; Ierardi, R.; Alborelli, I.; Fugazza, C.; Cassinelli, L.; Piconese, S.; Bose, F.; Ottolenghi, S.; Ferrari, G.; Ronchi, A. Sox6 enhances erythroid differentiation in human erythroid progenitors. *Blood* **2011**, *117*, 3669-3679, doi:10.1182/blood-2010-04-282350.
135. Kooreman, N.G.; de Almeida, P.E.; Stack, J.P.; Nelakanti, R.V.; Diecke, S.; Shao, N.Y.; Swijnenburg, R.J.; Sanchez-Freire, V.; Matsa, E.; Liu, C., et al. Alloimmune Responses of Humanized Mice to Human Pluripotent Stem Cell Therapeutics. *Cell reports* **2017**, *20*, 1978-1990, doi:10.1016/j.celrep.2017.08.003.
136. Mogilenko, D.A.; Kudriavtsev, I.V.; Trulioff, A.S.; Shavva, V.S.; Dizhe, E.B.; Missyul, B.V.; Zhakhov, A.V.; Ischenko, A.M.; Perevozchikov, A.P.; Orlov, S.V. Modified low density lipoprotein stimulates complement C3 expression and secretion via liver X receptor and Toll-like receptor 4 activation in human macrophages. *The Journal of biological chemistry* **2012**, *287*, 5954-5968, doi:10.1074/jbc.M111.289322.
137. Kefaloyianni, E.; Muthu, M.L.; Kaeppler, J.; Sun, X.; Sabbisetti, V.; Chalaris, A.; Rose-John, S.; Wong, E.; Sagi, I.; Waikar, S.S., et al. ADAM17 substrate release in proximal tubule drives kidney fibrosis. *JCI insight* **2016**, *1*, doi:10.1172/jci.insight.87023.
138. Pravenec, M.; Kajiya, T.; Zidek, V.; Landa, V.; Mlejnek, P.; Simakova, M.; Silhavy, J.; Malinska, H.; Oliyarnyk, O.; Kazdova, L., et al. Effects of human C-reactive protein on pathogenesis of features of the metabolic syndrome. *Hypertension* **2011**, *57*, 731-737, doi:10.1161/HYPERTENSIONAHA.110.164350.
139. Das, H.; Koizumi, T.; Sugimoto, T.; Chakraborty, S.; Ichimura, T.; Hasegawa, K.; Nishimura, R. Quantitation of Fas and Fas ligand gene expression in human ovarian, cervical and endometrial carcinomas using real-time quantitative RT-PCR. *British journal of cancer* **2000**, *82*, 1682-1688, doi:10.1054/bjoc.2000.1118.
140. Jais, A.; Einwallner, E.; Sharif, O.; Gossens, K.; Lu, T.T.; Soyal, S.M.; Medgyesi, D.; Neureiter, D.; Paier-Pourani, J.; Dalgaard, K., et al. Heme oxygenase-1 drives metaflammation and insulin resistance in mouse and man. *Cell* **2014**, *158*, 25-40, doi:10.1016/j.cell.2014.04.043.
141. Di, D.; Chen, L.; Wang, L.; Sun, P.; Liu, Y.; Xu, Z.; Ju, J. Downregulation of human intercellular adhesion molecule-1 attenuates the metastatic ability in human breast cancer cell lines. *Oncology reports* **2016**, *35*, 1541-1548, doi:10.3892/or.2016.4543.
142. Narantuya, D.; Nagai, A.; Sheikh, A.M.; Masuda, J.; Kobayashi, S.; Yamaguchi, S.; Kim,

S.U. Human microglia transplanted in rat focal ischemia brain induce neuroprotection and behavioral improvement. *PloS one* **2010**, *5*, e11746, doi:10.1371/journal.pone.0011746.

143. Flannery, C.A.; Rowzee, A.M.; Choe, G.H.; Saleh, F.L.; Radford, C.C.; Taylor, H.S.; Wood, T.L. Development of a Quantitative PCR Assay for Detection of Human Insulin-Like Growth Factor Receptor and Insulin Receptor Isoforms. *Endocrinology* **2016**, *157*, 1702-1708, doi:10.1210/en.2015-1698.
144. Zannetti, C.; Roblot, G.; Charrier, E.; Ainouze, M.; Tout, I.; Briat, F.; Isorce, N.; Faure-Dupuy, S.; Michelet, M.; Marotel, M., et al. Characterization of the Inflammasome in Human Kupffer Cells in Response to Synthetic Agonists and Pathogens. *Journal of immunology* **2016**, *197*, 356-367, doi:10.4049/jimmunol.1502301.
145. Steensberg, A.; Keller, C.; Starkie, R.L.; Osada, T.; Febbraio, M.A.; Pedersen, B.K. IL-6 and TNF-alpha expression in, and release from, contracting human skeletal muscle. *American journal of physiology. Endocrinology and metabolism* **2002**, *283*, E1272-1278, doi:10.1152/ajpendo.00255.2002.
146. Nacul, A.P.; Lecke, S.B.; Edelweiss, M.I.; Morsch, D.M.; Spritzer, P.M. Gene expression of leptin and long leptin receptor isoform in endometriosis: a case-control study. *Obstetrics and gynecology international* **2013**, *2013*, 879618, doi:10.1155/2013/879618.
147. Pettinelli, P.; Videla, L.A. Up-regulation of PPAR-gamma mRNA expression in the liver of obese patients: an additional reinforcing lipogenic mechanism to SREBP-1c induction. *The Journal of clinical endocrinology and metabolism* **2011**, *96*, 1424-1430, doi:10.1210/jc.2010-2129.
148. Xie, S.; Macedo, P.; Hew, M.; Nassenstein, C.; Lee, K.Y.; Chung, K.F. Expression of transforming growth factor-beta (TGF-beta) in chronic idiopathic cough. *Respiratory research* **2009**, *10*, 40, doi:10.1186/1465-9921-10-40.
149. Grenon, S.M.; Jeanne, M.; Aguado-Zuniga, J.; Conte, M.S.; Hughes-Fulford, M. Effects of gravitational mechanical unloading in endothelial cells: association between caveolins, inflammation and adhesion molecules. *Scientific reports* **2013**, *3*, 1494, doi:10.1038/srep01494.
150. Carmona Arana, J.A.; Seher, A.; Neumann, M.; Lang, I.; Siegmund, D.; Wajant, H. TNF Receptor-Associated Factor 1 is a Major Target of Soluble TWEAK. *Frontiers in immunology* **2014**, *5*, 63, doi:10.3389/fimmu.2014.00063.
151. Chang, C.C.; Huang, C.C.; Yang, S.H.; Chien, C.C.; Lee, C.L.; Huang, C.J. Data on clinical significance of GAS2 in colorectal cancer cells. *Data in brief* **2016**, *8*, 82-86, doi:10.1016/j.dib.2016.05.010.
152. Yates, B.; Braschi, B.; Gray, K.A.; Seal, R.L.; Tweedie, S.; Bruford, E.A. Genenames.org: the HGNC and VGNC resources in 2017. *Nucleic acids research* **2017**, *45*, D619-D625, doi:10.1093/nar/gkw1033.
153. Pasolli, E.; Schiffer, L.; Manghi, P.; Renson, A.; Obenchain, V.; Truong, D.T.; Beghini, F.; Malik, F.; Ramos, M.; Dowd, J.B., et al. Accessible, curated metagenomic data through ExperimentHub. *Nature methods* **2017**, *14*, 1023-1024, doi:10.1038/nmeth.4468.

154. Rani, J.; Shah, A.B.; Ramachandran, S. pubmed.mineR: an R package with text-mining algorithms to analyse PubMed abstracts. *Journal of biosciences* **2015**, *40*, 671-682, doi:10.1007/s12038-015-9552-2.
155. Lam, F.; Lalansingh, C.M.; Babaran, H.E.; Wang, Z.; Prokopec, S.D.; Fox, N.S.; Boutros, P.C. VennDiagramWeb: a web application for the generation of highly customizable Venn and Euler diagrams. *BMC bioinformatics* **2016**, *17*, 401, doi:10.1186/s12859-016-1281-5.
156. Cook, H.V.; Doncheva, N.T.; Szklarczyk, D.; von Mering, C.; Jensen, L.J. Viruses.STRING: A Virus-Host Protein-Protein Interaction Database. *Viruses* **2018**, *10*, doi:10.3390/v10100519.
157. Han, H.; Cho, J.W.; Lee, S.; Yun, A.; Kim, H.; Bae, D.; Yang, S.; Kim, C.Y.; Lee, M.; Kim, E., et al. TRRUST v2: an expanded reference database of human and mouse transcriptional regulatory interactions. *Nucleic acids research* **2018**, *46*, D380-D386, doi:10.1093/nar/gkx1013.
158. Essaghir, A.; Toffalini, F.; Knoops, L.; Kallin, A.; van Helden, J.; Demoulin, J.B. Transcription factor regulation can be accurately predicted from the presence of target gene signatures in microarray gene expression data. *Nucleic acids research* **2010**, *38*, e120, doi:10.1093/nar/gkq149.
159. Marbach, D.; Lamparter, D.; Quon, G.; Kellis, M.; Kutalik, Z.; Bergmann, S. Tissue-specific regulatory circuits reveal variable modular perturbations across complex diseases. *Nature methods* **2016**, *13*, 366-370, doi:10.1038/nmeth.3799.
160. Darzynkiewicz, Z.; Halicka, H.D.; Zhao, H. Analysis of cellular DNA content by flow and laser scanning cytometry. *Advances in experimental medicine and biology* **2010**, *676*, 137-147, doi:10.1007/978-1-4419-6199-0_9.
161. Bassaneze, V.; Miyakawa, A.A.; Krieger, J.E. A quantitative chemiluminescent method for studying replicative and stress-induced premature senescence in cell cultures. *Analytical biochemistry* **2008**, *372*, 198-203, doi:10.1016/j.ab.2007.08.016.
162. Mery, B.; Guy, J.B.; Vallard, A.; Espenel, S.; Ardail, D.; Rodriguez-Lafrasse, C.; Rancoule, C.; Magne, N. In Vitro Cell Death Determination for Drug Discovery: A Landscape Review of Real Issues. *Journal of cell death* **2017**, *10*, 1179670717691251, doi:10.1177/1179670717691251.
163. Cecchini, M.J.; Amiri, M.; Dick, F.A. Analysis of cell cycle position in mammalian cells. *Journal of visualized experiments : JoVE* **2012**, 10.3791/3491, doi:10.3791/3491.
164. Livneh, I.; Cohen-Kaplan, V.; Cohen-Rosenzweig, C.; Avni, N.; Ciechanover, A. The life cycle of the 26S proteasome: from birth, through regulation and function, and onto its death. *Cell research* **2016**, *26*, 869-885, doi:10.1038/cr.2016.86.
165. Munafo, D.B.; Colombo, M.I. A novel assay to study autophagy: regulation of autophagosome vacuole size by amino acid deprivation. *Journal of cell science* **2001**, *114*, 3619-3629.
166. Morciano, G.; Sarti, A.C.; Marchi, S.; Missiroli, S.; Falzoni, S.; Raffaghello, L.; Pistoia, V.; Giorgi, C.; Di Virgilio, F.; Pinton, P. Use of luciferase probes to measure ATP in living cells and animals. *Nature protocols* **2017**, *12*, 1542-1562, doi:10.1038/nprot.2017.052.

167. Desjardins, P.; Conklin, D. NanoDrop microvolume quantitation of nucleic acids. *Journal of visualized experiments : JoVE* **2010**, 10.3791/2565, doi:10.3791/2565.
168. Valones, M.A.; Guimaraes, R.L.; Brandao, L.A.; de Souza, P.R.; de Albuquerque Tavares Carvalho, A.; Crovela, S. Principles and applications of polymerase chain reaction in medical diagnostic fields: a review. *Brazilian journal of microbiology : [publication of the Brazilian Society for Microbiology]* **2009**, *40*, 1-11, doi:10.1590/S1517-83822009000100001.
169. Ye, J.; Coulouris, G.; Zaretskaya, I.; Cutcutache, I.; Rozen, S.; Madden, T.L. Primer-BLAST: a tool to design target-specific primers for polymerase chain reaction. *BMC bioinformatics* **2012**, *13*, 134, doi:10.1186/1471-2105-13-134.
170. Pfaffl, M.W. A new mathematical model for relative quantification in real-time RT-PCR. *Nucleic acids research* **2001**, *29*, e45, doi:10.1093/nar/29.9.e45.
171. Georgiou, C.D.; Grintzalis, K.; Zervoudakis, G.; Papapostolou, I. Mechanism of Coomassie brilliant blue G-250 binding to proteins: a hydrophobic assay for nanogram quantities of proteins. *Analytical and bioanalytical chemistry* **2008**, *391*, 391-403, doi:10.1007/s00216-008-1996-x.
172. Mahmood, T.; Yang, P.C. Western blot: technique, theory, and trouble shooting. *North American journal of medical sciences* **2012**, *4*, 429-434, doi:10.4103/1947-2714.100998.
173. Chen, L.; Deng, H.; Cui, H.; Fang, J.; Zuo, Z.; Deng, J.; Li, Y.; Wang, X.; Zhao, L. Inflammatory responses and inflammation-associated diseases in organs. *Oncotarget* **2018**, *9*, 7204-7218, doi:10.18632/oncotarget.23208.
174. Garcia-Unzueta, M.T.; Pesquera, C.; Calzada, E.; De la Mora, A.; Munoz, P.; Llorca, J.; Morchon, N.; Fernandez-Gonzalez, M.D.; Amado, J.A. Blood-soluble Fas levels are increased in type 2 diabetic patients with peripheral vascular disease. *Hormone and metabolic research = Hormon- und Stoffwechselforschung = Hormones et metabolisme* **2006**, *38*, 673-677, doi:10.1055/s-2006-954585.
175. Troyanov, S.; Hebert, M.J.; Masse, M.; Vigneault, N.; Sirois, I.; Madore, F. Soluble Fas: a novel predictor of atherosclerosis in dialysis patients. *American journal of kidney diseases : the official journal of the National Kidney Foundation* **2003**, *41*, 1043-1051, doi:10.1016/s0272-6386(03)00202-6.
176. Zhu, A.; Wang, M.; Zhou, G.; Zhang, H.; Liu, R.; Wang, Y. Fas/FasL, Bcl2 and Caspase-8 gene polymorphisms in Chinese patients with rheumatoid arthritis. *Rheumatology international* **2016**, *36*, 807-818, doi:10.1007/s00296-016-3443-1.
177. Rajasekhar, M.; Olsson, A.M.; Steel, K.J.; Georgouli, M.; Ranasinghe, U.; Brender Read, C.; Frederiksen, K.S.; Taams, L.S. MicroRNA-155 contributes to enhanced resistance to apoptosis in monocytes from patients with rheumatoid arthritis. *Journal of autoimmunity* **2017**, *79*, 53-62, doi:10.1016/j.jaut.2017.01.002.
178. Sievers, M.; Walker, U.A.; Sevastianova, K.; Setzer, B.; Wagsater, D.; Eriksson, P.; Yki-Jarvinen, H.; Sutinen, J. Gene expression and immunohistochemistry in adipose tissue of HIV type 1-infected patients with nucleoside analogue reverse-transcriptase inhibitor-associated lipoatrophy. *The Journal of infectious diseases* **2009**, *200*, 252-

262, doi:10.1086/599986.

179. Freyschmidt, J.; Klempa, I.; Gutberlet, K. [Successful use of transvenous angio-multidetector-CT in diagnosing cecal angiodysplasia as the cause of peranal hemorrhage]. *RoFo : Fortschritte auf dem Gebiete der Rontgenstrahlen und der Nuklearmedizin* **2003**, *175*, 855-857, doi:10.1055/s-2003-39930.
180. Wei, W.M.; Wu, X.Y.; Li, S.T.; Shen, Q. PPARG gene C161T CT/TT associated with lower blood lipid levels and ischemic stroke from large-artery atherosclerosis in a Han population in Guangdong. *Neurological research* **2016**, *38*, 620-624, doi:10.1080/01616412.2016.1189056.
181. Butt, C.; Gladman, D.; Rahman, P. PPAR-gamma gene polymorphisms and psoriatic arthritis. *J Rheumatol* **2006**, *33*, 1631-1633.
182. Giaginis, C.; Giagini, A.; Theocharis, S. Peroxisome proliferator-activated receptor-gamma (PPAR-gamma) ligands as potential therapeutic agents to treat arthritis. *Pharmacol Res* **2009**, *60*, 160-169, doi:10.1016/j.phrs.2009.02.005.
183. Victoria, B.; Cabezas-Agricola, J.M.; Gonzalez-Mendez, B.; Lattanzi, G.; Del Coco, R.; Loidi, L.; Barreiro, F.; Calvo, C.; Lado-Abeal, J.; Araujo-Vilar, D. Reduced adipogenic gene expression in fibroblasts from a patient with type 2 congenital generalized lipodystrophy. *Diabet Med* **2010**, *27*, 1178-1187, doi:10.1111/j.1464-5491.2010.03052.x.
184. Jiang, C.; Ting, A.T.; Seed, B. PPAR-gamma agonists inhibit production of monocyte inflammatory cytokines. *Nature* **1998**, *391*, 82-86, doi:10.1038/34184.
185. Gaspar, N.K. DHEA and frontal fibrosing alopecia: molecular and physiopathological mechanisms. *An Bras Dermatol* **2016**, *91*, 776-780, doi:10.1590/abd1806-4841.20165029.
186. Harries, M.J.; Paus, R. Scarring alopecia and the PPAR-gamma connection. *J Invest Dermatol* **2009**, *129*, 1066-1070, doi:10.1038/jid.2008.425.
187. Dinh, Q.N.; Chrissobolis, S.; Diep, H.; Chan, C.T.; Ferens, D.; Drummond, G.R.; Sobey, C.G. Advanced atherosclerosis is associated with inflammation, vascular dysfunction and oxidative stress, but not hypertension. *Pharmacol Res* **2017**, *116*, 70-76, doi:10.1016/j.phrs.2016.12.032.
188. Harrington, J.R. The Role of MCP-1 in Atherosclerosis. *STEM CELLS* **2000**, *18*, 65-66, doi:10.1634/stemcells.18-1-65.
189. Haringman, J.J.; Gerlag, D.M.; Smeets, T.J.; Baeten, D.; van den Bosch, F.; Bresnihan, B.; Breedveld, F.C.; Dinant, H.J.; Legay, F.; Gram, H., et al. A randomized controlled trial with an anti-CCL2 (anti-monocyte chemotactic protein 1) monoclonal antibody in patients with rheumatoid arthritis. *Arthritis Rheum* **2006**, *54*, 2387-2392, doi:10.1002/art.21975.
190. Villarroya, J.; Diaz-Delfin, J.; Hyink, D.; Domingo, P.; Giralt, M.; Klotman, P.E.; Villarroya, F. HIV type-1 transgene expression in mice alters adipose tissue and adipokine levels: towards a rodent model of HIV type-1 lipodystrophy. *Antivir Ther* **2010**, *15*, 1021-1028, doi:10.3851/IMP1669.
191. Wee, K.; Yang, W.; Sugii, S.; Han, W. Towards a mechanistic understanding of

lipodystrophy and seipin functions. *Biosci Rep* **2014**, *34*, doi:10.1042/BSR20140114.

192. Hong, S.B.; Jin, S.Y.; Park, H.J.; Jung, J.H.; Sim, W.Y. Analysis of the monocyte chemoattractant protein 1 -2518 promoter polymorphism in Korean patients with alopecia areata. *J Korean Med Sci* **2006**, *21*, 90-94, doi:10.3346/jkms.2006.21.1.90.
193. Alzolibani, A.A.; Zari, S.; Ahmed, A.A. Epidemiologic and genetic characteristics of alopecia areata (part 2). *Acta dermatovenerologica Alpina, Pannonica, et Adriatica* **2012**, *21*, 15-19.
194. Misiakos, E.P.; Kouraklis, G.; Agapitos, E.; Perrea, D.; Karatzas, G.; Boudoulas, H.; Karayannakos, P.E. Expression of PDGF-A, TGFb and VCAM-1 during the developmental stages of experimental atherosclerosis. *Eur Surg Res* **2001**, *33*, 264-269, doi:10.1159/000049716.
195. Laviades, C.; Varo, N.; Diez, J. Transforming growth factor beta in hypertensives with cardiorenal damage. *Hypertension* **2000**, *36*, 517-522.
196. Niu, Q.; Cai, B.; Huang, Z.C.; Shi, Y.Y.; Wang, L.L. Disturbed Th17/Treg balance in patients with rheumatoid arthritis. *Rheumatol Int* **2012**, *32*, 2731-2736, doi:10.1007/s00296-011-1984-x.
197. Sugiura, Y.; Niimi, T.; Sato, S.; Yoshinouchi, T.; Banno, S.; Naniwa, T.; Maeda, H.; Shimizu, S.; Ueda, R. Transforming growth factor beta1 gene polymorphism in rheumatoid arthritis. *Ann Rheum Dis* **2002**, *61*, 826-828.
198. Clouthier, D.E.; Comerford, S.A.; Hammer, R.E. Hepatic fibrosis, glomerulosclerosis, and a lipodystrophy-like syndrome in PEPCK-TGF-beta1 transgenic mice. *J Clin Invest* **1997**, *100*, 2697-2713, doi:10.1172/JCI119815.
199. Lu, G.Q.; Wu, Z.B.; Chu, X.Y.; Bi, Z.G.; Fan, W.X. An investigation of crosstalk between Wnt/beta-catenin and transforming growth factor-beta signaling in androgenetic alopecia. *Medicine (Baltimore)* **2016**, *95*, e4297, doi:10.1097/MD.0000000000004297.
200. Kizilay Mancini, Ö.; Lora, M.; Shum-Tim, D.; Nadeau, S.; Rodier, F.; Colmegna, I. A Proinflammatory Secretome Mediates the Impaired Immunopotency of Human Mesenchymal Stromal Cells in Elderly Patients with Atherosclerosis. *STEM CELLS Translational Medicine* **2017**, *6*, 1132-1140, doi:10.1002/sctm.16-0221.
201. Abke, S.; Neumeier, M.; Weigert, J.; Wehrwein, G.; Eggenhofer, E.; Schaffler, A.; Maier, K.; Aslanidis, C.; Scholmerich, J.; Buechler, C. Adiponectin-induced secretion of interleukin-6 (IL-6), monocyte chemotactic protein-1 (MCP-1, CCL2) and interleukin-8 (IL-8, CXCL8) is impaired in monocytes from patients with type I diabetes. *Cardiovasc Diabetol* **2006**, *5*, 17, doi:10.1186/1475-2840-5-17.
202. Koenen, R.R.; Weber, C. Therapeutic targeting of chemokine interactions in atherosclerosis. *Nat Rev Drug Discov* **2010**, *9*, 141-153, doi:10.1038/nrd3048.
203. Manivel, V.A.; Sohrabian, A.; Ronnelid, J. Granulocyte-augmented chemokine production induced by type II collagen containing immune complexes is mediated via TLR4 in rheumatoid arthritis patients. *Eur J Immunol* **2016**, *46*, 2822-2834, doi:10.1002/eji.201646496.
204. Szekanecz, Z.; Kim, J.; Koch, A.E. Chemokines and chemokine receptors in rheumatoid arthritis. *Semin Immunol* **2003**, *15*, 15-21.

205. He, G.; Andersen, O.; Haugaard, S.B.; Lihn, A.S.; Pedersen, S.B.; Madsbad, S.; Richelsen, B. Plasminogen activator inhibitor type 1 (PAI-1) in plasma and adipose tissue in HIV-associated lipodystrophy syndrome. Implications of adipokines. *Eur J Clin Invest* **2005**, *35*, 583-590, doi:10.1111/j.1365-2362.2005.01547.x.
206. Gallego-Escuredo, J.M.; Villarroya, J.; Domingo, P.; Targarona, E.M.; Alegre, M.; Domingo, J.C.; Villarroya, F.; Giralt, M. Differentially altered molecular signature of visceral adipose tissue in HIV-1-associated lipodystrophy. *J Acquir Immune Defic Syndr* **2013**, *64*, 142-148, doi:10.1097/QAI.0b013e31829bdb67.
207. Zhang, X.; Zhao, Y.; Ye, Y.; Li, S.; Qi, S.; Yang, Y.; Cao, H.; Yang, J.; Zhang, X. Lesional infiltration of mast cells, Langerhans cells, T cells and local cytokine profiles in alopecia areata. *Arch Dermatol Res* **2015**, *307*, 319-331, doi:10.1007/s00403-015-1539-1.
208. Barahmani, N.; Lopez, A.; Babu, D.; Hernandez, M.; Donley, S.E.; Duvic, M. Serum T helper 1 cytokine levels are greater in patients with alopecia areata regardless of severity or atopy. *Clinical and experimental dermatology* **2010**, *35*, 409-416, doi:10.1111/j.1365-2230.2009.03523.x.
209. Marzolla, V.; Armani, A.; Mammi, C.; Moss, M.E.; Pagliarini, V.; Pontecorvo, L.; Antelmi, A.; Fabbri, A.; Rosano, G.; Jaffe, I.Z., et al. Essential role of ICAM-1 in aldosterone-induced atherosclerosis. *Int J Cardiol* **2017**, *232*, 233-242, doi:10.1016/j.ijcard.2017.01.013.
210. Kitagawa, K.; Matsumoto, M.; Sasaki, T.; Hashimoto, H.; Kuwabara, K.; Ohtsuki, T.; Hori, M. Involvement of ICAM-1 in the progression of atherosclerosis in APOE-knockout mice. *Atherosclerosis* **2002**, *160*, 305-310.
211. Garg, N.; Krishan, P.; Syngle, A. Atherosclerosis in Psoriatic Arthritis: A Multiparametric Analysis Using Imaging Technique and Laboratory Markers of Inflammation and Vascular Function. *Int J Angiol* **2016**, *25*, 222-228, doi:10.1055/s-0036-1584918.
212. Yang, C.M.; Luo, S.F.; Hsieh, H.L.; Chi, P.L.; Lin, C.C.; Wu, C.C.; Hsiao, L.D. Interleukin-1beta induces ICAM-1 expression enhancing leukocyte adhesion in human rheumatoid arthritis synovial fibroblasts: involvement of ERK, JNK, AP-1, and NF-kappaB. *J Cell Physiol* **2010**, *224*, 516-526, doi:10.1002/jcp.22153.
213. Melendez, M.M.; McNurlan, M.A.; Mynarcik, D.C.; Khan, S.; Gelato, M.C. Endothelial adhesion molecules are associated with inflammation in subjects with HIV disease. *Clin Infect Dis* **2008**, *46*, 775-780, doi:10.1086/527563.
214. Gilhar, A.; Landau, M.; Assy, B.; Ullmann, Y.; Shalaginov, R.; Serafimovich, S.; Kalish, R.S. Transfer of alopecia areata in the human scalp graft/Prkdc(scid) (SCID) mouse system is characterized by a TH1 response. *Clin Immunol* **2003**, *106*, 181-187.
215. Gupta, A.K.; Ellis, C.N.; Cooper, K.D.; Nickoloff, B.J.; Ho, V.C.; Chan, L.S.; Hamilton, T.A.; Tellner, D.C.; Griffiths, C.E.; Voorhees, J.J. Oral cyclosporine for the treatment of alopecia areata. A clinical and immunohistochemical analysis. *J Am Acad Dermatol* **1990**, *22*, 242-250.
216. Pleskovič, A.; Letonja, M.Š.; Vujkovac, A.C.; Starčević, J.N.; Gazdikova, K.; Caprnda, M.; Gaspar, L.; Kruzliak, P.; Petrovič, D. C-reactive protein as a marker of progression of carotid atherosclerosis in subjects with type 2 diabetes mellitus. *Vasa* **2017**, *46*, 187-

192, doi:10.1024/0301-1526/a000614.

217. Paffen, E.; DeMaat, M.P. C-reactive protein in atherosclerosis: A causal factor? *Cardiovasc Res* **2006**, *71*, 30-39, doi:10.1016/j.cardiores.2006.03.004.
218. Yu, Q.; Li, Y.; Wang, Y.; Zhao, S.; Yang, P.; Chen, Y.; Fan, J.; Liu, E. C-reactive protein levels are associated with the progression of atherosclerotic lesions in rabbits. *Histol Histopathol* **2012**, *27*, 529-535, doi:10.14670/HH-27.529.
219. Sarkar, S.; Alam, M.M.; Das, G.; Datta, S. Inflammatory Markers and Disease Activity in Juvenile Idiopathic Arthritis. *Indian J Pediatr* **2017**, *84*, 349-356, doi:10.1007/s12098-017-2292-6.
220. Kim, K.W.; Kim, B.M.; Moon, H.W.; Lee, S.H.; Kim, H.R. Role of C-reactive protein in osteoclastogenesis in rheumatoid arthritis. *Arthritis Res Ther* **2015**, *17*, 41, doi:10.1186/s13075-015-0563-z.
221. Miehle, K.; Ebert, T.; Kralisch, S.; Hoffmann, A.; Kratzsch, J.; Schlogl, H.; Stumvoll, M.; Fasshauer, M. Progranulin is increased in human and murine lipodystrophy. *Diabetes Res Clin Pract* **2016**, *120*, 1-7, doi:10.1016/j.diabres.2016.07.017.
222. Samaras, K.; Gan, S.K.; Peake, P.W.; Carr, A.; Campbell, L.V. Proinflammatory markers, insulin sensitivity, and cardiometabolic risk factors in treated HIV infection. *Obesity (Silver Spring)* **2009**, *17*, 53-59, doi:10.1038/oby.2008.500.
223. Mahamid, M.; Abu-Elhija, O.; Samamra, M.; Mahamid, A.; Nseir, W. Association between vitamin D levels and alopecia areata. *Isr Med Assoc J* **2014**, *16*, 367-370.
224. Howard, A.N.; Thurnham, D.I. Lutein and atherosclerosis: Belfast versus Toulouse revisited. *Med Hypotheses* **2017**, *98*, 63-68, doi:10.1016/j.mehy.2016.10.030.
225. Buono, C.; Come, C.E.; Witztum, J.L.; Maguire, G.F.; Connelly, P.W.; Carroll, M.; Lichtman, A.H. Influence of C3 deficiency on atherosclerosis. *Circulation* **2002**, *105*, 3025-3031.
226. Ballanti, E.; Perricone, C.; di Muzio, G.; Kroegler, B.; Chimenti, M.S.; Graceffa, D.; Perricone, R. Role of the complement system in rheumatoid arthritis and psoriatic arthritis: relationship with anti-TNF inhibitors. *Autoimmun Rev* **2011**, *10*, 617-623, doi:10.1016/j.autrev.2011.04.012.
227. Jansen, J.; Delaere, L.; Spielberg, L.; Leys, A. Long-term fundus changes in acquired partial lipodystrophy. *BMJ Case Rep* **2013**, *2013*, doi:10.1136/bcr-2013-201218.
228. Savage, D.B.; Semple, R.K.; Clatworthy, M.R.; Lyons, P.A.; Morgan, B.P.; Cochran, E.K.; Gorden, P.; Raymond-Barker, P.; Murgatroyd, P.R.; Adams, C., et al. Complement abnormalities in acquired lipodystrophy revisited. *J Clin Endocrinol Metab* **2009**, *94*, 10-16, doi:10.1210/jc.2008-1703.
229. Yavuz, S.; Acarturk, T.O. Acquired partial lipodystrophy with C3 hypocomplementemia and antiphospholipid and anticardiolipin antibodies. *Pediatr Dermatol* **2010**, *27*, 504-508, doi:10.1111/j.1525-1470.2010.01255.x.
230. Kulkarni, S.; Punia, R.S.; Kundu, R.; Thami, G.P.; Mohan, H. Direct immunofluorescence pattern and histopathological staging in alopecia areata. *Int J Trichology* **2014**, *6*, 164-167, doi:10.4103/0974-7753.142859.
231. Fairhurst, D.A.; Mitra, A.; MacDonald-Hull, S. Direct Immunofluorescence studies of

patients with alopecia areata in affected and clinically normal areas of scalp. *J Eur Acad Dermatol Venereol* **2009**, *23*, 347-348, doi:10.1111/j.1468-3083.2008.02853.x.

232. Zirlik, A.; Bavendiek, U.; Libby, P.; MacFarlane, L.; Gerdes, N.; Jagielska, J.; Ernst, S.; Aikawa, M.; Nakano, H.; Tsitsikov, E., et al. TRAF-1, -2, -3, -5, and -6 are induced in atherosclerotic plaques and differentially mediate proinflammatory functions of CD40L in endothelial cells. *Arterioscler Thromb Vasc Biol* **2007**, *27*, 1101-1107, doi:10.1161/ATVBAHA.107.140566.
233. Missiou, A.; Kostlin, N.; Varo, N.; Rudolf, P.; Aichele, P.; Ernst, S.; Munkel, C.; Walter, C.; Stachon, P.; Sommer, B., et al. Tumor necrosis factor receptor-associated factor 1 (TRAF1) deficiency attenuates atherosclerosis in mice by impairing monocyte recruitment to the vessel wall. *Circulation* **2010**, *121*, 2033-2044, doi:10.1161/CIRCULATIONAHA.109.895037.
234. Cheng, T.; Sun, X.; Wu, J.; Wang, M.; Eisenberg, R.A.; Chen, Z. Increased serum levels of tumor necrosis factor receptor-associated factor 1 (TRAF1) correlate with disease activity and autoantibodies in rheumatoid arthritis. *Clin Chim Acta* **2016**, *462*, 103-106, doi:10.1016/j.cca.2016.08.021.
235. de Souza Dantas Oliveira, S.H.; de Souza Aarão, T.L.; da Silva Barbosa, L.; Souza Lisbôa, P.G.; Tavares Dutra, C.D.; Margalho Sousa, L.; Simões Quaresma, J.A.; Feio Libonati, R.M. Immunohistochemical analysis of the expression of TNF-alpha, TGF-beta, and caspase-3 in subcutaneous tissue of patients with HIV Lipodystrophy Syndrome. *Microbial Pathogenesis* **2014**, *67*, 41-47, doi:http://dx.doi.org/10.1016/j.micpath.2014.02.004.
236. de Oliveira Pinto, L.M.; Garcia, S.; Lecoeur, H.; Rapp, C.; Gougeon, M.-L. Increased sensitivity of T lymphocytes to tumor necrosis factor receptor 1 (TNFR1)– and TNFR2-mediated apoptosis in HIV infection: relation to expression of Bcl-2 and active caspase-8 and caspase-3. *Blood* **2002**, *99*, 1666-1675, doi:10.1182/blood.V99.5.1666.
237. Redler, S.; Brockschmidt, F.F.; Forstbauer, L.; Giehl, K.A.; Herold, C.; Eigelshoven, S.; Hanneken, S.; De Weert, J.; Lutz, G.; Wolff, H., et al. The TRAF1/C5 locus confers risk for familial and severe alopecia areata. *Br J Dermatol* **2010**, *162*, 866-869, doi:10.1111/j.1365-2133.2009.09598.x.
238. Paramel Varghese, G.; Folkersen, L.; Strawbridge, R.J.; Halvorsen, B.; Yndestad, A.; Ranheim, T.; Krohg‐Sørensen, K.; Skjelland, M.; Espevik, T.; Aukrust, P., et al. NLRP3 Inflammasome Expression and Activation in Human Atherosclerosis. *Journal of the American Heart Association* **2016**, *5*, doi:10.1161/jaha.115.003031.
239. Tenger, C.; Sundborger, A.; Jawien, J.; Zhou, X. IL-18 accelerates atherosclerosis accompanied by elevation of IFN-gamma and CXCL16 expression independently of T cells. *Arterioscler Thromb Vasc Biol* **2005**, *25*, 791-796, doi:10.1161/01.ATV.0000153516.02782.65.
240. Meiler, S.; Lutgens, E.; Weber, C.; Gerdes, N. Atherosclerosis: cell biology and lipoproteins-focus on interleukin-18 signaling, chemotactic heteromers, and microRNAs. *Curr Opin Lipidol* **2016**, *27*, 308-309, doi:10.1097/MOL.0000000000000305.

241. Kanameishi, S.; Nakamizo, S.; Endo, Y.; Fujisawa, A.; Dainichi, T.; Tanaka, T.; Izawa, K.; Nishikomori, R.; Kabashima, K. High level of serum human interleukin-18 in a patient with pyogenic arthritis, pyoderma gangrenosum and acne syndrome. *J Eur Acad Dermatol Venereol* **2017**, *31*, e115-e116, doi:10.1111/jdv.13856.
242. Gracie, J.A.; Forsey, R.J.; Chan, W.L.; Gilmour, A.; Leung, B.P.; Greer, M.R.; Kennedy, K.; Carter, R.; Wei, X.Q.; Xu, D., et al. A proinflammatory role for IL-18 in rheumatoid arthritis. *J Clin Invest* **1999**, *104*, 1393-1401, doi:10.1172/JCI7317.
243. Lindegaard, B.; Hansen, A.B.; Pilegaard, H.; Keller, P.; Gerstoft, J.; Pedersen, B.K. Adipose tissue expression of IL-18 and HIV-associated lipodystrophy. *AIDS* **2004**, *18*, 1956-1958.
244. Lee, D.; Hong, S.K.; Park, S.W.; Hur, D.Y.; Shon, J.H.; Shin, J.G.; Hwang, S.W.; Sung, H.S. Serum levels of IL-18 and sIL-2R in patients with alopecia areata receiving combined therapy with oral cyclosporine and steroids. *Exp Dermatol* **2010**, *19*, 145-147, doi:10.1111/j.1600-0625.2009.00937.x.
245. Lee, J.H.; Cho, D.H.; Park, H.J. IL-18 and Cutaneous Inflammatory Diseases. *Int J Mol Sci* **2015**, *16*, 29357-29369, doi:10.3390/ijms161226172.
246. Soler Palacios, B.; Estrada-Capetillo, L.; Izquierdo, E.; Criado, G.; Nieto, C.; Municio, C.; González-Alvaro, I.; Sánchez-Mateos, P.; Pablos, J.L.; Corbí, A.L., et al. Macrophages from the synovium of active rheumatoid arthritis exhibit an activin A-dependent pro-inflammatory profile. *The Journal of Pathology* **2015**, *235*, 515-526, doi:10.1002/path.4466.
247. van den Berg, W.B. The role of cytokines and growth factors in cartilage destruction in osteoarthritis and rheumatoid arthritis. *Z Rheumatol* **1999**, *58*, 136-141.
248. Hui, W.; Rowan, A.D.; Cawston, T. Modulation of the expression of matrix metalloproteinase and tissue inhibitors of metalloproteinases by TGF-beta1 and IGF-1 in primary human articular and bovine nasal chondrocytes stimulated with TNF-alpha. *Cytokine* **2001**, *16*, 31-35, doi:10.1006/cyto.2001.0950.
249. Boucher, J.; Softic, S.; El Ouaamari, A.; Krumpoch, M.T.; Kleinridders, A.; Kulkarni, R.N.; O'Neill, B.T.; Kahn, C.R. Differential Roles of Insulin and IGF-1 Receptors in Adipose Tissue Development and Function. *Diabetes* **2016**, *65*, 2201-2213, doi:10.2337/db16-0212.
250. Bergfeld, W.F. Growth hormone deficiency in a young patient with alopecia areata. *J Investig Dermatol Symp Proc* **2013**, *16*, S54-55, doi:10.1038/jidsymp.2013.21.
251. Tang, L.; Bernardo, O.; Bolduc, C.; Lui, H.; Madani, S.; Shapiro, J. The expression of insulin-like growth factor 1 in follicular dermal papillae correlates with therapeutic efficacy of finasteride in androgenetic alopecia. *J Am Acad Dermatol* **2003**, *49*, 229-233.
252. Leung, V.; Chiu, Y.L.; Kotler, D.P.; Albu, J.; Zhu, Y.S.; Ham, K.; Engelson, E.S.; Hammad, H.; Christos, P.; Donovan, D.S., et al. Effect of Recombinant Human Growth Hormone and Rosiglitazone for HIV-Associated Abdominal Fat Accumulation on Adiponectin and other Markers of Inflammation. *HIV Clin Trials* **2016**, *17*, 55-62, doi:10.1080/15284336.2015.1126424.

253. Okazaki, S.; Sakaguchi, M.; Miwa, K.; Furukado, S.; Yamagami, H.; Yagita, Y.; Mochizuki, H.; Kitagawa, K. Association of interleukin-6 with the progression of carotid atherosclerosis: a 9-year follow-up study. *Stroke* **2014**, *45*, 2924-2929, doi:10.1161/STROKEAHA.114.005991.
254. Hartman, J.; Frishman, W.H. Inflammation and atherosclerosis: a review of the role of interleukin-6 in the development of atherosclerosis and the potential for targeted drug therapy. *Cardiol Rev* **2014**, *22*, 147-151, doi:10.1097/CRD.0000000000000021.
255. Dong, S.; Xia, T.; Wang, L.; Zhao, Q.; Tian, J. Investigation of candidate genes for osteoarthritis based on gene expression profiles. *Acta Orthop Traumatol Turc* **2016**, *50*, 686-690, doi:10.1016/j.aott.2016.04.002.
256. Kim, G.W.; Lee, N.R.; Pi, R.H.; Lim, Y.S.; Lee, Y.M.; Lee, J.M.; Jeong, H.S.; Chung, S.H. IL-6 inhibitors for treatment of rheumatoid arthritis: past, present, and future. *Arch Pharm Res* **2015**, *38*, 575-584, doi:10.1007/s12272-015-0569-8.
257. Loonam, C.R.; O'Dell, S.D.; Sharp, P.A.; Mullen, A. Microarray Analysis Reveals Altered Lipid and Glucose Metabolism Genes in Differentiated, Ritonavir-Treated 3T3-L1 Adipocytes. *Current HIV research* **2016**, *14*, 37-46.
258. Kannisto, K.; Sutinen, J.; Korsheninnikova, E.; Fisher, R.M.; Ehrenborg, E.; Gertow, K.; Virkamaki, A.; Nyman, T.; Vidal, H.; Hamsten, A., et al. Expression of adipogenic transcription factors, peroxisome proliferator-activated receptor gamma co-activator 1, IL-6 and CD45 in subcutaneous adipose tissue in lipodystrophy associated with highly active antiretroviral therapy. *AIDS* **2003**, *17*, 1753-1762, doi:10.1097/01.aids.0000076305.76477.ce.
259. Rossi, A.; Cantisani, C.; Carlesimo, M.; Scarno, M.; Scali, E.; Mari, E.; Garelli, V.; Maxia, C.; Calvieri, S. Serum concentrations of IL-2, IL-6, IL-12 and TNF-alpha in patients with alopecia areata. *International journal of immunopathology and pharmacology* **2012**, *25*, 781-788.
260. Yu, M.; Kissling, S.; Freyschmidt-Paul, P.; Hoffmann, R.; Shapiro, J.; McElwee, K.J. Interleukin-6 cytokine family member oncostatin M is a hair-follicle-expressed factor with hair growth inhibitory properties. *Exp Dermatol* **2008**, *17*, 12-19, doi:10.1111/j.1600-0625.2007.00643.x.
261. Bruunsgaard, H.; Skinhoj, P.; Pedersen, A.N.; Schroll, M.; Pedersen, B.K. Ageing, tumor necrosis factor-alpha (TNF-alpha) and atherosclerosis. *Clin Exp Immunol* **2000**, *121*, 255-260.
262. Kleinbongard, P.; Heusch, G.; Schulz, R. TNFalpha in atherosclerosis, myocardial ischemia/reperfusion and heart failure. *Pharmacol Ther* **2010**, *127*, 295-314, doi:10.1016/j.pharmthera.2010.05.002.
263. Jia, G.; Cheng, G.; Gangahar, D.M.; Agrawal, D.K. Insulin-like growth factor-1 and TNF-alpha regulate autophagy through c-jun N-terminal kinase and Akt pathways in human atherosclerotic vascular smooth cells. *Immunol Cell Biol* **2006**, *84*, 448-454, doi:10.1111/j.1440-1711.2006.01454.x.
264. Mewar, D.; Wilson, A.G. Treatment of rheumatoid arthritis with tumor necrosis factor inhibitors. *Br J Pharmacol* **2011**, *162*, 785-791, doi:10.1111/j.1476-5381.2010.01099.x.

265. Muller-Ladner, U.; Pap, T.; Gay, R.E.; Neidhart, M.; Gay, S. Mechanisms of disease: the molecular and cellular basis of joint destruction in rheumatoid arthritis. *Nat Clin Pract Rheumatol* **2005**, *1*, 102-110, doi:10.1038/ncprheum0047.
266. Brennan, F.M.; Chantry, D.; Jackson, A.; Maini, R.; Feldmann, M. Inhibitory effect of TNF alpha antibodies on synovial cell interleukin-1 production in rheumatoid arthritis. *Lancet* **1989**, *2*, 244-247.
267. Moelants, E.A.; Mortier, A.; Van Damme, J.; Proost, P. Regulation of TNF-alpha with a focus on rheumatoid arthritis. *Immunol Cell Biol* **2013**, *91*, 393-401, doi:10.1038/icb.2013.15.
268. Mahajan, S.D.; Gaekwad, A.; Pawar, J.; Tripathy, S.; Ghate, M.; Bhattacharya, J.; Singh, H.O.; Schwartz, S.A.; Paranjape, R.; Gangakhedkar, R. Cardiac morbidity in an HIV-1 lipodystrophy patient cohort expressing the TNF-alpha-238 G/A single nucleotide gene polymorphism. *Curr HIV Res* **2015**, *13*, 98-108.
269. Prins, J.B.; Niesler, C.U.; Winterford, C.M.; Bright, N.A.; Siddle, K.; O'Rahilly, S.; Walker, N.I.; Cameron, D.P. Tumor necrosis factor-alpha induces apoptosis of human adipose cells. *Diabetes* **1997**, *46*, 1939-1944.
270. Lichtenstein, K.A. Redefining lipodystrophy syndrome: risks and impact on clinical decision making. *J Acquir Immune Defic Syndr* **2005**, *39*, 395-400.
271. Kasumagic-Halilovic, E.; Prohic, A.; Cavaljuga, S. Tumor necrosis factor-alpha in patients with alopecia areata. *Indian journal of dermatology* **2011**, *56*, 494-496, doi:10.4103/0019-5154.87124.
272. Philpott, M.P.; Sanders, D.A.; Bowen, J.; Kealey, T. Effects of interleukins, colony-stimulating factor and tumor necrosis factor on human hair follicle growth in vitro: a possible role for interleukin-1 and tumor necrosis factor-alpha in alopecia areata. *Br J Dermatol* **1996**, *135*, 942-948.
273. Brydun, A.; Watari, Y.; Yamamoto, Y.; Okuhara, K.; Teragawa, H.; Kono, F.; Chayama, K.; Oshima, T.; Ozono, R. Reduced expression of heme oxygenase-1 in patients with coronary atherosclerosis. *Hypertens Res* **2007**, *30*, 341-348, doi:10.1291/hypres.30.341.
274. Wu, M.L.; Ho, Y.C.; Lin, C.Y.; Yet, S.F. Heme oxygenase-1 in inflammation and cardiovascular disease. *Am J Cardiovasc Dis* **2011**, *1*, 150-158.
275. Zwerina, J.; Tzima, S.; Hayer, S.; Redlich, K.; Hoffmann, O.; Hanslik-Schnabel, B.; Smolen, J.S.; Kollias, G.; Schett, G. Heme oxygenase 1 (HO-1) regulates osteoclastogenesis and bone resorption. *FASEB J* **2005**, *19*, 2011-2013, doi:10.1096/fj.05-4278fje.
276. Rueda, B.; Oliver, J.; Robledo, G.; Lopez-Nevot, M.A.; Balsa, A.; Pascual-Salcedo, D.; Gonzalez-Gay, M.A.; Gonzalez-Escribano, M.F.; Martin, J. HO-1 promoter polymorphism associated with rheumatoid arthritis. *Arthritis Rheum* **2007**, *56*, 3953-3958, doi:10.1002/art.23048.
277. Manente, L.; Lucariello, A.; Costanzo, C.; Viglietti, R.; Parrella, G.; Parrella, R.; Gargiulo, M.; De Luca, A.; Chirianni, A.; Esposito, V. Suppression of pre adipocyte differentiation and promotion of adipocyte death by anti-HIV drugs. *In Vivo* **2012**, *26*, 287-291.

278. Yun, S.J.; Kim, H.S.; Choi, J.Y.; Lee, J.B.; Kim, S.J.; Won, Y.H.; Lee, S.C. Decreased heme oxygenase-1 expression in the scalp of patients with alopecia areata: the pathogenic role of heme oxygenase-1. *Journal of dermatological science* **2009**, *54*, 43-45, doi:10.1016/j.jdermsci.2008.11.009.
279. Payne, G.A.; Tune, J.D.; Knudson, J.D. Leptin-induced endothelial dysfunction: a target for therapeutic interventions. *Curr Pharm Des* **2014**, *20*, 603-608.
280. Abella, V.; Scotece, M.; Conde, J.; Pino, J.; Gonzalez-Gay, M.A.; Gomez-Reino, J.J.; Mera, A.; Lago, F.; Gomez, R.; Gualillo, O. Leptin in the interplay of inflammation, metabolism and immune system disorders. *Nat Rev Rheumatol* **2017**, *13*, 100-109, doi:10.1038/nrrheum.2016.209.
281. Paz-Filho, G.; Mastronardi, C.A.; Licinio, J. Leptin treatment: facts and expectations. *Metabolism* **2015**, *64*, 146-156, doi:10.1016/j.metabol.2014.07.014.
282. Yang, C.C.; Chung, P.L.; Lin, L.Y.; Hughes, M.W.; Tsai, Y.S. Higher plasma leptin is associated with higher risk of androgenetic alopecia in men. *Experimental dermatology* **2017**, *26*, 524-526, doi:10.1111/exd.13369.
283. Lee, Y.W.; Hirani, A.A. Role of interleukin-4 in atherosclerosis. *Arch Pharm Res* **2006**, *29*, 1-15.
284. Wojdasiewicz, P.; Poniatowski, L.A.; Szukiewicz, D. The role of inflammatory and anti-inflammatory cytokines in the pathogenesis of osteoarthritis. *Mediators Inflamm* **2014**, *2014*, 561459, doi:10.1155/2014/561459.
285. Dragovic, G.; Dimitrijevic, B.; Khawla, A.M.; Soldatovic, I.; Andjic, M.; Jevtovic, D.; Nair, D. Lower levels of IL-4 and IL-10 influence lipodystrophy in HIV/AIDS patients under antiretroviral therapy. *Exp Mol Pathol* **2017**, *102*, 210-214, doi:10.1016/j.yexmp.2017.02.001.
286. Alli, R.; Nguyen, P.; Boyd, K.; Sundberg, J.P.; Geiger, T.L. A mouse model of clonal CD8+ T lymphocyte-mediated alopecia areata progressing to alopecia universalis. *J Immunol* **2012**, *188*, 477-486, doi:10.4049/jimmunol.1100657.
287. McLaren, J.E.; Ramji, D.P. Interferon gamma: a master regulator of atherosclerosis. *Cytokine Growth Factor Rev* **2009**, *20*, 125-135, doi:10.1016/j.cytogfr.2008.11.003.
288. Lee, S.H.; Kwon, J.Y.; Kim, S.Y.; Jung, K.; Cho, M.L. Interferon-gamma regulates inflammatory cell death by targeting necroptosis in experimental autoimmune arthritis. *Sci Rep* **2017**, *7*, 10133, doi:10.1038/s41598-017-09767-0.
289. Liu, Y.; Ramot, Y.; Torrelo, A.; Paller, A.S.; Si, N.; Babay, S.; Kim, P.W.; Sheikh, A.; Lee, C.C.; Chen, Y., et al. Mutations in proteasome subunit beta type 8 cause chronic atypical neutrophilic dermatosis with lipodystrophy and elevated temperature with evidence of genetic and phenotypic heterogeneity. *Arthritis and rheumatism* **2012**, *64*, 895-907, doi:10.1002/art.33368.
290. Castelar, L.; Silva, M.M.; Castelli, E.C.; Deghaide, N.H.; Mendes-Junior, C.T.; Machado, A.A.; Donadi, E.A.; Fernandes, A.P. Interleukin-18 and interferon-gamma polymorphisms in Brazilian human immunodeficiency virus-1-infected patients presenting with lipodystrophy syndrome. *Tissue Antigens* **2010**, *76*, 126-130, doi:10.1111/j.1399-0039.2010.01471.x.

291. Arca, E.; Musabak, U.; Akar, A.; Erbil, A.H.; Tastan, H.B. Interferon-gamma in alopecia areata. *Eur J Dermatol* **2004**, *14*, 33-36.
292. Szklarczyk, D.; Morris, J.H.; Cook, H.; Kuhn, M.; Wyder, S.; Simonovic, M.; Santos, A.; Doncheva, N.T.; Roth, A.; Bork, P., et al. The STRING database in 2017: quality-controlled protein-protein association networks, made broadly accessible. *Nucleic acids research* **2017**, *45*, D362-D368, doi:10.1093/nar/gkw937.
293. Min, E.Y.; Kim, I.H.; Lee, J.; Kim, E.Y.; Choi, Y.H.; Nam, T.J. The effects of fucodian on senescence are controlled by the p16INK4a-pRb and p14Arf-p53 pathways in hepatocellular carcinoma and hepatic cell lines. *International journal of oncology* **2014**, *45*, 47-56, doi:10.3892/ijo.2014.2426.
294. Bridger, J.M.; Kill, I.R.; O'Farrell, M.; Hutchison, C.J. Internal lamin structures within G1 nuclei of human dermal fibroblasts. *Journal of cell science* **1993**, *104 ( Pt 2)*, 297-306.
295. Tiniakos, D.; Jurk, D. A novel Sudan Black B-based analogue revives lipofuscin as a biomarker for in vivo senescence. *Virchows Archiv : an international journal of pathology* **2018**, *473*, 781-783, doi:10.1007/s00428-018-2452-8.
296. Lozano-Gerona, J.; Garcia-Otin, A.L. ImageJ-based semiautomatic method to analyze senescence in cell culture. *Analytical biochemistry* **2018**, *543*, 30-32, doi:10.1016/j.ab.2017.11.020.
297. Althubiti, M.; Lezina, L.; Carrera, S.; Jukes-Jones, R.; Giblett, S.M.; Antonov, A.; Barlev, N.; Saldanha, G.S.; Pritchard, C.A.; Cain, K., et al. Characterization of novel markers of senescence and their prognostic potential in cancer. *Cell death & disease* **2014**, *5*, e1528, doi:10.1038/cddis.2014.489.
298. Vermeulen, K.; Van Bockstaele, D.R.; Berneman, Z.N. The cell cycle: a review of regulation, deregulation and therapeutic targets in cancer. *Cell proliferation* **2003**, *36*, 131-149, doi:10.1046/j.1365-2184.2003.00266.x.
299. Neurohr, G.E.; Terry, R.L.; Lengefeld, J.; Bonney, M.; Brittingham, G.P.; Moretto, F.; Miettinen, T.P.; Vaites, L.P.; Soares, L.M.; Paulo, J.A., et al. Excessive Cell Growth Causes Cytoplasm Dilution And Contributes to Senescence. *Cell* **2019**, *176*, 1083-1097 e1018, doi:10.1016/j.cell.2019.01.018.
300. Ricklin, D.; Reis, E.S.; Mastellos, D.C.; Gros, P.; Lambris, J.D. Complement component C3 - The "Swiss Army Knife" of innate immunity and host defense. *Immunological reviews* **2016**, *274*, 33-58, doi:10.1111/imr.12500.
301. Pepys, M.B.; Hirschfield, G.M. C-reactive protein: a critical update. *The Journal of clinical investigation* **2003**, *111*, 1805-1812, doi:10.1172/JCI18921.
302. Strasser, A.; Jost, P.J.; Nagata, S. The many roles of FAS receptor signaling in the immune system. *Immunity* **2009**, *30*, 180-192, doi:10.1016/j.immuni.2009.01.001.
303. Origassa, C.S.; Camara, N.O. Cytoprotective role of heme oxygenase-1 and heme degradation derived end products in liver injury. *World journal of hepatology* **2013**, *5*, 541-549, doi:10.4254/wjh.v5.i10.541.
304. Schroder, K.; Hertzog, P.J.; Ravasi, T.; Hume, D.A. Interferon-gamma: an overview of signals, mechanisms and functions. *Journal of leukocyte biology* **2004**, *75*, 163-189, doi:10.1189/jlb.0603252.

305. Wrigley, S.; Arafa, D.; Tropea, D. Insulin-Like Growth Factor 1: At the Crossroads of Brain Development and Aging. *Frontiers in cellular neuroscience* **2017**, *11*, 14, doi:10.3389/fncel.2017.00014.
306. Tanaka, T.; Narazaki, M.; Kishimoto, T. IL-6 in inflammation, immunity, and disease. *Cold Spring Harbor perspectives in biology* **2014**, *6*, a016295, doi:10.1101/cshperspect.a016295.
307. Kaiko, G.E.; Horvat, J.C.; Beagley, K.W.; Hansbro, P.M. Immunological decision-making: how does the immune system decide to mount a helper T-cell response? *Immunology* **2008**, *123*, 326-338, doi:10.1111/j.1365-2567.2007.02719.x.
308. Yasuda, K.; Nakanishi, K.; Tsutsui, H. Interleukin-18 in Health and Disease. *International journal of molecular sciences* **2019**, *20*, doi:10.3390/ijms20030649.
309. Chhabra, M.; Sharma, S. Potential role of Peroxisome Proliferator Activated Receptor gamma analogues in regulation of endothelial progenitor cells in diabetes mellitus: An overview. *Diabetes & metabolic syndrome* **2019**, *13*, 1123-1129, doi:10.1016/j.dsx.2019.01.036.
310. Hata, A.; Chen, Y.G. TGF-beta Signaling from Receptors to Smads. *Cold Spring Harbor perspectives in biology* **2016**, *8*, doi:10.1101/cshperspect.a022061.
311. Parameswaran, N.; Patial, S. Tumor necrosis factor-alpha signaling in macrophages. *Critical reviews in eukaryotic gene expression* **2010**, *20*, 87-103, doi:10.1615/critreveukargeneexpr.v20.i2.10.
312. Shi, J.H.; Sun, S.C. Tumor Necrosis Factor Receptor-Associated Factor Regulation of Nuclear Factor kappaB and Mitogen-Activated Protein Kinase Pathways. *Frontiers in immunology* **2018**, *9*, 1849, doi:10.3389/fimmu.2018.01849.
313. Deshmane, S.L.; Kremlev, S.; Amini, S.; Sawaya, B.E. Monocyte chemoattractant protein-1 (MCP-1): an overview. *Journal of interferon & cytokine research : the official journal of the International Society for Interferon and Cytokine Research* **2009**, *29*, 313-326, doi:10.1089/jir.2008.0027.
314. Diamond, M.S.; Staunton, D.E.; de Fougerolles, A.R.; Stacker, S.A.; Garcia-Aguilar, J.; Hibbs, M.L.; Springer, T.A. ICAM-1 (CD54): a counter-receptor for Mac-1 (CD11b/CD18). *The Journal of cell biology* **1990**, *111*, 3129-3139, doi:10.1083/jcb.111.6.3129.
315. Rosenkilde, M.M.; Schwartz, T.W. The chemokine system -- a major regulator of angiogenesis in health and disease. *APMIS : acta pathologica, microbiologica, et immunologica Scandinavica* **2004**, *112*, 481-495, doi:10.1111/j.1600-0463.2004.apm11207-0808.x.
316. Zhou, Y.; Rui, L. Leptin signaling and leptin resistance. *Frontiers of medicine* **2013**, *7*, 207-222, doi:10.1007/s11684-013-0263-5.
317. Vidak, S.; Foisner, R. Molecular insights into the premature aging disease progeria. *Histochemistry and cell biology* **2016**, *145*, 401-417, doi:10.1007/s00418-016-1411-1.
318. Samavati, L.; Rastogi, R.; Du, W.; Huttemann, M.; Fite, A.; Franchi, L. STAT3 tyrosine phosphorylation is critical for interleukin 1 beta and interleukin-6 production in response to lipopolysaccharide and live bacteria. *Molecular immunology* **2009**, *46*,

1867-1877, doi:10.1016/j.molimm.2009.02.018.

319. Hu, X.; Ivashkiv, L.B. Cross-regulation of signaling pathways by interferon-gamma: implications for immune responses and autoimmune diseases. *Immunity* **2009**, *31*, 539-550, doi:10.1016/j.immuni.2009.09.002.
320. Fridman, J.S.; Scherle, P.A.; Collins, R.; Burn, T.C.; Li, Y.; Li, J.; Covington, M.B.; Thomas, B.; Collier, P.; Favata, M.F., et al. Selective inhibition of JAK1 and JAK2 is efficacious in rodent models of arthritis: preclinical characterization of INCB028050. *Journal of immunology* **2010**, *184*, 5298-5307, doi:10.4049/jimmunol.0902819.
321. Montecucco, A.; Zanetta, F.; Biamonti, G. Molecular mechanisms of etoposide. *EXCLI journal* **2015**, *14*, 95-108, doi:10.17179/excli2015-561.
322. Rodier, F.; Munoz, D.P.; Teachenor, R.; Chu, V.; Le, O.; Bhaumik, D.; Coppe, J.P.; Campeau, E.; Beausejour, C.M.; Kim, S.H., et al. DNA-SCARS: distinct nuclear structures that sustain damage-induced senescence growth arrest and inflammatory cytokine secretion. *Journal of cell science* **2011**, *124*, 68-81, doi:10.1242/jcs.071340.
323. Novakova, Z.; Hubackova, S.; Kosar, M.; Janderova-Rossmeislova, L.; Dobrovolna, J.; Vasicova, P.; Vancurova, M.; Horejsi, Z.; Hozak, P.; Bartek, J., et al. Cytokine expression and signaling in drug-induced cellular senescence. *Oncogene* **2010**, *29*, 273-284, doi:10.1038/onc.2009.318.
324. Coppe, J.P.; Desprez, P.Y.; Krtolica, A.; Campisi, J. The senescence-associated secretory phenotype: the dark side of tumor suppression. *Annual review of pathology* **2010**, *5*, 99-118, doi:10.1146/annurev-pathol-121808-102144.
325. Rea, I.M.; Gibson, D.S.; McGilligan, V.; McNerlan, S.E.; Alexander, H.D.; Ross, O.A. Age and Age-Related Diseases: Role of Inflammation Triggers and Cytokines. *Frontiers in immunology* **2018**, *9*, 586, doi:10.3389/fimmu.2018.00586.
326. Gordon, L.B.; Campbell, S.E.; Massaro, J.M.; D'Agostino, R.B., Sr.; Kleinman, M.E.; Kieran, M.W.; Moses, M.A. Survey of plasma proteins in children with progeria pre-therapy and on-therapy with lonafarnib. *Pediatric research* **2018**, *83*, 982-992, doi:10.1038/pr.2018.9.
327. Liu, Y.Z.; Wang, Y.X.; Jiang, C.L. Inflammation: The Common Pathway of Stress-Related Diseases. *Frontiers in human neuroscience* **2017**, *11*, 316, doi:10.3389/fnhum.2017.00316.
328. Franceschi, C.; Bonafe, M.; Valensin, S.; Olivieri, F.; De Luca, M.; Ottaviani, E.; De Benedictis, G. Inflamm-aging. An evolutionary perspective on immunosenescence. *Annals of the New York Academy of Sciences* **2000**, *908*, 244-254, doi:10.1111/j.1749-6632.2000.tb06651.x.

# Acknowledgement

Upon completion of this thesis, I am grateful to those who encouraged and supported me during my doctoral studies.

First of all, I would like to dedicate my most sincere gratitude to my advisor Professor Karima Djabali. I thank her for giving me this precious opportunity to join her laboratory and for guiding me throughout all my PhD time. Her profound knowledge, serious scientific attitude, and rigorous academic spirit have greatly impacted me. From the beginning of the project selection to the topic's completion, she always gave me careful guidance. Her meticulous guidance not only enabled me to set ambitious academic goals but also made me understand many philosophies about life. What impressed me the most was her rigorous scientific research attitude. Her attention to detail finally made me learn to set priorities and focus on crucial things; small details make a difference. Finally, she taught me how to think and criticize my work and conduct excellent research. I am very grateful that she has been my advisor. Thank you for everything!

Second, I would like to thank Professor Thomas Brück as my second advisor and Professor Wolfgang Domke as my mentor, both of whom were essential for the development and progress of my PhD. I would also like to thank Professor Brück for participating in my committee meetings and for his encouragement, advice and feedback throughout my study. I also want to thank Professor Domke for his great support during my PhD. Without their precious help, it would have been impossible for me to conduct this research.

Third, I want to mention the colleagues to whom I wish to express my gratitude. I would like to thank Rouven Arnold for helping me in the Western blot, qPCR research and paper writing. Every discussion with you makes me progress, and we grew with each other on this project. I hope that I can help you one day the way you helped me.

I also want to thank Gonçalo Henriques. I started this project almost at the same time as him. At that time, I was more involved in project design and methodology. Meanwhile, Gonçalo

spent more time reading the literature to support my data mining results. I think he is the hardest-working master's student I have ever met. He could solve all of the problems with me, no matter what they were.

Many thanks also to my fellow lab mates, Dr Leithe Budel, Dr Xiang Lu, Dr Diana Gabriel and Veronika Eisch, for the great help, exciting discussions and all of the good times we spent together inside and outside the lab. Special thanks to Leithe, with whom I am still in contact. I hope that one day we can complete our entrepreneurial dream together. Thanks to Luxiang; he encouraged me to join this lab, had lunch with me every day, and still shares my work experience to this day. Thanks to Diana and Veronika for all of the teamwork; they taught me many experimental techniques and helped me grow.

My thanks also go to Jennifer Röhrl, Farah Najdi, Elena Vehns and Peter Krüger. I loved burger day and karaoke night. We had a lot of fun together. The debates with Jennifer always helped me see things from different perspectives, and I learned a lot from her. Being from a non-EU country, Farah and I share many common emotions; our values are similar, and we have many common topics to share. Thanks to Elena, our laboratory became even more happy, tidy and clean. I learned many good habits from her and became more organized. Peter, although I met him very late, we had a great, happy time together. I often hear your stories, and it makes me feel like we have been friends for a long time.

Last but not least, my PhD would not have been possible to finish without my family. My parents were always there for me whenever I needed them. Their support accompanied me through every step.